

PROPERTIES OF THE BROMIDE ION AS A NUCLEAR MAGNETIC  
RESONANCE PROBE OF PROTEIN CONFORMATION:  
STUDIES ON METHEMOGLOBIN AND SIMPLE THIOLS

by

TERRYL RAND COLLINS

B.Sc. (Honours), Simon Fraser University, 1969

A DISSERTATION SUBMITTED IN PARTIAL FULFILLMENT  
OF THE REQUIREMENTS FOR THE DEGREE OF  
MASTER OF SCIENCE  
in the Department  
of  
Biological Sciences

© TERRYL RAND COLLINS, 1971

SIMON FRASER UNIVERSITY

APPROVAL

Name: Terryl Rand Collins

Degree: Master of Science

Title of Thesis: Properties of the Bromide Ion as a Nuclear  
Magnetic Resonance Probe of Protein  
Conformation: Studies on Methemoglobin  
and Simple Thiols.

Examining Committee:

Chairman: P. C. Oloffs

---

A. H. Burr  
Senior Supervisor

---

E. J. Wells

---

C. O. Parkes

---

H. L. Speer

---

J. S. Barlow

Date Approved: July 15, 1971

## ABSTRACT

The majority of NMR halide-probe studies on macromolecules to date have dealt with the estimation of the number of available metal-ion binding sites on proteins from  $^{35}\text{Cl}$  NMR linewidth measurements. This study is designed to investigate the feasibility of using  $^{81}\text{Br}$  and  $^{79}\text{Br}$  induction decay-rate measurements to obtain the correlation time ( $\tau_c$ ) for reorientation of the bound probe and the rate of exchange of halide ions ( $k_1$ ) at the binding site.

A general theoretical treatment of the halide-exchange phenomenon is presented. The inadequacy of present theoretical models for movement of the bound probe imposes limitations on the treatment of the quadrupolar transverse relaxation time  $T_2$ . Two-species Bloch equations including the chemical exchange give an expression relating  $k_1$  and  $\tau_c$  to the slope  $\alpha$  of the curve for titration of the protein binding sites by the probe. The implications of the three limiting regions which follow from this equation are discussed.

Titration of four simple thiols (mercaptosuccinic acid, cysteine, glutathione, and mercaptoethanol) with  $\text{HgCl}_2$  in 2.0 molar NaBr at pH 2, 6, and 11 revealed that formation of the dimer  $\text{RS-Hg-SR}$  occurs under these conditions, with a distinct

endpoint being observed only at the latter two pH values. Presence of an observable concentration of mercuric tetrabromide ion at acid pH indicates that the dimer is unstable under these conditions. Consideration of the chemical equilibria present at acidic pH yields a third-order equation for  $[\text{HgBr}_4^{2-}]$  in terms of the pH and equilibrium constants of the species involved. Decay rates calculated from this equation were found to fit the observed titration curves to within experimental error.

The conformational changes induced in equine methemoglobin by basic pH were chosen as a model system for evaluating the capabilities of the bromide-probe method. The hemoglobin samples used were 85% hemoglobin by weight, with approximately 98% of the hemoglobin being in the ferric form. Titration of the  $\beta$ -chain sulphhydryl groups of this protein with  $\text{HgCl}_2$  yielded a sulphhydryl titer of 1.2-1.5 groups per molecule.  $\alpha$  did not change between pH 7.0 and 8.5 but decreased to half by pH 10.0, suggesting that a conformational change occurred between pH 8.5 and 10.0 but not between pH 7.0 and 8.5. This conclusion is in agreement with the ultracentrifuge studies of Kurihara and Shibata.  $k_1$  and  $\tau_c$  were calculated at pH 7.0 and 10.0 from the dependence of  $\alpha$  on the bromide concentration in the range 0.5-3.0 molar.  $k_1$  decreased from  $3.27 \times 10^7$  liter mole<sup>-1</sup>sec<sup>-1</sup> at pH 7.0 to  $1.2 \times 10^7$  liter mole<sup>-1</sup>sec<sup>-1</sup> at pH 10.0, suggesting that the

accessibility of the  $\beta$  chain sulphhydryl group to free halide ions decreased at basic pH.  $\tau_c$  decreased from  $0.74 \times 10^{-10}$  sec at pH 7.0 to  $0.4 \times 10^{-10}$  sec at pH 10.0, indicating that there is enhanced flexibility of the  $\beta$  chain at or near the sulphhydryl site in basic medium. Since previous halide-probe studies on proteins have dealt only with changes in  $\alpha$ , the fact that this method has proven capable of separating the contributions of  $k_1$  and  $\tau_c$  to alterations in  $\alpha$  represents a considerable advance in the specificity of the halide-probe technique as a tool for the study of protein conformational changes.

vi

To Janie

who helped to make it all possible

Forward and backward I have gone, and for me it has been an immense journey....I have done all in my power to avoid errors in fact. I have given the record of what one man thought as he pursued research and pressed his hands against the confining walls of scientific method in his time. It is not, I must confess at the outset, an account of discovery so much as a confession of ignorance and of the final illumination that sometimes comes to a man....But men see differently. I can at best report only from my own wilderness. The important thing is that each man possess such a wilderness and that he consider what marvels are to be observed there.

Loren Eiseley,  
The Immense Journey

## ACKNOWLEDGEMENTS

I would like to express my gratitude to Dr. A.H. Burr for his support and guidance during this project and for the valuable opportunity to study at the Marine Biological Laboratory in Woods Hole. I want also to thank Dr. H.L. Speer, Dr. E.M. Voigt, and Dr. L.J. Albright for their helpful suggestions and criticism during the course of this study.

To Dr. E.J. Wells I am deeply indebted for his support and patience during every phase of this project. Without his encouragement and the use of this equipment this study would not have been possible.

My thanks go particularly to Dr. C.O. Parkes for his patient answers to many, many questions about protein chemistry.

I would like to express my special thanks to Dr. Z. Starcuk for working with me on the first part of this project and for sharing many small frustrations and triumphs. Dr. Starcuk is responsible for developing the theory explaining pH effects in simple thiols and contributed greatly to our derivation of the exchange-rate theory.

I am grateful to the National Research Council of Canada from granting me a postgraduate scholarship.

Finally, I wish to express my deepest thanks and gratitude to my wife Janie for typing this rather formidable manuscript



and for sharing with me the successes and failures of the last two years.

## TABLE OF CONTENTS

	Page
Examining Committee Approval . . . . .	ii
Abstract . . . . .	iii
Dedication . . . . .	vi
Acknowledgments . . . . .	vii
Table of Contents . . . . .	ix
List of Tables . . . . .	xi
List of Figures . . . . .	xii
Introduction . . . . .	1
Theory of Pulsed NMR	
I. Classical Treatment: Motion of the Magnetization	5
II. Quantum-Mechanical Treatment: Spin Relaxation . .	9
Theory of the Exchange Effect . . . . .	24
Description of NMR Apparatus and Methods . . . . .	46
Studies on Simple Thiols	
I. Introduction . . . . .	55
II. Theory . . . . .	56
III. Experimental . . . . .	67
IV. Results and Discussion . . . . .	69
Studies on Hemoglobin	
I. Introduction . . . . .	84

	Page
II. Characterization of the Hemoglobin Preparation	
A. Experimental . . . . .	91
B. Results and Discussion . . . . .	94
III. NMR Studies	
A. Experimental . . . . .	108
B. Results . . . . .	112
C. Discussion . . . . .	122
Studies on Other Proteins	
I. Papain . . . . .	129
II. Ovalbumin . . . . .	132
General Conclusions	
I. Comparison of Chloride, Bromide, and Iodide as NMR Probes . . . . .	135
II. Improvements to the Spectrometer and Data Acquisition System . . . . .	136
III. Other Possible Probes . . . . .	138
Bibliography . . . . .	141
Curriculum Vitae . . . . .	149

## LIST OF TABLES

		Page
Table I	Equilibrium constants for thiols at 25 °C.	58
Table II	Values of $\alpha$ for $[\text{HgBr}_4]^{2-}$ in 2.0 molar NaBr, 26 °C . . . . .	69
Table III	Absorptivities of equine methemoglobin in 0.2 molar phosphate buffer at pH 7.0 . .	97
Table IV	Molecular weight of hemoglobin measured by different methods . . . . .	103
Table V	Experimental values of $k_1$ and $T_{2B}/n$ . . .	121

## LIST OF FIGURES

	Page
Figure 1	Classical description of the free induction experiment . . . . . 8
Figure 2	Behaviour of $G_{qq'}(\tau)$ . . . . . 11
Figure 3	Behaviour of $J_{qq'}(\omega)$ for three values of correlation time . . . . . 12
Figure 4	Program used to calculate the values of $\alpha$ shown in Figures 5-10 . . . . . 36
Figure 5	Calculated dependence of $\alpha$ on the rate of halide exchange for 2.0 molar bromide . . . 37
Figure 6	Calculated dependence of $\alpha$ on the correla- tion time for 2.0 molar bromide . . . . . 38
Figure 7	Calculated dependence of $\alpha$ on the rate of halide exchange for 0.5 molar bromide . . . 39
Figure 8	Calculated dependence of $\alpha$ on the correla- tion time for 0.5 molar bromide . . . . . 40
Figure 9	Calculated dependence of $\alpha$ on the rate of halide exchange for 2.0 molar chloride . . . 41
Figure 10	Calculated dependence of $\alpha$ on the correla- tion time for 2.0 molar chloride . . . . . 42
Figure 11	Block diagram of pulsed NMR spectrometer and signal averaging system . . . . . 47

	Page
Figure 12	Typical raw and averaged $^{81}\text{Br}$ free induction decays from aqueous NaBr solutions . . . . . 49
Figure 13	Graph of $\ln(\text{Signal Amplitude})$ versus time for a typical $^{81}\text{Br}$ decay . . . . . 52
Figure 14	Two-point method of determining $T_2$ . . . . . 54
Figure 15	Program used to solve equation (61) . . . . . 61
Figure 16	Simulated titration curves for simple thiols at low pH produced by solution of equation (61) . . . . . 62
Figure 17	Minimum pH for which the condition $R < 10^{-10}$ can be met as a function of bromide concen- tration . . . . . 64
Figure 18	Dependence of $R_2$ on the concentration of mer- curic ion in 2.0 molar sodium bromide solution at pH 2.2 . . . . . 70
Figure 19	Dependence of $R_2$ on the concentration of mer- curic ion in 2.0 molar sodium bromide solution at pH 6.1 . . . . . 71
Figure 20	Dependence of $R_2$ on the concentration of mer- curic ion in 2.0 molar sodium bromide solution at pH 11.1 . . . . . 72
Figure 21	Titration of $1.2 \times 10^{-3}$ molar mercaptosuccinic acid with $\text{HgCl}_2$ . . . . . 73

	Page
Figure 22	Titration of $1.2 \times 10^{-3}$ molar cysteine with HgCl <sub>2</sub> . . . . . 74
Figure 23	Titration of $1.0 \times 10^{-3}$ molar glutathione with HgCl <sub>2</sub> . . . . . 75
Figure 24	Titration of $1.25 \times 10^{-3}$ molar mercaptoethanol with HgCl <sub>2</sub> . . . . . 76
Figure 25	Dependence of the mercaptosuccinic acid titration curve at low pH on the bromide con- centration . . . . . 81
Figure 26	Structure of the hemoglobin molecule . . . . . 87
Figure 27	Effect of high pH on the S <sub>w,20</sub> of horse hemo- globin in 0.2 molar phosphate buffer . . . . . 88
Figure 28	Absorption spectrum of equine methemoglobin . . . . . 96
Figure 29	Gel filtration of Mann equine methemoglobin on G-75 Sephadex . . . . . 99
Figure 30	Gel filtration of Mann equine methemoglobin on G-75 Sephadex . . . . . 100
Figure 31	Chromatography of Mann equine methemoglobin on DEAE Sephadex A-50 in 0.1 molar tris-HCl buffer at pH 8.5 . . . . . 101
Figure 32	Titration curve of 0.2 molar mixed buffer . . . . . 110
Figure 33	Titration of $3.8 \times 10^{-5}$ molar equine met- hemoglobin in 2.0 molar NaBr in 0.05 molar

	Page
	sodium phosphate buffer, pH 7.0 . . . . . 113
Figure 34	Titration of $2.5 \times 10^{-3}$ molar equine met- hemoglobin in 2.0 molar NaBr in 0.2 molar mixed buffer at pH 7.0 and 8.5 . . . . . 114
Figure 35	Titration of $3.8 \times 10^{-5}$ molar equine met- hemoglobin in 2.0 molar NaBr in 0.05 molar sodium bicarbonate buffer, pH 10.0 . . . . . 115
Figure 36	Dependence of $R_2$ on the methemoglobin con- centration in the absence of mercury . . . . . 117
Figure 37	Determination of $k_1$ and $T_{2B}$ for equine met- hemoglobin at pH 7.0 and 10.0 . . . . . 119
Figure 38	Titration curves of papain . . . . . 131
Figure 39	Titration of $5.9 \times 10^{-5}$ molar ovalbumin in 2.0 molar NaBr in 0.05 molar phosphate buf- fer, pH 7.0 . . . . . 134
Figure 40	Calculated dependence of $\alpha$ on the rate of halide exchange for 2.0 molar iodide . . . . . 137



## INTRODUCTION

Numerous investigations in recent years (1-5) attest to the growing importance of probe techniques for the elucidation of structural changes in macromolecules. In this method, a specific site in the biopolymer is tagged with one or more small reporter molecules called "probes" and an easily-observable parameter of the probe such as fluorescence yield or ESR linewidth is measured as the macromolecule undergoes conformational change. If the environment of the probe is altered by this structural rearrangement, the nature of the change may be inferred from its effect on the bound probe.

Recently there has been considerable interest (4-21) in the application of nuclear magnetic resonance (NMR) probes to this type of study. The work described here is an extension of the halide probe technique developed by Stengle and Baldeschwieler to the study of protein conformational changes. Present results indicate that this method has great potential for the elucidation of certain structural and mechanistic problems.

The NMR halide probe experiments are based on changes in the effective halide transverse relaxation time  $T_2$  (to be discussed in detail later) as a result of halide exchange between symmetrically solvated halide ion ( $T_2$  long) and a site where the quadru-

polar halide nucleus is bound tightly to a specific region within a protein ( $T_2$  short). The resulting relaxation time is dependent on the relative concentration of each binding site and the physical environment of the bound halide, as well as the frequency with which the halide nucleus samples the two sites. In the method of Stengle and Baldeschwieler (4-6), a solution of protein is prepared in aqueous sodium halide, and specific binding sites on the protein are titrated with a mercury compound which binds only to these sites. Since chloride, bromide, and iodide form weak covalent bonds to mercury under these conditions, for these elements halide exchange can occur between the bound mercurial and the solution. This method leads in principle to the determination of the number of binding sites on the protein, the correlation time for re-orientation of the halogen-protein bond, and the average rate of halogen exchange from the binding sites. The latter two parameters are sensitive to conformational changes at the halide binding site. As the probe may be tailor-made to fit any binding site, a large number of mercury compounds are potentially useful in this application, yet little research has been done in this field to date. In most cases, the mercurial has been simply the mercury salt of the halide concerned, with the result that a complex of the form Protein-S-Hg $\cdots$ X is created with cysteine residues in the protein. The present work deals with a probe of this sort.

The halide probe experiment may be carried out using the chlorine, bromine, or iodine resonance. For the most part, chloride probes observed by broad-line NMR have been used to date. The present study is an evaluation of the feasibility of using pulsed NMR to observe protein structural changes by following the  $T_2$  of bromine rather than chlorine nuclei. The use of pulsed NMR to observe bromide resonances represents a considerable improvement over broad-line chloride probe techniques for a number of reasons:

1. Pulsed NMR techniques permit observation of the shape of the decay signal, with the result that deviations from the ideal exponential decay will be readily detectable.
2. Broad-line NMR techniques require modulation of the resonance signal in order to obtain a usable signal-to-noise ratio. Overmodulation may lead to modulation distortion and an apparent increase in the linewidth.
3. Efficient signal averaging is possible with pulsed NMR. For measurements taken over the same time interval, the pulsed NMR method with signal averaging will yield greater sensitivity than will continuous-wave techniques.

4. The theoretical treatment to be presented in this work demonstrates that the observed  $T_2$  for the bromide probe experiment is intrinsically more sensitive to changes in the rate of exchange between the free and bound sites than is the case for the chloride probe. Consequently, the bromide ion is, in theory, a more powerful tool for examining protein conformational changes than is the chloride ion.

By observing the resonance of  $^{81}\text{Br}$ , an attempt was made to obtain information about the  $T_2$  for the bound bromide and the rate of exchange when the bromide probe was bound to the sulphhydryl groups of equine methemoglobin. This technique has also been applied to the study of the mercury complexes of a number of simple sulphhydryl compounds in order to gain some insight into the stability of the mercury-sulphur complex under a variety of conditions.

THEORY OF PULSED NMR

I. Classical Treatment: Motion of the Magnetization

The classical description presented in this section is mainly intended to introduce the NMR methodology used in this study, and therefore will be brief. A more detailed quantum-mechanical treatment of the decay time changes observed here will be presented in the following sections.

Consider a static magnetic field  $\vec{H}_0$  applied to an ensemble of nuclei, each with nuclear magnetic moment  $\vec{u}$  and gyromagnetic ratio  $\gamma$ . Let  $\vec{H}_0$  define the Z direction of a set of Cartesian coordinates. Since the nuclear magnetic moment and the angular momentum  $\hbar\vec{I}$  are related by

$$\vec{u} = \gamma\hbar\vec{I} \tag{1}$$

and since the rate of change of angular momentum of a system equals the torque on the system, the classical equation of motion for an individual moment may be written (22) as

$$\frac{d\vec{u}}{dt} = \gamma(\vec{u} \times \vec{H}_0) \tag{2}$$

Classically, this is equivalent to the precession of the magnetic vector around  $\vec{H}_0$  with Larmor frequency  $\omega_0 = \gamma H_0$  (Fig. 1a). For an equilibrium ensemble of moments precessing about  $\vec{H}_0$  with random phase, the resultant bulk magnetization vector

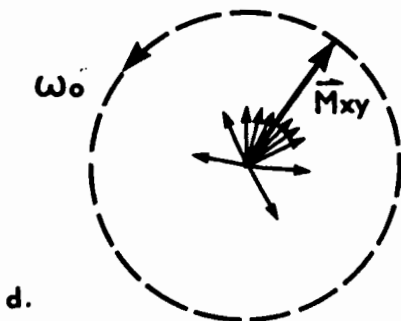
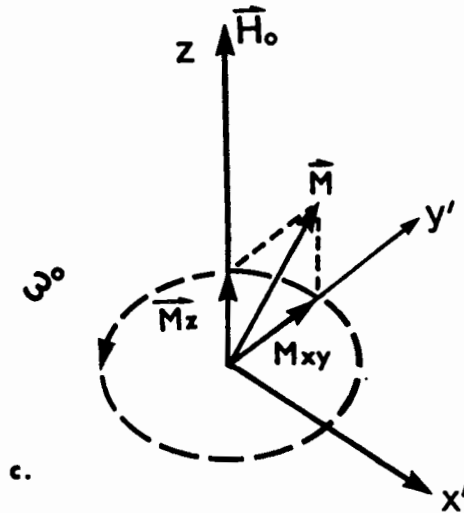
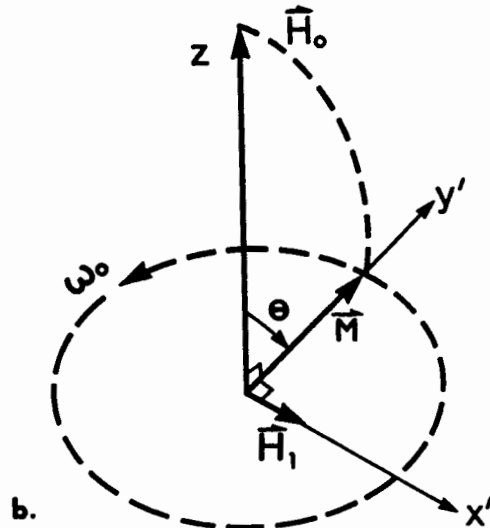
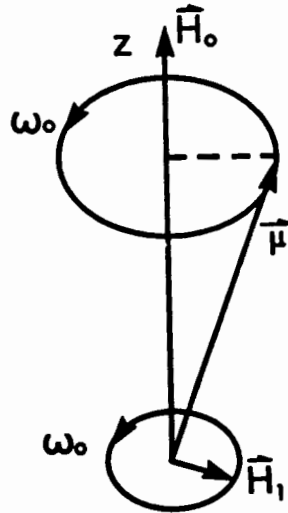
$$\vec{M} = \sum_i \vec{u}_i \text{ is parallel to } \vec{H}_0.$$

Now consider a weak radio-frequency field of frequency  $\omega_0$  applied at right angles to  $\vec{H}_0$  in a pulse of length  $t$ . This sinusoidally oscillating field may be resolved into two components of equal magnitude rotating in opposite directions about  $\vec{H}_0$  in the XY plane, with the component rotating in the opposite direction to  $\vec{u}$  having negligible effect for large  $\vec{H}_0$ . At this point, it is best to consider  $\vec{M}$  in relation to a set of axes X'Y'Z rotating with frequency  $\omega_0$  about  $H_0$ ;  $H_1$  may be considered to always lie along the X' axis. In this frame of reference, the effect of  $H_1$  will be to rotate  $\vec{M}$  about X' by an angle  $\theta = \gamma H_1 t$ . In free induction decay studies,  $H_1$  and  $t$  are chosen so that  $\gamma H_1 t = \frac{\pi}{2}$  ( $90^\circ$  pulse) and  $\vec{M}$  is turned into the X'Y' plane perpendicular to  $H_1$  (Fig. 1b). When the pulse ceases,  $\vec{M}$  will begin to swing back along  $\vec{H}_0$  and  $\vec{M}_z$  will recover to  $\vec{M}_0$  at an exponential rate described by the spin-lattice relaxation time  $T_1$  (Fig. 1c). Because of imperfections in the applied static field  $\vec{H}_0$ , and magnetic fields from other nuclei in the ensemble of spins, the magnitude of  $\vec{H}_0$  perceived by each nucleus may be different, with resulting variation in the individual Larmor frequencies of precession. This will cause the XY components of the magnetic moments composing  $\vec{M}$  to lose coherence and fan out in the XY plane after the pulse (Fig. 1d). Since a receiver coil oriented along the Y axis will respond only to the vector

sum of the XY components, that is,  $\vec{M}_{xy} = \sum_i \vec{u}_i$ , the amplitude of the detected induced signal will decay to zero with inhomogeneous spin-spin relaxation time  $T_2^*$  (23), or with the natural relaxation time  $T_2$  if the static field is sufficiently homogeneous across the sample.  $T_2$  can never be longer than  $T_1$ , but may be considerably shorter.

Fig. 1. Classical description of the free induction experiment.

- a. Individual magnetic moment  $\vec{\mu}_i$  precessing about  $\vec{H}_0$  with Larmor frequency  $\omega_0$ .  $\vec{H}_1$  turned on and moving with the same angular frequency.
- b.  $X'Y'$  axes rotating about the Z axis with angular frequency  $\omega_0$ . Magnetization vector  $\vec{M}$  turned into the  $X'Y'$  plane by a  $90^\circ$  pulse of  $\vec{H}_1$ .
- c.  $\vec{M}$  swinging back along  $\vec{H}_0$  after end of pulse.  $M_z$  recovering to  $M_0$  at a rate described by the spin-lattice relaxation time  $T_1$ .
- d.  $M_{xy}$  decreasing with spin-spin relaxation time  $T_2$  as the  $X'Y'$  components of the  $\vec{\mu}_i$  lose coherence and fan out in the  $X'Y'$  plane.





## II. Quantum-Mechanical Treatment: Spin Relaxation

In order to put forward a meaningful theoretical treatment of the halide-probe exchange phenomenon, it is first necessary to discuss the manner in which the expression for the transverse relaxation time  $T_2$  is derived and the limitations imposed by this derivation. For the case of a system of nuclei undergoing quadrupolar relaxation, the standard treatment of this problem has been that of Abragam (24). This derivation yields  $T_2$  in a form suitable for halide-exchange studies on proteins, but is complex. Huntress (25), in dealing with small molecules, has recast this problem in a more sophisticated formulation. The present derivation will utilize the latter formulation to treat the relaxation of protein-bound quadrupolar nuclei.

Consider a system of nuclear spins described by a stationary Hamiltonian  $\mathcal{H}_0$  (in angular frequency units) to which a random perturbation expressed by the fluctuating Hamiltonian  $\mathcal{H}_1(t)$  is applied. The existence of  $\mathcal{H}_1(t)$  is due to coupling between the nuclear quadrupole moment (aligned along the nuclear spin vector which is Zeeman quantized along the large applied  $H_0$ ) and the electric field gradient tensor, which has a fixed orientation with respect to a molecule-fixed coordinate system. As all or part of the molecule tumbles in

solution, random variations in the angles between the molecular and laboratory frames of reference result in an interaction Hamiltonian which is a random function of time. In the laboratory frame, this Hamiltonian may be expressed (24, 25) as the scalar invariant of two spherically irreducible tensors of the second rank:

$$\mathcal{H}_1(t) = \underset{\approx}{A}(\vec{I}) \cdot \underset{\approx}{F}(\Omega, t) = \sum_{q=-2}^2 (-1)^q \underset{\approx}{A}^{(-q)}(\vec{I}) \underset{\approx}{F}^{(q)}(\Omega, t) \quad (3)$$

Here  $\underset{\approx}{A}(\vec{I})$  is the nuclear spin tensor derived from the electric quadrupole moment operator,  $\underset{\approx}{F}(\Omega, t)$  describes both the magnitude and symmetry of the electric field gradient and its orientation with respect to the nuclear quadrupole moment, and  $\Omega$  stands for the three Euler angles  $\alpha, \beta, \gamma$  defining the orientation of the molecule with respect to the laboratory frame. Since  $\underset{\approx}{A}(\vec{I})$  is both traceless and symmetric for quadrupolar interaction, only terms of the second rank need be considered in (3). The elements  $\underset{\approx}{F}^{(q)}(\Omega, t)$  of  $\underset{\approx}{F}$  will be random functions of time.

At this point, it is necessary to introduce the correlation functions

$$G_{qq'}(\tau) = \overline{F^{(q)}(t)F^{(-q')}^*(t + \tau)} \quad (4)$$

(the bar indicates an ensemble average) and their Fourier transforms

$$J_{qq'}(\omega) = \int_{-\infty}^{\infty} G_{qq'}(\tau) e^{-i\omega\tau} d\tau \quad (5)$$

Equation (4) expresses the ensemble-average correlation between the value of  $F^{(q)}$  at time  $t$  and the value of  $F^{(q')}$  at time  $(t + \tau)$ . For times less than a critical time  $\tau_c$  (the correlation time) the motion of the nuclei relative to each other may be considered negligible, so that  $\kappa_1(t) \approx \kappa_1(t + \tau)$ . For  $\tau > \tau_c$ , the value of  $\kappa_1(t + \tau)$  becomes progressively less correlated to  $\kappa_1(t)$  as  $\tau$  increases, and  $G_{qq'}(\tau)$  goes to zero, as shown in Fig. 2.

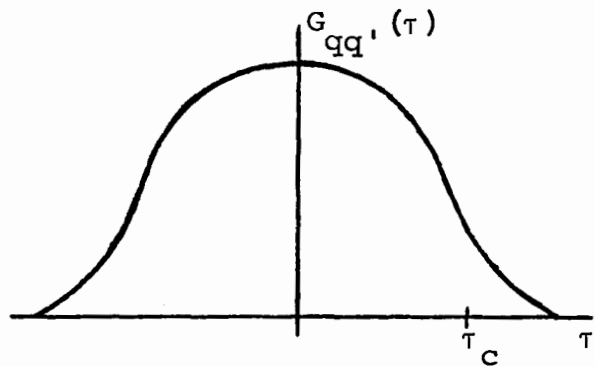


Fig. 2. Behaviour of  $G_{qq'}(\tau)$ .

$\tau_c$  is generally defined (26) as the normalized area under the correlation function:

$$\tau_c = \frac{1}{2G_{qq'}(0)} \int_{-\infty}^{\infty} G_{qq'}(\tau) d\tau \quad (6)$$

$J_{qq'}(\omega)$  may be thought of as the spectral density of the correlation function  $G_{qq'}(\tau)$  and will contain frequencies up to the order of  $1/\tau_c$ . It may be shown (27) that

$$G_{qq'}(0) = \frac{1}{2\pi} \int_{-\infty}^{\infty} J_{qq'}(\omega) d\omega \quad (7)$$

so that the area of the spectral density curve remains fixed as  $\tau_c$  changes. This constraint results in spectral density curves of the type shown in Fig. 3.

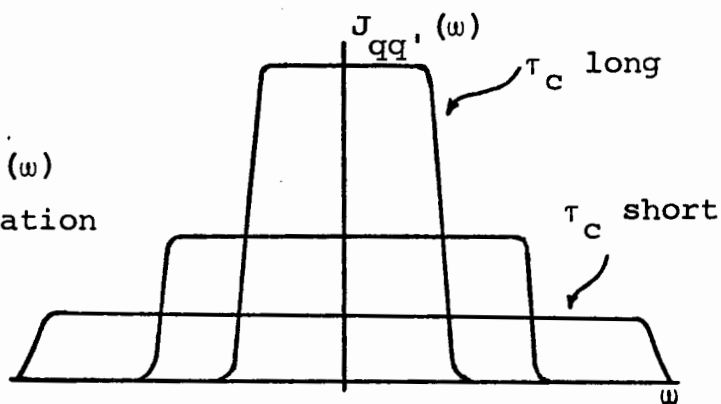


Fig. 3. Behaviour of  $J_{qq'}(\omega)$  for three values of correlation time.

If the observed nuclear transition has frequency  $\omega_o$ ,  $J_{qq'}(\omega_o)$  will be found to have a maximum when  $\tau_c = 1/\omega_o$ . This result is not surprising, since one would expect fluctuations at or

near the Larmor frequency to be most effective in inducing nuclear transitions. Later in this discussion, the importance of the limit  $\tau_c \ll 1/\omega_0$  will become apparent, because it causes  $J_{qq'}(\omega)$  to extend far above the transition frequency. This is the "extreme narrowing limit" and

$$J_{qq'}(\omega) = J_{qq'}(0) \quad (8)$$

It is now possible to use the theory of density matrices to obtain the equation of motion for the nuclear spins which will yield  $T_2$ . The density matrix operator  $\sigma$  (the quantum-mechanical analogue of the classical thermodynamic density of states) is defined following Dirac (28). Consider a dynamical system which is at a certain time in one of a set of discrete states labelled by the parameter  $m$ . If the probability of the system being in the  $m$ th state is  $P_m$ , then the density matrix operator may be defined by

$$\sigma = \sum_m |m\rangle P_m \langle m| \quad (9)$$

Since the effect of  $H_1$  will be to alter the magnitude of the elements of  $\sigma$ , it is necessary to consider both the value of  $\sigma$  at time  $t$ ,  $\sigma(t)$ , and the equilibrium value at  $t=\infty$ ,  $\sigma_0$ , and deal with the deviation from equilibrium  $[\sigma(t) - \sigma_0]$ . In order to remove any

time dependence due to  $\mathcal{K}_0$ ,  $\sigma(t)$  will in general be written in the interaction representation

$$\sigma'(t) = e^{i\mathcal{K}_0 t} \sigma(t) e^{-i\mathcal{K}_0 t} \quad (10)$$

which has the effect of transforming  $\sigma(t)$  into the set of spectroscopic frames of reference rotating with angular velocities  $\omega_{\alpha\beta}$ , where  $\alpha$  and  $\beta$  are eigenstates of  $H_0$ . For the same reason,  $\mathcal{K}_1(t)$  must also be written in this representation and, for a spectrum consisting of a single line at frequency  $\omega_0$ ,

$$\mathcal{K}'_1(t) = e^{i\mathcal{K}_0 t} \mathcal{K}_1(t) e^{-i\mathcal{K}_0 t} = \sum_q (-1)^q F^{(q)}(t) A^{(-q)} e^{-iq\omega_0 t} \quad (11)$$

The derivation of the expressions for  $T_2$  will begin with two familiar results of density matrix theory. Firstly, given some operator  $Q$  acting on the system, the ensemble average of the corresponding observable  $q(t)$  will be given (29) by

$$q(t) = \langle Q \rangle = \text{tr} \{ \sigma(t) Q \} \quad (12)$$

Secondly, the equation of motion for the ensemble-averaged density matrix may be shown (30) to be

$$\frac{d\sigma'}{dt} = - \int_0^\infty \overline{[\mathcal{K}'_1(t), [\mathcal{K}'_1(t+\tau), \sigma'(t) - \sigma_0]]} d\tau \quad (13)$$

Substituting  $\mathcal{K}_1'(t)$  into equation (13) one obtains (25)

$$\frac{d\sigma'(t)}{dt} = -\sum_{q, q'} (-1)^q e^{-i(q+q')\omega_0 t} \cdot \left[ A^{(-q')}, [A^{(-q)}, \sigma'(t) - \sigma_0] \right] J_{qq'}(\omega) \quad (14)$$

If appropriate expressions for  $A^{(q)}(\vec{I})$  and  $J_q(\omega)$  can be found, it will be possible to obtain the time dependence of  $\vec{I}_x$  from (12) and (14) and therefore to obtain a relationship for  $T_2$ .

Since nuclear resonance is observed in the laboratory frame, both  $\underline{A}$  and  $\underline{F}$  must be written in terms of this coordinate system. Suitable  $A^{(q)}(\vec{I})$  may be obtained (31, 25) from the components of the nuclear quadrupole moment operator by means of the Wigner-Eckart theorem and will be given here without further discussion of their derivation:

$$A^0 = \frac{(eQ/\hbar)^2}{2I(2I-1)} \left[ 3\vec{I}_z^2 - I(I+1) \right] \quad (15a)$$

$$A^{(\pm 1)} = \frac{\sqrt{3}(eQ/\hbar)^2}{2I(2I-1)} \left[ \vec{I}_z \vec{I}_\pm + \vec{I}_\pm \vec{I}_z \right] \quad (15b)$$

$$A^{(\pm 2)} = \frac{\sqrt{6}(eQ/\hbar)^2}{2I(2I-1)} \left[ \vec{I}_\pm^2 \right] \quad (15c)$$

Here  $I$  is the total nuclear spin,  $\vec{I}_z$  is the operator corresponding to the Z-component, and  $\vec{I}_+$  and  $\vec{I}_-$  are the raising and lowering operators. Determination of the  $F^{(q)}(\rho, t)$  is a more complex problem. The  $F^{(q)}$  are known explicitly only in

the molecular coordinate system, where they are simply the components of the irreducible field-gradient tensor, denoted by  $\mathfrak{J}^{(q)}$ . Consequently, the random time-dependence of the orientation must be absorbed into the Wigner rotation matrices  $D_{q,m}^{(2)}$  (32) transforming the molecular  $\mathfrak{J}^{(q)}$  into the laboratory coordinate system:

$$F^{(q)}(\mathbf{r}, t) = \sum_m D_{q,m}^{(2)*} \mathfrak{J}^{(m)} = \sum_m (-1)^{q-m} D_{-q,-m}^{(2)} \mathfrak{J}^{(m)} \quad (16)$$

Consideration of the exact nature of the  $\mathfrak{J}^{(q)}$  required will permit considerable simplification of this transformation. In the irreducible representation, the electric field gradient tensor  $\underset{\approx}{V}$  in the molecular frame can be written (33):

$$V^{(0)} = \frac{1}{2} V_{zz} \quad (17a)$$

$$V^{(\pm 1)} = \frac{1}{\sqrt{6}} (V_{zx} \pm iV_{zy}) \quad (17b)$$

$$V^{(\pm 2)} = \frac{1}{\sqrt{6}} (V_{xx} - V_{yy} \pm 2iV_{xy}) \quad (17c)$$

If molecular axes that diagonalize  $\underset{\approx}{V}$  are chosen, that is,

$V_{xz} = V_{yz} = V_{xy} = 0$ ,  $|V_{zz}| \gg |V_{xx}|, |V_{yy}|$ , one can define

$$eq = V_{zz} \quad (18a)$$

$$\eta = \frac{V_{xx} - V_{yy}}{V_{zz}} \quad (18b)$$



(where  $\eta$  will be referred to as the "asymmetry parameter")

and can write the  $\mathfrak{J}^{(q)}$  in terms of these two parameters:

$$\mathfrak{J}^{(0)} = \frac{eq}{2} \quad (19a)$$

$$\mathfrak{J}^{(\pm 1)} = 0 \quad (19b)$$

$$\mathfrak{J}^{(\pm 2)} = \frac{eq}{2\sqrt{6}} \eta \quad (19c)$$

If the field gradient in the Hg-Br bond is assumed to possess cylindrical symmetry, that is,  $\eta = 0$ , the contribution from (19c) may be neglected and (16) becomes

$$F^{(q)}(\mathbf{n}, t) = \frac{eq}{2} (-1)^q D_{-q, 0}^{(2)} \quad (20)$$

The required Wigner matrix elements are (25):

$$D_{0, 0}^{(2)} = \frac{1}{2} (3\cos^2\beta - 1) = \sqrt{\frac{4\pi}{5}} Y_0^2(\beta, \alpha) \quad (21a)$$

$$D_{\pm 1, 0}^{(2)} = \mp \sqrt{\frac{3}{2}} \sin\beta \cos\beta e^{\mp i\alpha} = -\sqrt{\frac{4\pi}{5}} Y_{\mp 1}^2(\beta, \alpha) \quad (21b)$$

$$D_{\pm 2, 0}^{(2)} = \sqrt{\frac{3}{8}} \sin^2\beta e^{\pm 2i\alpha} = \sqrt{\frac{4\pi}{5}} Y_{\pm 2}^2(\beta, \alpha) \quad (21c)$$

where the  $Y_q^2(\beta, \alpha)$  are the spherical harmonics of order two.

The correlation function now becomes

$$G_{q, q'}(\tau) = \frac{4\pi}{5} \left(\frac{eq}{2}\right)^2 \overline{Y_q^2(t) Y_{-q'}^{2*}(t+\tau)} \quad (22)$$

If the orientation of a molecule is  $\Omega_0$  at time  $t$  and  $\Omega$  at time  $(t + \tau)$ , then the ensemble average in equation (22) becomes (34,35)

$$\overline{Y_q^2(t) Y_{-q}^{2*}(t+\tau)} = \iint Y_q^2(\Omega) Y_{-q}^2(\Omega) P(\Omega_0) \cdot P(\Omega_0 | \Omega, t) d\Omega d\Omega_0 \quad (23)$$

where  $P(\Omega_0) = 1/4\pi$  (assuming an isotropic liquid) is the probability that a molecule has orientation  $\Omega_0$  at time  $t$ , and  $P(\Omega_0 | \Omega, t)$  is the probability that if the molecule has initial orientation  $\Omega_0$ , then at a later time  $(t + \tau)$  its orientation will be  $\Omega$ .

Up to this point, the derivation has been quite general; no assumptions have been made concerning the exact nature of the molecular motion involved in the halide probe experiment. Before proceeding to write down  $P(\Omega_0 | \Omega, t)$  and the correlation functions, it is necessary to pause in order to examine the approximations inherent in the description of the motion of the probe. Proteins in solution may be expected to undergo three classes of molecular movement:

1. Diffusional rotation and translation of the molecule as a whole.

2. Motion of the polypeptide chains relative to one another. Free portions of the polypeptide chain may be expected to execute random diffusional movement with respect to the molecular coordinate system.
3. Rotation of individual bonds and side-groups on the chain. Whether this movement is diffusional or involves transitions between potential minima will depend upon the steric hindrances affecting the group in question.

Diffusional rotation is described by the rigid-sphere model assumed by Abragam in his original treatment of quadrupolar relaxation; (2) and (3) have so far resisted adequate theoretical description. Wallach (26) has put forth a general formulation which makes provision for intramolecular motion at the probe site but was unable to derive the exact form of the correlation functions involved. If internal rotations are absent or are much slower than the overall macromolecular rotation rate, then the system may be treated as a rigid sphere undergoing diffusional rotation. If the rate of internal rotation of the probe is sufficiently greater than the rate of macromolecular rotation, then the observed correlation time will be dependent on the intramolecular rotations.

The exact theoretical description of this case is quite complex, particularly as the observed correlation time may be an average over the motions of all of the bonds holding the probe to the protein. If the rates of macromolecular tumbling and intramolecular rotation are comparable, the expressions for the two motions are inseparable and no quantum-mechanical solution for  $\tau_c$  can be found at present. For lack of a more satisfactory theoretical model, the present treatment will be restricted to the assumption of a rigid macromolecule undergoing diffusional rotation.

Based on this assumption, an expression has been derived (36) for  $P(\rho_0 | \rho, t)$  in terms of the spherical harmonics:

$$P(\rho_0 | \rho, t) = \sum_{l, m} Y_m^{l*}(\rho_0) Y_m^l(\rho) e^{-t/\tau_c} \quad (24)$$

Substituting (24) into (23), rearranging terms, and applying the orthogonality properties of the spherical harmonics (37) yields

$$\begin{aligned} G_{q, q'}(\tau) &= \frac{(eq)^2}{20} \sum_{l, m} \int Y_q^l(\rho_0) Y_m^{l*}(\rho_0) d\rho_0 \cdot \\ &\cdot \int Y_{-q'}^{2*}(\rho) Y_m^l(\rho) d\rho e^{-t/\tau_c} \\ &= \delta(q', -q) \frac{(eq)^2}{20} e^{-t/\tau_c} \end{aligned} \quad (25)$$

The delta function follows from the orthogonality of the spherical harmonics and eliminates any cross-correlation terms. From (6), the spectral density becomes

$$J_q(\omega) = \frac{(eq)^2}{10} \frac{\tau_c}{1 + (q\omega_0\tau_c)^2} \quad (26)$$

Unless the extreme narrowing condition  $J(\omega) = J(0)$  holds, it is not possible to evaluate the commutators in (15) to obtain an exponential decay; hence it is necessary to assume  $\omega_0\tau_c \ll 1$ . In this limit, it can be shown that  $T_1 = T_2$  (38). Hence one may evaluate equation (15) in terms of  $I_z$  rather than  $I_+$  or  $I_x$ , thereby achieving some simplification of the commutators. Multiplying both sides of equation (15) by  $I_z$ , applying the condition  $q' = -q$ , and taking the trace gives rise to the equation of motion of  $I_z$  in the rotating frame:

$$\frac{d\langle I_z \rangle}{dt} = -J(0) \sum_q (-1)^q \text{Tr} \left\{ \left( \left[ A^{(q)}, [A^{(-q)}, I_z] \right] \right) (\sigma'(t) - \sigma_0) \right\} \quad (27)$$

since in taking the trace the order of operations is permutable (39). The commutators are (34):

$$\left[ A^{(0)}, [A^{(0)}, I_z] \right] = 0 \quad (29a)$$

$$[A^{(\pm 1)}, [A^{(\mp 1)}, I_z]] = - \frac{3(eQ)^2}{8[I(2I-1)]^2 \hbar^2} \cdot \left( -16I_z^3 - I_z[8I(I+1) - 2] \right) \quad (28b)$$

$$[A^{(\pm 2)}, [A^{(\mp 2)}, I_z]] = \frac{3(eQ)^2}{8[I(2I-1)]^2 \hbar^2} \cdot \left( -16I_z^3 + I_z[16I(I+1) - 8] \right) \quad (28c)$$

Substituting these operators into equation (27) yields

$$\frac{d\langle I_z' \rangle}{dt} = - \frac{3(eQ)^3(2I+3)}{2\hbar^2 I^2(2I-1)} J(0) \left( \langle I_z' \rangle - \langle I_z' \rangle_0 \right) \quad (29)$$

Using the expression for  $J(0)$  derived from equation (26), equation (29) yields the final expression for  $T_2$  in the case of quadrupolar relaxation within the extreme narrowing limit:

$$\boxed{R_2 = \frac{1}{T_2} = R_1 = \frac{1}{T_1} = \frac{3}{20} \left( \frac{2I+3}{I^2(2I-1)} \right) \left( \frac{e^2 qQ}{\hbar} \right)^2 \tau_c} \quad (30)$$

Equation (30) predicts an  $R_2$  that is a factor of two greater than that derived by Abragam (38). Since Abragam has neglected to include the commutators  $[A^{(1)}, [A^{(-1)}, I_z]]$  and  $[A^{(2)}, [A^{(-2)}, I_z]]$  as part of the sum in his equation (135), this discrepancy appears to be the result of an error on his part. Huntress (25, 34) has obtained the same expression

for  $R_2$  as Abragam; however, calculation of  $R_2$  from equation (4.26) of reference (25) yields a relation that agrees with the present result, suggesting that Huntress is also in error. Note that there is a typographical error in the second term of equation (4.26). The correct commutators should be taken from equation (3B.2) of reference (34).

### THEORY OF THE EXCHANGE EFFECT

At the present time, the observation of individual groups within a protein is a problem of considerable technical difficulty, largely because of the low relative concentration of individual nuclei within high molecular weight biopolymers. Some means of increasing the sensitivity of present NMR methods is therefore eminently desirable. This section presents a theoretical treatment of the manner in which the halide-probe technique accomplishes this end.

If the effect of the rate of exchange of halide nuclei between the free and bound sites is neglected, the observed decay rate  $R_2$  may be written (5) in terms of the decay rates  $R_{2F}$  and  $R_{2B}$  of halide nuclei in the free and bound sites.

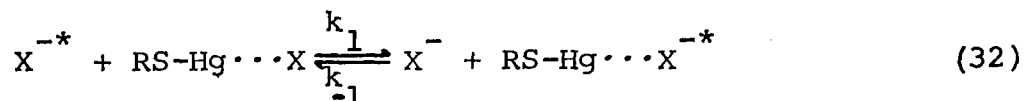
$$R_2 = R_{2F} P_F + R_{2B} P_B \quad (31)$$

where  $P_F$  and  $P_B$  are the probabilities of a halide nucleus being found in the free or bound site. The sensitivity of the halide probe method depends directly on the difference between the decay rates of halide nuclei in the two sites. For chlorine and bromine nuclei in dilute aqueous solution, the solvation of the ion is essentially symmetric and the electric field gradient at the nucleus is small. This situation results in a



decay rate of approximately  $1400 \text{ sec}^{-1}$  for dilute (0.5-4.0 molar) aqueous solutions of NaBr. When the bromide ion participates in covalent bonding, the field gradient is large and a corresponding increase occurs in the decay rate. For the  $[\text{HgBr}_4]^{2-}$  ion, for example,  $R_{2B}$  is approximately  $10^6 \text{ sec}^{-1}$ . With  $R_{2B}$  values of this magnitude or greater, a very small concentration ( $\sim 10^{-5}$  molar) of a protein binding site will produce an observable effect on the overall decay rate. Hence the exchange process functions as a chemical amplifier, permitting the halide ion to be used as a probe for interesting sites in low concentrations. A theoretical treatment of this phenomenon which accounts for the effects of the rate of halide exchange will now be presented.

The effect of mercuric halide-free halide exchange on halide decay lifetimes has been dealt with extensively by O'Reilly (40) using three-species Bloch equations. The present theory is a modification of this derivation for the case of halide exchange occurring between free halide in solution and halide bound to a mercury-sulphydryl complex  $\text{RS-Hg}\cdots$  at a specific site in a macromolecule. This exchange may be represented by the equilibrium



Let the free halide concentration be represented by [X] and the bound halide concentration by [B]. A relationship will now be derived for the observed  $R_2$  in terms of the rate constants and the concentrations of the various species in the solution.

As before, it will be necessary to consider axes  $X', Y'$  rotating about  $H_0$  with angular frequency  $\omega_0 = \gamma H_0$  where the  $X'$  axis is defined to be the direction of  $H_1$ . Representing the  $X'$  components of magnetization for free bromide in solution and bound bromide by  $u_F$  and  $u_B$  respectively, one can write the two-species Bloch equations in the absence of exchange:

$$\frac{du_F}{dt} = \frac{-u_F}{T_{2F}} + (\omega_F - \omega_0) v_F \quad (33)$$

$$\frac{du_B}{dt} = \frac{-u_B}{T_{2B}} + (\omega_B - \omega_0) v_B \quad (34)$$

where  $v_F$  and  $v_B$  are the  $Y'$  components of nuclear magnetization and  $\omega_F, \omega_B$  are the Larmor frequencies of the free and bound halides. If exchange occurs between the two sites, there will be a transfer of spin magnetization between the two environments. Assuming that the rate of transfer of transverse magnetization from a given site is proportional to the trans-

verse magnetization at that site, one obtains

$$\left(\frac{du_F}{dt}\right)_{\text{ex}} = \frac{-u_F}{\tau_{FB}} + \frac{u_B}{\tau_{BF}} \quad (35)$$

$$\left(\frac{du_B}{dt}\right)_{\text{ex}} = \frac{-u_B}{\tau_{BF}} + \frac{u_F}{\tau_{FB}} \quad (36)$$

where  $\tau_{FB}$  and  $\tau_{BF}$  are lifetimes for exchange out of the free and bound sites, respectively. Equations (33) and (34) now take the following form:

$$\frac{du_F}{dt} = \frac{-u_F}{\tau_{2F}} + (\omega_F - \omega_O)v_F + \frac{u_B}{\tau_{BF}} \quad (37)$$

$$\frac{du_B}{dt} = \frac{-u_B}{\tau_{2B}} + (\omega_B - \omega_O)v_B + \frac{u_F}{\tau_{FB}} \quad (38)$$

where

$$\frac{1}{\tau_{2F}} = \frac{1}{\tau_{2F}} + \frac{1}{\tau_{FB}} \quad (39)$$

$$\frac{1}{\tau_{2B}} = \frac{1}{\tau_{2B}} + \frac{1}{\tau_{BF}} \quad (40)$$

If  $H_1$  is assumed to be rotating at the Larmor frequency  $\omega_F$  of the free halide, the simplifying assumption that the second term on the right side of equation (38) is negligible may be made. This assumption is justified by the fact that

chemical shifts in halide compounds do not exceed one part in  $10^2$  (41) and  $T_{2B}$  (and hence  $\tau_{2B}$ ) is of the order of  $10^{-7}$  second. Hence  $u_B/T_{2B} \gg (\omega_B - \omega_o)v_B$ . Also, since  $T_{2B} \ll T_{2F}$ , system B will reach a steady state in a time which is short compared to the time for  $du_F/dt$  to reach zero; consequently  $du_B/dt \cong 0$ . These conditions result in considerable simplification of equations (37) and (38):

$$\frac{du_F}{dt} = \frac{-u_F}{2F} + \frac{u_B}{\tau_{BF}} \quad (41)$$

$$0 = \frac{-u_B}{\tau_{2B}} + \frac{u_F}{\tau_{FB}} \quad (42)$$

Combining equations (41) and (42) yields the equation for the exponential decay rate  $R_2$  of  $u_F$ :

$$\frac{du_F}{dt} = -u_F R_2 \quad (43)$$

$$\frac{1}{T_2} = \frac{1}{T_{2F}} + \frac{1}{\tau_{FB}} - \frac{\tau_{2B}}{\tau_{FB} \tau_{BF}} \quad (44)$$

Referring back to the original equilibrium equation (32), one can see that the exchange lifetimes  $\tau_{FB}$  and  $\tau_{BF}$  may be expressed in terms of the pseudo-first-order rate constants  $k_1$  and

$k_{-1}$ . Since the rates of the forward and reverse reactions must be equal if a state of equilibrium is to exist,  $k_1 = k_{-1}$ , and therefore (15, 40)

$$\frac{1}{\tau_{FB}} = k_1 [B] \quad (45)$$

$$\frac{1}{\tau_{BF}} = k_1 [X] \quad (46)$$

Substituting (40) for  $\tau_{2B}$  in (44) and using (45) and (46), one obtains the expression for the observed decay rate  $R_2$ :

$$\boxed{R_2 = R_{2F} + \alpha[B]} \quad (47)$$

where the constant  $\alpha$  is given by

$$\boxed{\alpha^{-1} = \frac{1}{k_1} + T_{2B}[X]} \quad (48)$$

In the case where there are  $n$  equivalent binding sites,  $k_1 = nk_{-1}$  and  $T_{2B}$  is replaced by  $(T_{2B}/n)$  in equation (48). When species B relaxes by a quadrupolar mechanism,  $T_{2B}$  has the form (30) and hence, for a spin 3/2 nucleus

$$\alpha^{-1} = \frac{1}{k_1} + 10 \left( \frac{\hbar}{2e^2qQ} \right)^2 \frac{[X]}{\tau_{app}} \quad (49)$$

where  $\tau_{app}$ , the apparent correlation time, will be defined.

The expression for  $T_{2B}$  derived by Abragam (24) has been used here to facilitate comparison with other data.

One further consideration is required before a general equation for  $\alpha$  in the presence of chemical exchange can be obtained. Marshall (42) has demonstrated that when the exchange lifetime  $\tau_{BF}$  for bound halogen becomes comparable to the actual rotational correlation time  $\tau_c$  of the protein, the apparent correlation time is dependent on both terms:

$$\frac{1}{\tau_{app}} = \frac{1}{\tau_c} + \frac{1}{\tau_{BF}} \quad (50)$$

When  $\tau_c$  and  $\tau_{BF}$  are comparable, two relaxation mechanisms are operational: the expected contribution from relaxation induced by reorientation of the electric field gradient at the halide nucleus caused by molecular tumbling (expressed by  $\tau_c$  in equation (50)) and an additional contribution due to the change in the direction of the electric field gradient tensor each time there is a change in site (expressed by  $\tau_{BF}$ ). Equation (50) is derived under the condition  $\tau_{BF} \ll T_{2B}$ ; however, in the region where this requirement is not met, the term in  $\tau_{BF}$  will be quite negligible and no contradiction between the conditions under which equations (49) and (50) are derived will arise. A more detailed treatment of the derivation of

the above result is beyond the scope of the present discussion.

Equation (49) may now be given in its most general form:

$$\alpha^{-1} = \frac{1}{k_1} + 10 \left( \frac{\hbar}{e^2 q Q} \right)^2 \left( \frac{[X]}{\tau_c} + k_1 [X]^2 \right) \quad (51)$$

or in terms of  $\tau_{BF}$ :

$$(\alpha')^{-1} = \frac{\alpha^{-1}}{[X]} = \tau_{BF} + 10 \left( \frac{\hbar}{e^2 q Q} \right)^2 \left( \frac{1}{\tau_c} + \frac{1}{\tau_{BF}} \right) \quad (52)$$

Three limiting cases for halide exchange follow naturally from the general equations (51) and (52):

1.  $T_{2F} \gg \tau_{BF} > T_{2B}$  (SLOW EXCHANGE LIMIT)

In this case, the exchange lifetime  $\tau_{BF}$  is long enough compared to  $T_{2B}$  to permit all the transferred halogen nuclei to relax during the interval when they are bound to the protein; in other words, the protein site behaves as an infinite magnetization sink to spins transferred from the free site.  $\alpha$  is determined solely by the rate of exchange out of the free site.

2.  $\tau_c \ll \tau_{BF} \ll T_{2B}$  (FAST EXCHANGE LIMIT)

If this condition holds, relaxation in the protein site occurs primarily through changes in the direc-

tion of the electric field gradient as the protein or a portion thereof tumbles in solution; the molecule tumbles quickly enough so that rotation occurs during the interval that the halide is bound. In this limit,  $\alpha$  is dominated by  $T_{2B}$  and equation (47) reduces to the form assumed by Stengle and Baldeschwieler (4-6):

$$R_2 = R_{2F} + R_{2B} \frac{[\text{Protein-Hg}]}{[X]} \quad (53)$$

3.  $\tau_{BF} \ll \tau_c$  (EXTREMELY FAST EXCHANGE LIMIT)

Here changes in site are the dominant means of relaxation; the exchange lifetime is so short that appreciable rotation of the protein cannot occur in this interval. Relaxation occurs because the direction of the electric field gradient tensor is altered each time there is a change in environment.  $\alpha$  is again dependent only on  $k_1$ .

It is worthwhile at this point to pause and consider the exact significance of the results of this derivation. Equation (47) may be rewritten as

$$R_2 = R_{2F} + \frac{\alpha' [B]}{[X]} \quad (54)$$



which is equivalent to

$$R_2 = R_{2F} P_F + \alpha' P_B \quad (55)$$

where  $P_F \approx 1$  (provided that the concentration of protein binding sites is small) and  $P_B = [B]/[X]$  are simply the relative probabilities of finding a halide nucleus in solution or attached to the protein binding site. Consider a protein dissolved in a solution of a halide NaX. The decay rate of this solution will be approximately  $R_{2F}$  if little non-specific binding of halide to the protein occurs. As  $HgX_2$  is added, the decay rate will increase linearly with slope  $\alpha$  until all of the binding sites have been filled. A sharp break in the curve will then occur and  $R_2$  will continue to increase linearly with a slope characteristic of  $\alpha$  for  $[HgX_4]^{2-}$  ions. From equation (47) it is apparent that repeating the titration at a number of different concentrations of halide and plotting  $\alpha^{-1}$  as a function of the halide concentration will yield a straight line with intercept  $1/k_1$  and slope  $T_{2B}$ , allowing calculation of both quantities simultaneously. A notable point arising from equation (51) and (52) is that the parameter  $\alpha$  is isotope-dependent via the isotopic dependence of  $eQ$ . Thus an independent check on the separation of the contributions from  $k_1$  and

$\tau_c$  to  $\alpha$  can be had from measurement of the decay rates of two halide isotopes, for example,  $^{35}\text{Cl}$  and  $^{37}\text{Cl}$ , or  $^{79}\text{Br}$  and  $^{81}\text{Br}$ . The existence of only one naturally-occurring iodine isotope,  $^{127}\text{I}$ , precludes this check for an iodide probe.

A program to generate  $\alpha$  as a function of  $k_1$  and  $\tau_c$  was set up on an IBM 360 computer (Fig. 4), resulting in the families of curves shown in Figures 5 through 10. The values (34) of 320 MHz and 40 MHz for the quadrupolar coupling constants of  $^{81}\text{Br}$  and  $^{35}\text{Cl}$  were used in this calculation.

It is important to be aware that the values of  $e^2 Qq/\hbar$  used here are at best an educated guess at the quadrupolar coupling constants for halides complexed through mercury to a sulphhydryl site. The nuclear quadrupole moment  $eQ/\hbar$  is presumably independent of the nuclear environment, but the field gradient  $q$  at the nucleus will be strongly dependent on the electron configuration about that nucleus. To date, it has been assumed that the majority of the field gradient at the halide nucleus has been due to the polarity of the Hg-Br bond (17), and that this gradient will be relatively immune to outside influences. For this reason, coupling constants for  $\text{HgBr}_2$  or  $\text{HgCl}_2$  have been applied to calculations involving protein-bound halides. At present it is not possible to either refute or verify

the validity of this approximation. However, it appears likely that the character of the mercury-bromine bond will change when mercury is complexed to the sulphur atom rather than to a second atom of bromine. As a result of this change in the orbital structure of the bond, the coupling constant for the sulphydryl complex will in all likelihood be different from the value of 320 MHz calculated for  $\text{Hg}^{81}\text{Br}_2$  (34).

With these considerations in mind, Figures 5 through 10 may now be discussed. Figure 5 shows  $\alpha$  plotted against  $k_1$  for different correlation times, a manner of presentation which makes the three limiting cases dramatically apparent. For slow exchange ( $k_1 \sim 10^5, 10^6$ ) and long correlation times ( $\tau_c \sim 10^{-9}, 10^{-10}$ ),  $\alpha$  is dependent only on  $k_1$  (linear portion of Figure 5) and measurements of  $\alpha$  under these conditions can only yield values for the exchange rate. The extremely fast exchange limit ( $\tau_c$  long,  $k_1$  large) presents a similar case where only  $k_1$  can be determined. In the fast exchange limit,  $\alpha$  is dependent exclusively on  $\tau_c$  (flat regions of Fig. 5) and only this quantity can be determined. A different picture of the fast exchange limit can be obtained from Fig. 6, a plot of  $\alpha$  versus  $\tau_c$  for different exchange rates. Here the dashed line represents the dependence expected if the exchange rate

Fig. 4. Program used to calculate the values of  $\alpha$  shown in Figures 5-10. A sample of the data output is included.

```

0001 C
0002 RAND COLLINS--PROGRAM TO CALCULATE ALPHA AS A FUNCTION OF K1 AND TAU
0003 IMPLICIT REAL*8 (A-H,O-Z)
0004 DIMENSION X(6),A(12),VWUN(30)
0005 READ (5,1) (X(I), I=1,6)
0006 1 FORMAT (F2.1)
0007 QUAD = .320D09
0008 PI = 3.1416D0
0009 EM = 5.00/(2.0*PI**2*(QUAD**2))
0010 FREQ = 0.15D08
0011 OMEGA = 2.0*PI*FREQ
0012 DO 55 I=1,6
0013 WRITE (6,2)
0014 2 FORMAT (1H1,1TABLE OF VALUES OF ALPHA AS A FUNCTION OF K1 FOR BROM
0015 CINE 81 *****1//)
0016 WRITE (6,3) QUAD
0017 3 FORMAT (1H0,1THE QUADROPOLAR COUPLING CONSTANT IS ,D9.2,'HZ.1')
0018 WRITE (6,4) EM
0019 4 FORMAT (1H,1THE VALUE OF M IS ,D9.2//)
0020 WRITE (6,5) X(1)
0021 5 FORMAT (1H,1THE NABR MOLARITY IS ,F3.1)
0022 WRITE (6,6)
0023 6 FORMAT (1 TAURDT IS EXPRESSED AS A POWER OF TEN//)
0024 WRITE (6,7)
0025 7 FORMAT (1H0,1 TAURDT= -7 -121) -8 -9
0026 C
0027 -10
0028 WRITE (6,8)
0029 8 FORMAT (1 K11)
0030 DO 30 N=5,21,4
0031 VWUN(1) = 0.1D06
0032 VWUN(2) = 0.2D06
0033 VWUN(3) = 0.4D06
0034 VWUN(4) = 0.7D06
0035 VWUN(N) = VWUN(N-4)*10.0
0036 VWUN(N+1) = VWUN(N-3)*10.0
0037 VWUN(N+2) = VWUN(N-2)*10.0
0038 VWUN(N+3) = VWUN(N-1)*10.0
0039 30 CONTINUE
0040 DO 40 IK=1,24
0041 DO 35 IT=7,12
0042
0043
0044
0045
0046
0047
0048
0049
0050
0051
0052
0053
0054
0055
0056
0057
0058
0059
0060
0061
0062
0063
0064
0065
0066
0067
0068
0069
0070
0071
0072
0073
0074
0075
0076
0077
0078
0079
0080
0081
0082
0083
0084
0085
0086
0087
0088
0089
0090
0091
0092
0093
0094
0095
0096
0097
0098
0099
0100
0101
0102
0103
0104
0105
0106
0107
0108
0109
0110
0111
0112
0113
0114
0115
0116
0117
0118
0119
0120
0121
0122
0123
0124
0125
0126
0127
0128
0129
0130
0131
0132
0133
0134
0135
0136

```

```

0037 TAU = 1.D1**(-IT)
0038 T2B = (EM/TAU)
0039 A(IT) = 1.DO/((1.DO/ VWUN(IK))+(EM*VWUN(IK)*(X(I)**2))+(X(I)*T2B))
0040 35 CONTINUE
0041 WRITE (6,9) VWUN(IK),A(7),A(8),A(9),A(10),A(11),A(12)
0042 9 FORMAT (1H ,D9.2,6(3X,D11.4))
0043 40 CONTINUE
0044 WRITE (6,10)
0045 10 FORMAT (1H1,1TABLE OF VALUES OF ALPHA AS A FUNCTION OF TAU FOR BRO
      CMINE 81 *****
0046 WRITE (6,11) QUAD
0047 11 FORMAT (1H0,1THE QUADRUPLAR COUPLING CONSTANT IS ',D9.2,'HZ.1)
0048 WRITE (6,12) EM
0049 12 FORMAT (1H ,1THE VALUE OF M IS ',D9.2,/)
0050 WRITE (6,13) X(I)
0051 13 FORMAT (1H ,1THE NABR MOLARITY IS ',F3,1)
0052 WRITE (6,14)
0053 14 FORMAT (' K1 IS EXPRESSED AS A POWER OF TEN')
0054 WRITE (6,15)
0055 15 FORMAT (1H0,1 K1 = 5 6 7
      C 8 9 10)
0056 WRITE (6,16)
0057 16 FORMAT (' TAU')
0058 DO 45 M=1,24
0059 ZED= 0.1D18
0060 VWUN(M) = VWUN(M)/ZED
0061 45 CONTINUE
0062 DO 55 IT=1,24
0063 DO 50 IK=5,10
0064 VARK = 1.D1**IK
0065 T2B = (EM/VWUN(IT))
0066 A(IK) = 1.DO/((1.DO/VARK)+(EM*VARK*(X(I)**2))+(X(I)*T2B))
0067 50 CONTINUE
0068 WRITE (6,17) VWUN(IT),A(5),A(6),A(7),A(8),A(9),A(10)
0069 17 FORMAT (1H ,D9.2,6(3X,D11.4))
0070 55 CONTINUE
0071 STOP
0072 END

```

TABLE OF VALUES OF ALPHA AS A FUNCTION OF TAU FOR BROMINE 81 \*\*\*\*\*

THE QUADRUPOLE COUPLING CONSTANT IS 0.32D 09HZ.  
 THE VALUE OF M IS 0.25D-17

THE NMR MOLARITY IS 2.0  
 KI IS EXPRESSED AS A POWER OF TEN

TAU	KI = 5	6	7	8	9	10
0.10D-11	0.6690D 05	0.1681D 06	0.1981D 06	0.2017D 06	0.2017D 06	0.1982D 06
0.20D-11	0.8017D 05	0.2879D 06	0.3885D 06	0.4025D 06	0.4025D 06	0.3887D 06
0.40D-11	0.8899D 05	0.4471D 06	0.7480D 06	0.8014D 06	0.8015D 06	0.7486D 06
0.70D-11	0.9340D 05	0.5859D 06	0.1239D 07	0.1393D 07	0.1393D 07	0.1241D 07
0.10D-10	0.9529D 05	0.6690D 06	0.1681D 07	0.1977D 07	0.1978D 07	0.1684D 07
0.20D-10	0.9759D 05	0.8017D 06	0.2878D 07	0.3871D 07	0.3872D 07	0.2887D 07
0.40D-10	0.9878D 05	0.8899D 06	0.4469D 07	0.7425D 07	0.7431D 07	0.4490D 07
0.70D-10	0.9930D 05	0.9340D 06	0.5856D 07	0.1225D 08	0.1226D 08	0.5892D 07
0.10D-09	0.9951D 05	0.9529D 06	0.6686D 07	0.1654D 08	0.1657D 08	0.6733D 07
0.20D-09	0.9975D 05	0.9759D 06	0.8011D 07	0.2799D 08	0.2807D 08	0.8079D 07
0.40D-09	0.9988D 05	0.9878D 06	0.8891D 07	0.4281D 08	0.4299D 08	0.8976D 07
0.70D-09	0.9993D 05	0.9930D 06	0.9331D 07	0.5538D 08	0.5567D 08	0.9424D 07
0.10D-08	0.9995D 05	0.9951D 06	0.9520D 07	0.6275D 08	0.6312D 08	0.9616D 07
0.20D-08	0.9998D 05	0.9975D 06	0.9749D 07	0.7428D 08	0.7480D 08	0.9850D 07
0.40D-08	0.9999D 05	0.9988D 06	0.9868D 07	0.8179D 08	0.8243D 08	0.9972D 07
0.70D-08	0.9999D 05	0.9993D 06	0.9920D 07	0.8550D 08	0.8620D 08	0.1002D 08
0.10D-07	0.1000D 06	0.9995D 06	0.9941D 07	0.8708D 08	0.8780D 08	0.1005D 08
0.20D-07	0.1000D 06	0.9997D 06	0.9965D 07	0.8899D 08	0.8975D 08	0.1007D 08
0.40D-07	0.1000D 06	0.9999D 06	0.9978D 07	0.8998D 08	0.9076D 08	0.1008D 08
0.70D-07	0.1000D 06	0.9999D 06	0.9983D 07	0.9041D 08	0.9120D 08	0.1009D 08
0.10D-06	0.1000D 06	0.9999D 06	0.9985D 07	0.9059D 08	0.9137D 08	0.1009D 08
0.20D-06	0.1000D 06	0.1000D 07	0.9988D 07	0.9079D 08	0.9158D 08	0.1009D 08
0.40D-06	0.1000D 06	0.1000D 07	0.9989D 07	0.9089D 08	0.9168D 08	0.1010D 08
0.70D-06	0.1000D 06	0.1000D 07	0.9989D 07	0.9094D 08	0.9173D 08	0.1010D 08

Fig. 5. Calculated dependence of  $\alpha$  on the rate of halide exchange for 2.0 molar bromide. Literature values of  $k_1$  and  $\tau_c$  (see text) for the mercuric tetrabromide ion place these quantities within the cross-hatched area. Note that since this species offers four sites for chemical exchange, the actual value of  $\alpha$  for the tetrabromide ion will be four times that predicted from this graph.



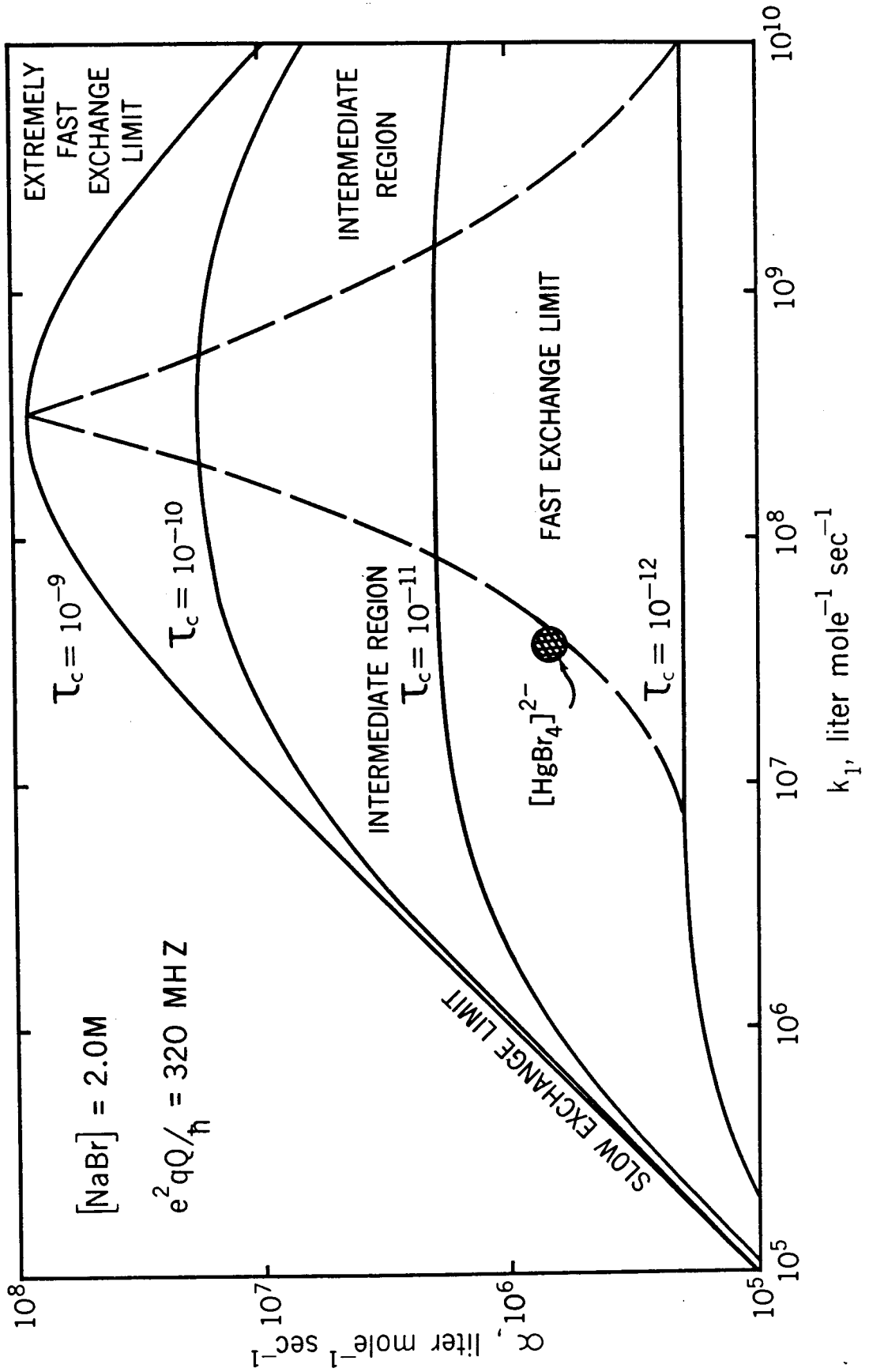


Fig. 6. Calculated dependence of  $\alpha$  on the correlation time for 2.0 molar bromide.

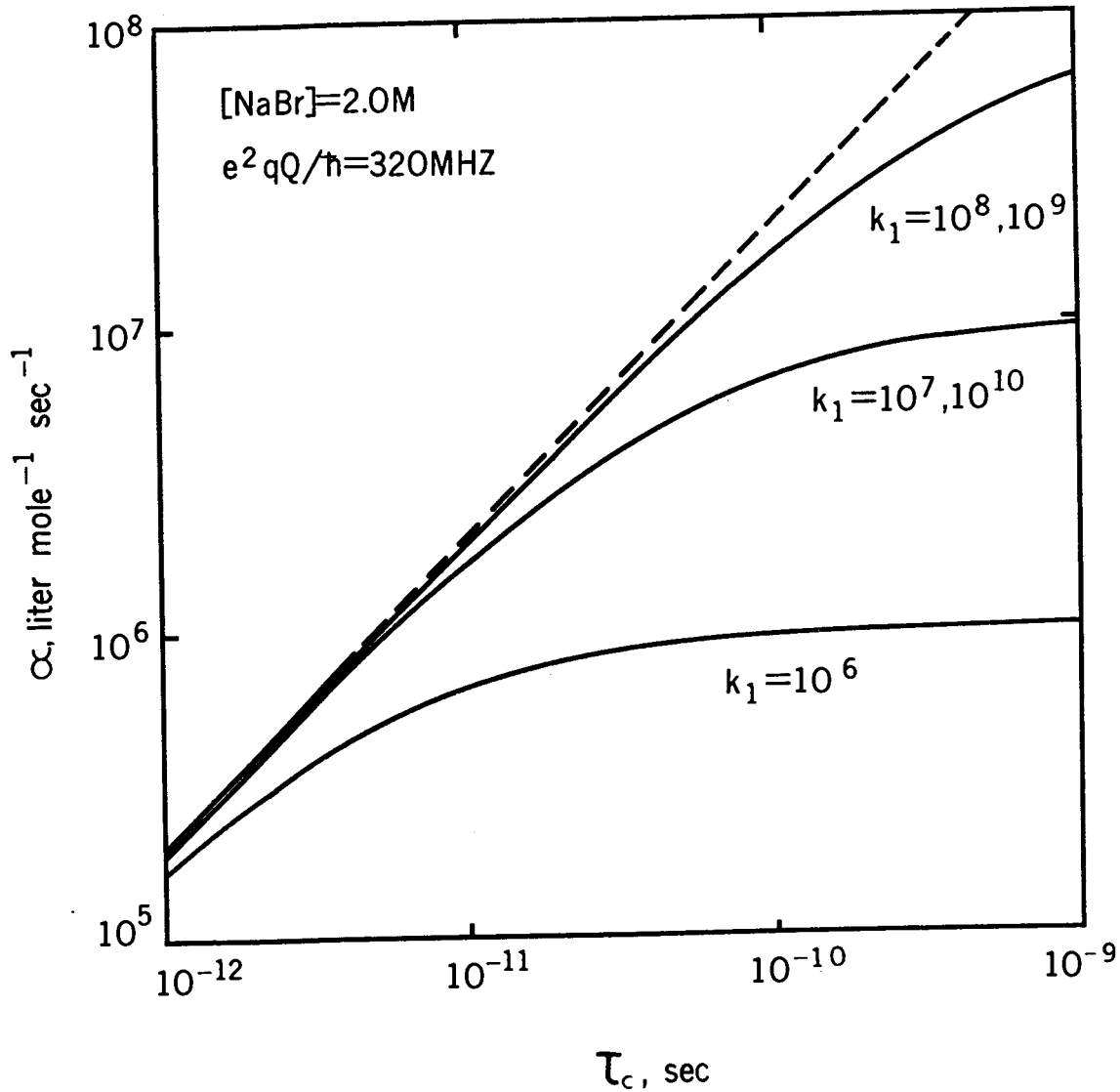


Fig. 7. Calculated dependence of  $\alpha$  on the rate of halide exchange for 0.5 molar bromide.

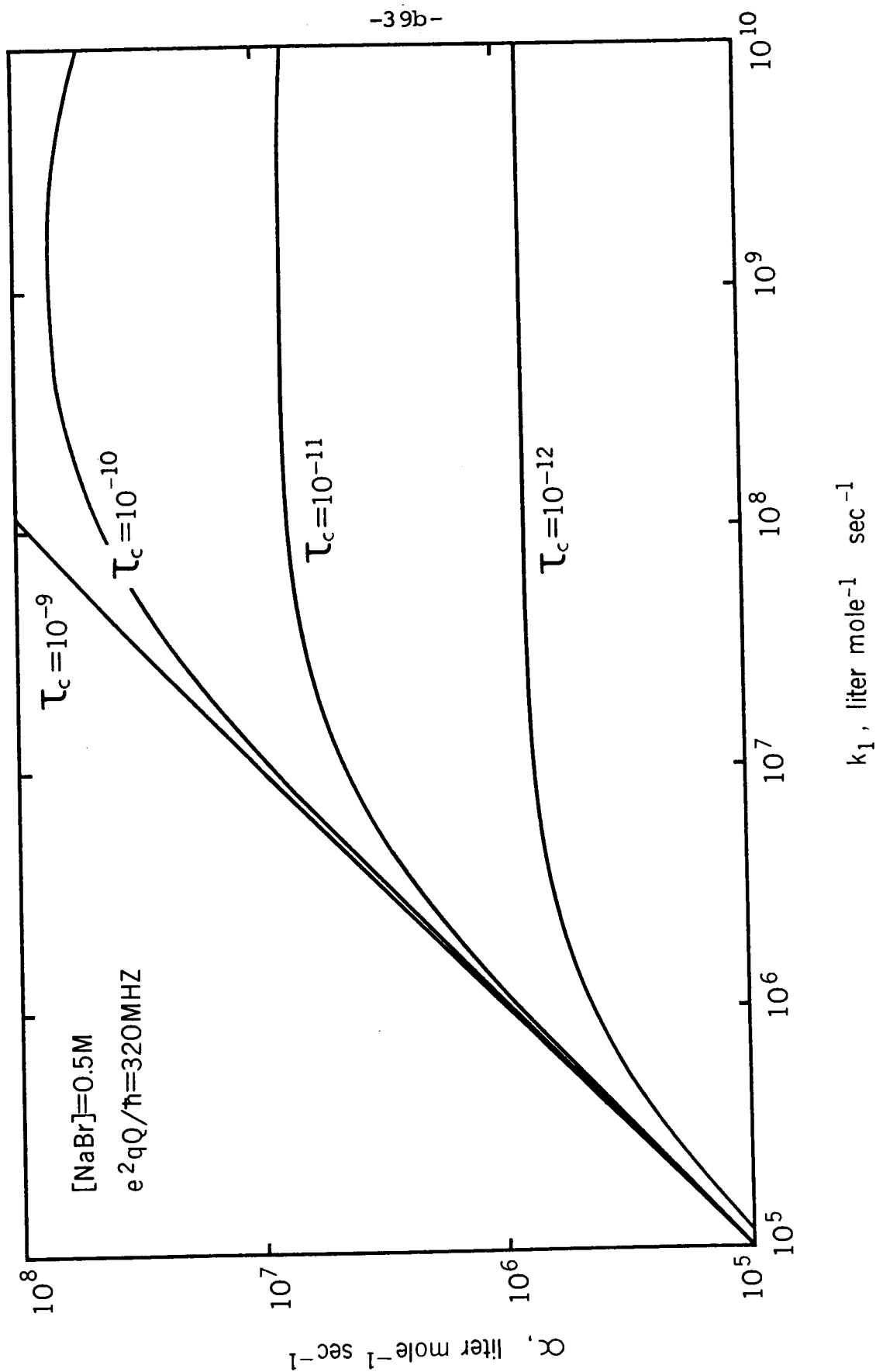


Fig. 8. Calculated dependence of  $\alpha$  on the correlation time for 0.5 molar bromide.

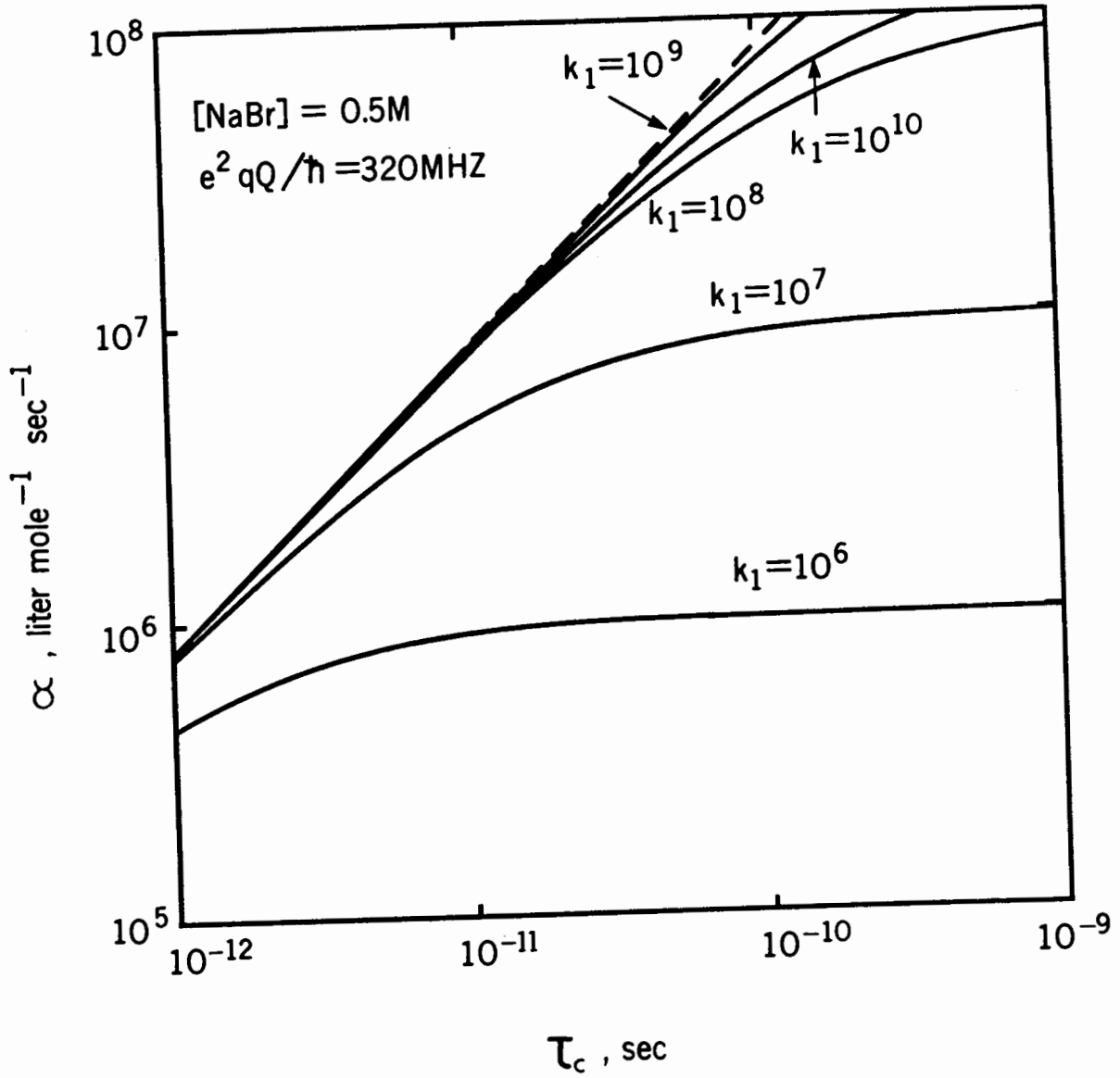


Fig. 9. Calculated dependence of  $\alpha$  on the rate of halide exchange for 2.0 molar chloride.



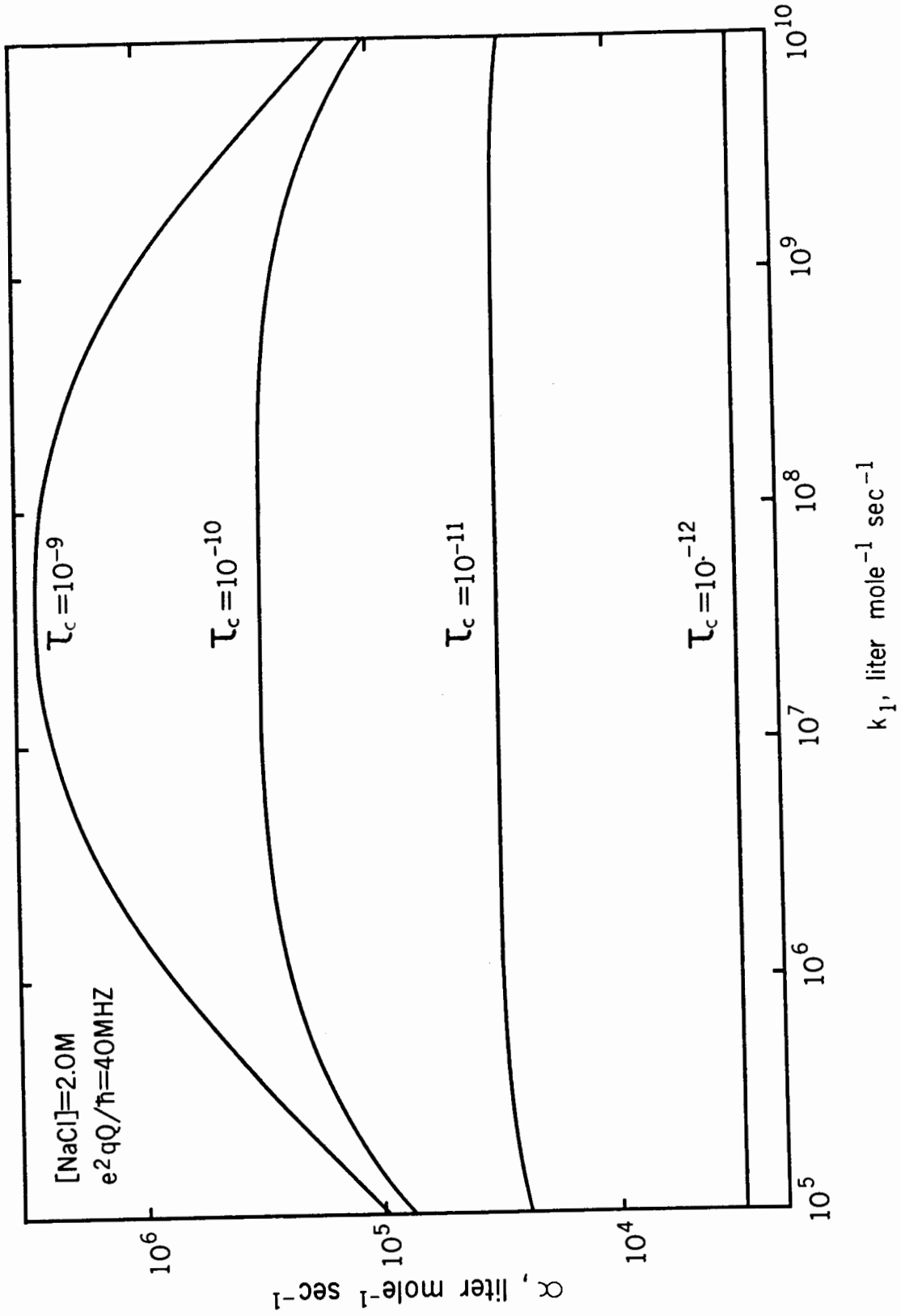
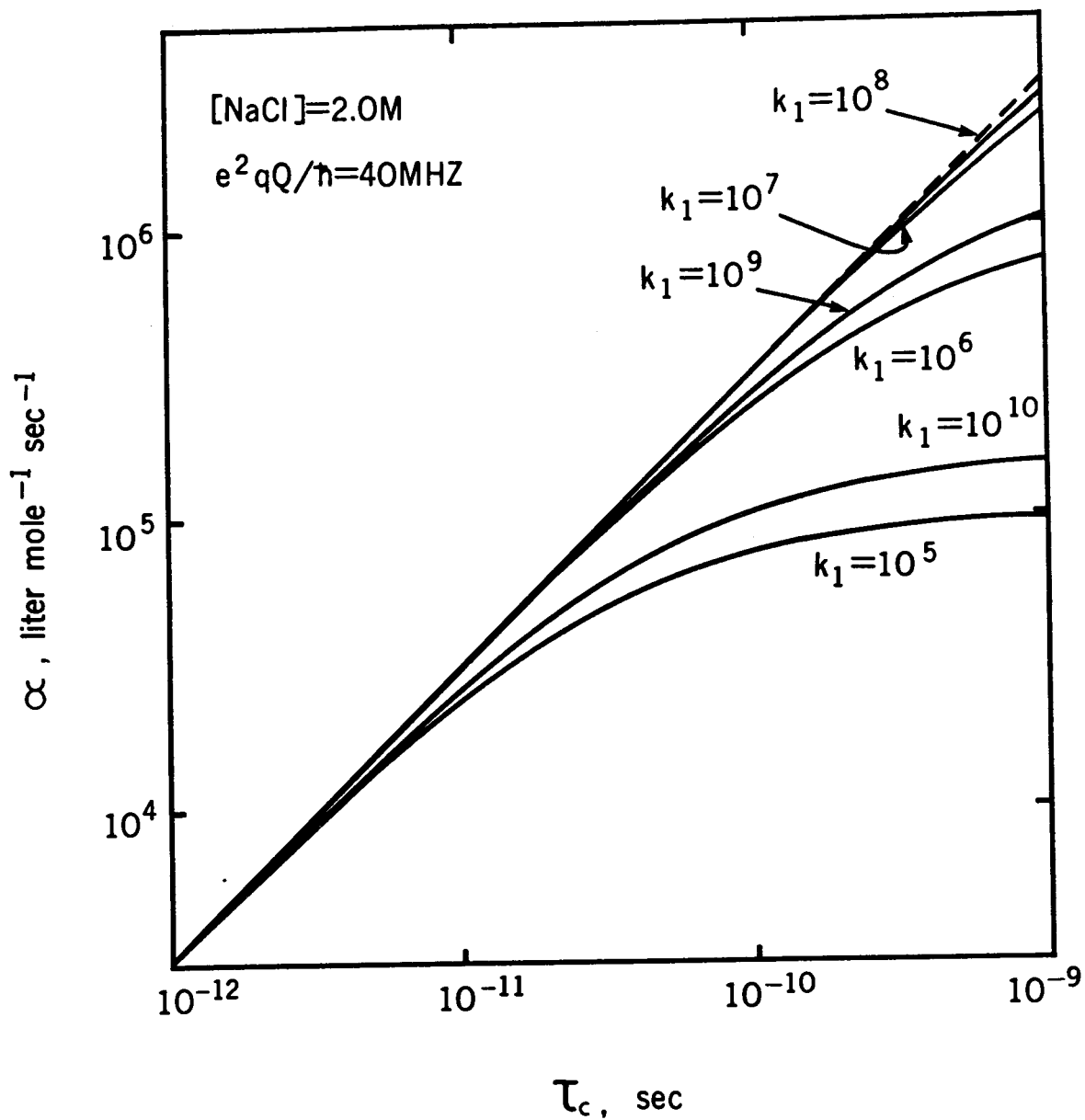


Fig. 10. Calculated dependence of  $\alpha$  on the correlation time for 2.0 molar chloride.



had no effect on  $\alpha$  (that is, the dependence assumed by Stengle and Baldeschwieler) and the fast exchange limit includes those values of  $\tau_c$  and  $k_1$  where the graph is asymptotic to this line.

Intermediate regions prove to be the most informative, with measurements of  $\alpha$  under these conditions yielding values for both  $k_1$  and  $\tau_c$ . Bromide-mercury complexes fall between the slow and fast exchange limits. O'Reilley et al (40) have calculated values of  $3.7 \pm 0.4 \times 10^7$  liter mole<sup>-1</sup>sec<sup>-1</sup> for  $k_1$ , and  $1.46 \pm 0.07 \times 10^{-6}$  sec<sup>-1</sup> for  $R_{2B}$  in the  $[\text{HgBr}_4]^{2-}$  ion. Assuming a quadrupolar coupling constant of 320 MHz, the latter quantity places  $\tau_c$  for this complex at  $3.6 \times 10^{-12}$  sec. Under the experimental conditions encountered in this work, hemoglobin-bound bromide was found to have exchange rates which placed it in this intermediate region also. This result is of the utmost importance, as it appears possible to measure two parameters characteristic of a protein binding site: the local correlation time and the exchange rate, the former quantity providing a measure of the rigidity of the sulphhydryl side-chain and the latter indicating the accessibility and hence reactivity of that site to the surrounding environment. For Figures 7 and 8, it may be seen that decreasing the halide concentration has the effect of shifting the curves to higher values of  $k_1$

and  $\alpha$  without appreciably changing their shape.

On the basis of the calculation whose results are shown in Figures 9 and 10, chloride ion may be expected to be much less liable to exchange effects than bromide. Since  $k_1$  for mercuric iodide is only twice as great as for mercuric bromide,  $9 \times 10^7$  liter mole<sup>-1</sup> sec<sup>-1</sup> (40), one may reasonably predict that mercury-chlorine complexes will also exhibit exchange rates close to those found for mercuric bromide. Hence, the behaviour of chloride complexes should deviate from the fast exchange limit only at correlation times of the order of  $10^{-9}$  second or longer. The information available from bromide exchange is therefore potentially much greater than that obtainable from chloride exchange.

Since (31) ceases to be a valid description of  $T_{2B}$  when the extreme narrowing approximation is violated, this derivation has been limited to the consideration of correlation times of the order of  $10^{-9}$  second or less for an operating frequency of 15 MHz. It is possible to make some correction for the effect of  $\omega\tau$  approaching unity by including terms in  $I_z^3$  in the derivation of (30) and expanding the resulting expression; however, such a treatment can only extend the theory to correlation times of the order of  $3 \times 10^{-9}$  second. Since the adjust-

ment to  $\alpha$  in this region would be quite negligible, there is little reason for discussing such corrections here. An extensive revision of the theory of quadrupolar broadening for the case where  $\omega\tau$  approaches and exceeds unity will be required before this situation can be treated theoretically in a meaningful manner. An empirical study of the dependence of the decay on the resonance frequency  $\omega_0$  may point the way to useful approximations.

## DESCRIPTION OF NMR APPARATUS AND METHODS

The 15 MHz  $^{79}\text{Br}$  and  $^{81}\text{Br}$  NMR signals were obtained as signal-averaged phase-detected free induction decays by standard pulse techniques. Fig. 11 shows the block diagram of the system employed in these experiments. A Varian V3600 low impedance twelve inch magnet equipped with high resolution pole caps and field homogeneity and sweep controls, the latter operating through a V3506 flux stabilizer, was used to provide  $\text{H}_2\text{O}$ . The pulse power amplifier was an NMR Specialties PS-60A low power unit tuned to 15 MHz and operating from either a Schomandl ND30M synthesizer or an internal 15 MHz crystal oscillator as frequency source. A home-built high resolution single coil probe containing a FET preamplifier was employed. The signal from the FET preamplifier mounted in the probe was amplified in a low-noise tube-type 15 MHz tuned IF strip and fed to the NMR Specialties phase detector and through an RC filter to the data acquisition system.

The 15MHz signal produced by the frequency source is amplified and fed into the probe in pulses whose rate and duration is governed by a gating voltage from the pulse programmer. The phase difference between the reference signal from the oscillator and the receiver output is detected and fed to the RC out-

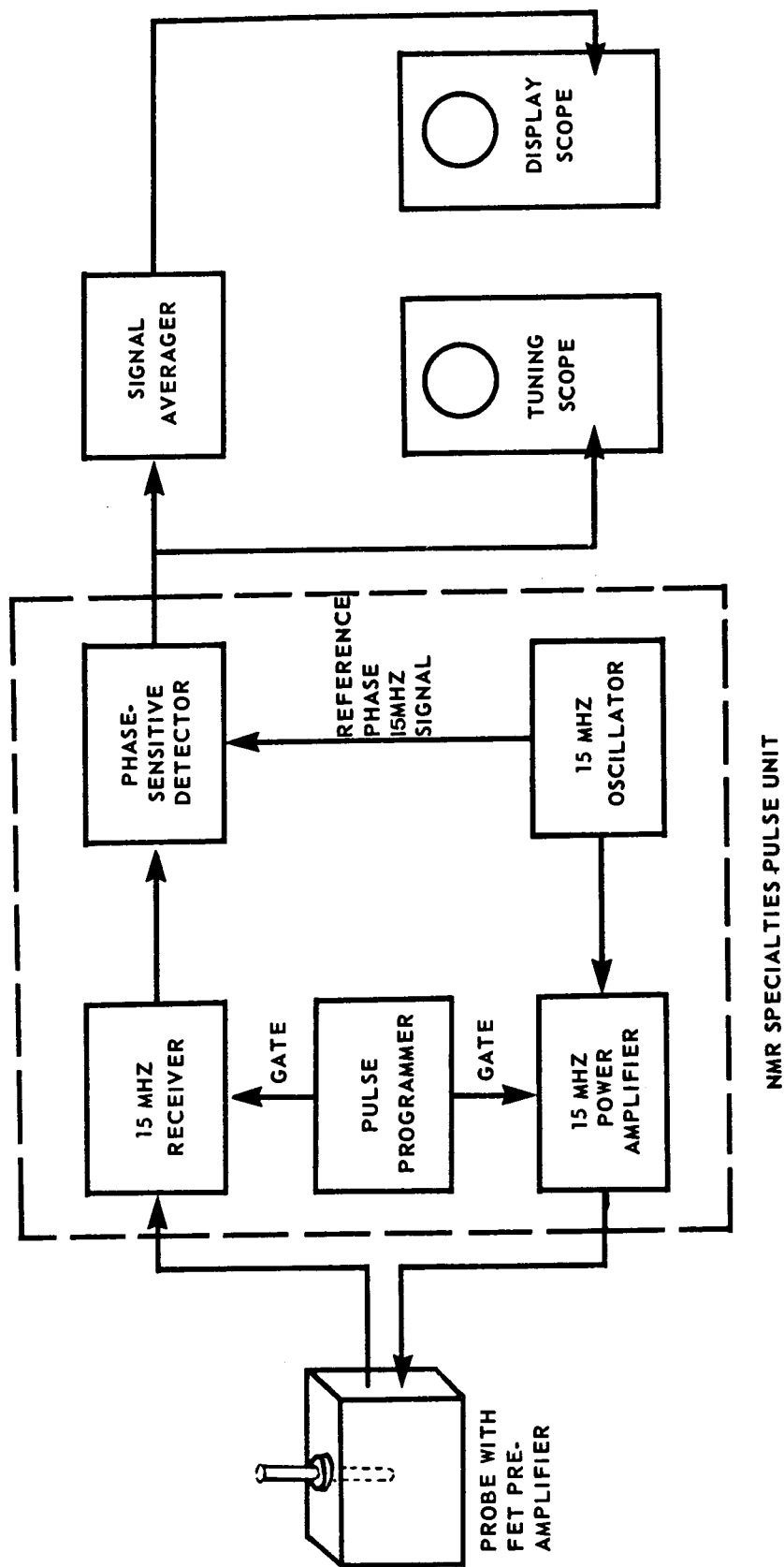


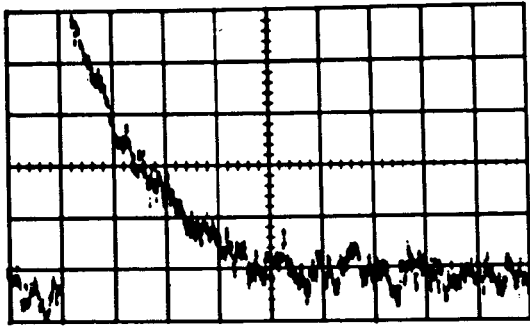
FIG. 11: BLOCK DIAGRAM OF PULSED NMR SPECTROMETER AND SIGNAL AVERAGING SYSTEM



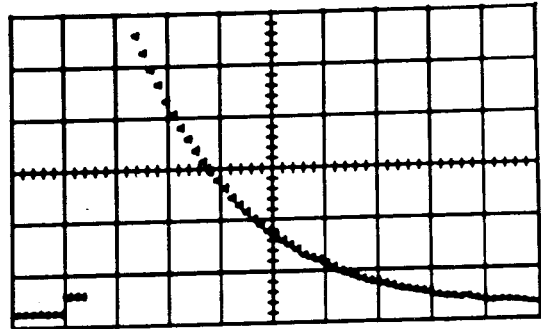
put circuit and thence to a Fabritek 1064 signal averager. For the  $^{81}\text{Br}$  resonance from 2 molar aqueous NaBr solution and 1  $\mu\text{sec}$  output time constant, the final signal available at the beginning of a single free induction decay was typically 2 volts with a signal-to-noise ratio of 10:1. With signal averaging, it was possible to obtain usable  $T_2$ 's from NaBr solutions with concentrations down to 0.25 molar. Figure 12 shows typical raw and averaged signals from NaBr in the concentration range 0.5 - 2.0 molar. The samples were contained either in Wilmad polished high resolution NMR tubes of 15 mm O.D. and 1 mm wall thickness or in 15 mm test tubes. Use of the latter was quite feasible because the sample was not spun.

The value of the bromide relaxation time could be obtained to within 15% from photographs or direct display of decay signals on a Tektronix 549 storage oscilloscope. The precision in all relaxation time measurements was increased by signal averaging. Usually 512-2048 scans were performed using a Fabritek signal averager with SW-2 sweep plug-in and SD-2 digitizer operating at 10 bit resolution. These plug-ins were limited to a minimum dwell time per channel of 50  $\mu\text{sec}$ , rather more than optimum for dealing with the moderately

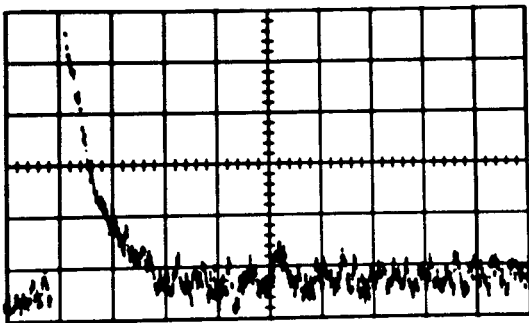
- Fig. 12. Typical raw and averaged  $^{81}\text{Br}$  free induction decays from aqueous NaBr solutions. a - c: vertical scale, 1.4 volts/division; horizontal scale, 500  $\mu\text{sec}$  /division. d - f: vertical scale 1.25 volts/division; horizontal scale, 50  $\mu\text{sec}$  /channel.
- a. 2 molar NaBr, raw signal.
  - b. 2 molar NaBr +  $7 \times 10^{-5}$  molar  $\text{HgCl}_2$ , raw signal.
  - c. 0.5 molar NaBr, raw signal.
  - d. 2 molar NaBr, average of 512 sweeps.
  - e. 2 molar NaBr +  $7 \times 10^{-5}$  molar  $\text{HgCl}_2$ , average of 512 sweeps.
  - f. 0.5 molar NaBr, average of 1024 sweeps.



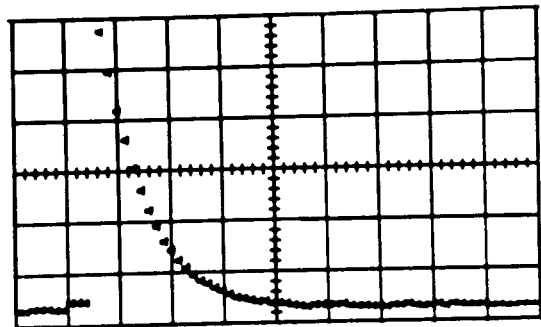
a



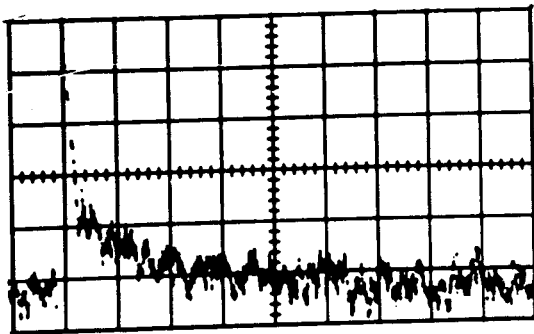
d



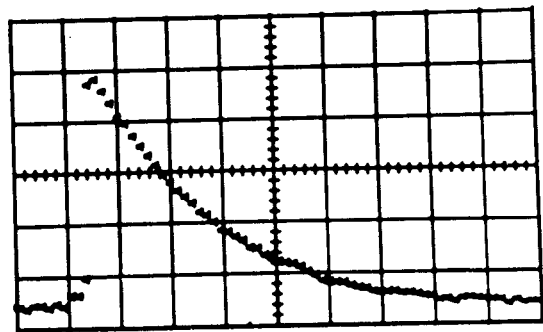
b



e



c



f

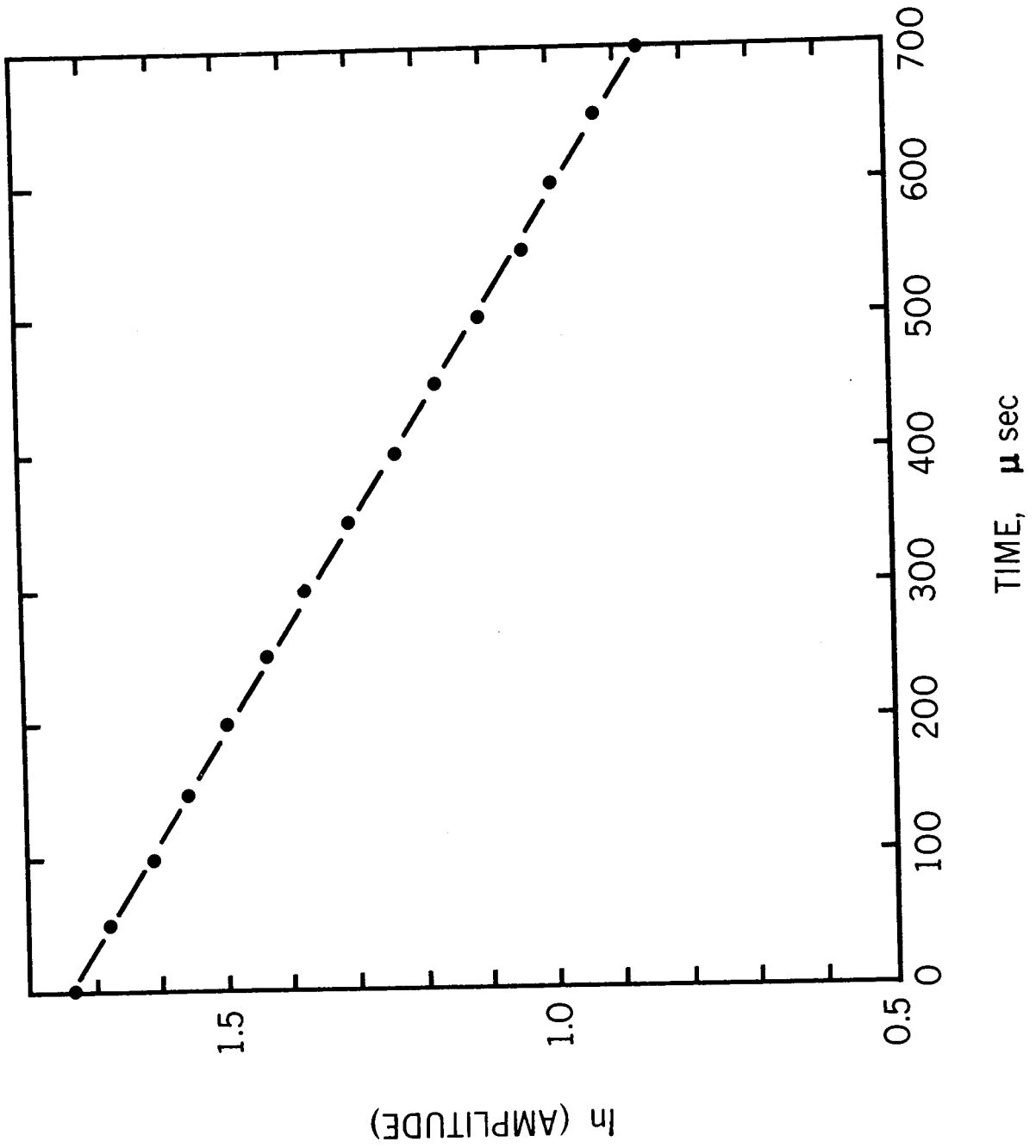
small values of  $^{81}\text{Br}$  and  $^{79}\text{Br}$  relaxation times experienced here (150 to 750  $\mu\text{sec}$ ).

Errors in the measured decay rates due to  $H_0$  inhomogeneity were minimized by shimming the magnet homogeneity on the sharp nearby  $\text{Na}^{23}$  resonance. The main contributions to the error in the measured decay rates were introduced by  $H_0$  drifts during averaging and by small initial deviations from the exact resonance condition, both of which effects introduce incipient modulation on the phase detected decay, reducing the observed relaxation time. Although  $H_0$  was stabilized, drift effects were occasionally noticed when averaging the longer decays and may introduce some random errors in these cases. They could not be detected over  $T_2$  decays less than 600  $\mu\text{sec}$  for averaging periods up to 30 seconds. The resonance condition was set by maximizing the decay amplitude over the time interval between one and two  $T_2$ 's. Resonance tuning was quite critical at long  $T_2$ . The inconvenience of having fewer points for the  $^{81}\text{Br}$  decay at shorter lifetimes was compensated for by the increased linewidth, which caused the drift in  $H_0$  and the initial adjustment of the resonance condition to be less critical. Consequently, the estimated error in the measured decay rate  $R_2$  was  $80 \text{ sec}^{-1}$  or better over the range 1200 to 3500  $\text{sec}^{-1}$ .

Before commencing a series of measurements, a flat baseline on the portion of the output signal where the decay was displayed was obtained by adjusting  $H_0$  completely off the  $^{81}\text{Br}$  resonance with the sample in the probe. Under these conditions, the signal appears as a series of pulses separated by a baseline whose slope is dependent on the detector phase setting. This setting was varied until the baseline on the averaged signal was as flat as possible, thus avoiding the necessity for any baseline correction. Unfortunately, the probe was detuned near the end of this series of experiments, and for some time it was not possible to retune it to obtain a flat baseline. Consequently, during some of the later work it was necessary to work with a curved baseline and subtract the averaged off-resonance baseline signal digitally in the averager memory.

Since the bromide decay was exponential at this frequency,  $T_2$  could be obtained from the slope of a linear plot of  $\ln$  (Signal Amplitude) versus time (Fig. 13). This proved to be a time-consuming process, however, and it was found that comparable results could be obtained by calculating  $T_2$  from the time interval between two points with known amplitude ratio on the averaged decay curve and repeating the measurement

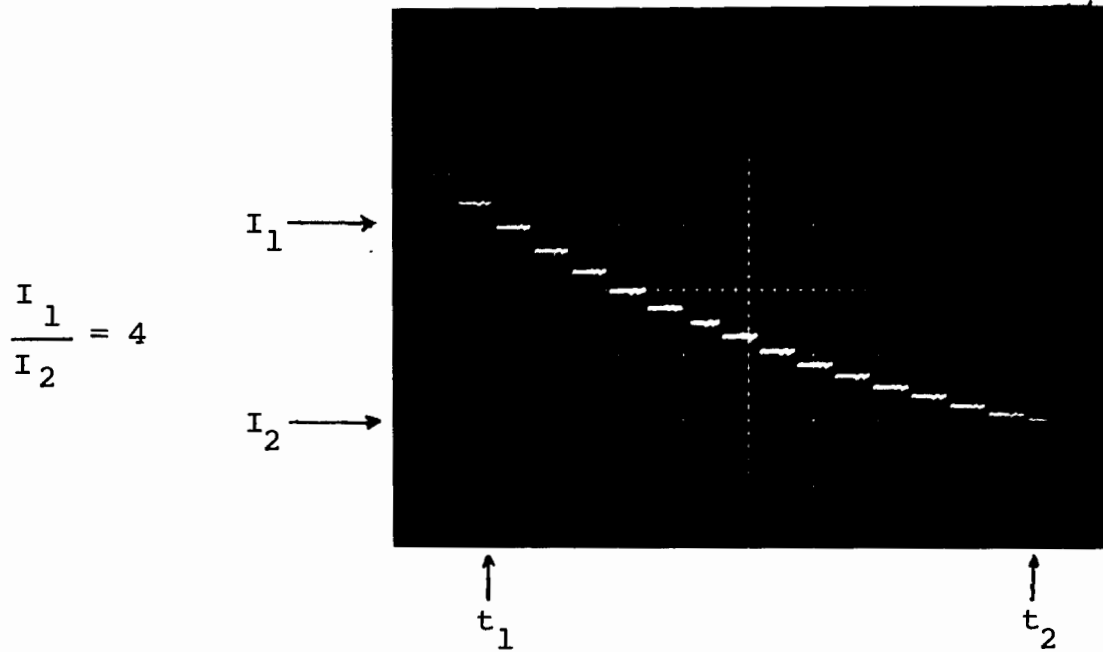
Fig. 13. Graph of  $\ln(\text{Signal Amplitude})$  versus time for a typical  $^{81}\text{Br}$  decay. In order to present data in this form, the decay curve was photographed and the signal voltage for each channel measured in units of centimeters on the oscilloscope graticule. Each data point corresponds to the output of one channel. The time interval between points was 50  $\mu\text{sec}$ , the minimum dwell time per channel.



several times, readjusting the resonance condition each time. This method of obtaining  $T_2$  is shown in Fig. 14. The present data were obtained by this two-point method. Deviations from linearity on the logarithmic plots were observed at the beginning and near the tail of the decay. Consequently, the first few points of the decay were excluded from the interval used to determine  $T_2$  whenever possible. Every relaxation rate given here is the average of several separately tuned and averaged relaxation decays.

Measurement of  $T_2$  by this method at bromide concentrations below 0.5 molar was made difficult by the presence of a 3 KHz signal originating in the pulse programmer. This signal, apparent in Fig. (12f), was synchronized with the pulse and appeared superimposed on the decay. Accurate measurement of decay rates under these conditions would have required graphical determination of  $T_2$  on a considerable number of decays. For this reason, experiments were not performed at halide concentrations below 0.5 molar.





For an exponential decay:

$$\ln (I_2/I_1) = (t_1 - t_2)/T_2$$

$$\therefore T_2 = (t_1 - t_2)/\ln 4$$

$$= (14.1 \text{ channels} \times 50 \mu\text{sec./ch.})/\ln 4$$

$$= 509 \mu\text{sec.}$$

Fig. 14. Two-point method of determining  $T_2$ .

## STUDIES ON SIMPLE THIOLS

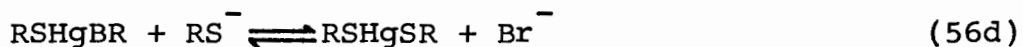
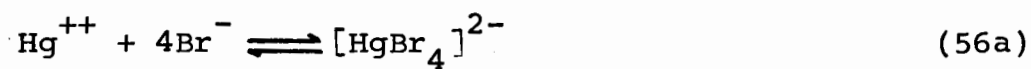
### I. Introduction

In order to gain a better understanding of the capabilities of the halide-probe technique, NMR titrations were performed on a series of simple sulphhydryl-containing compounds.

Exhaustive polarographic studies by Koltoff (43-47), with such compounds have demonstrated that in the presence of mercuric ion, thiol dimers of the form  $\text{RSHgSR}$  exist in equilibrium with small quantities of uncomplexed thiol. In the dimer, mercury-bromide binding cannot occur, and no chemical exchange will be observed as long as all available mercury is bound in this manner. However, the thiol-dimer equilibrium has been found to be strongly dependent on the pH and bromide concentration, and, under appropriate conditions, sufficient dissociation of the dimer occurs to permit the presence of appreciable quantities of  $[\text{HgBr}_4]^{2-}$  ion. Since the existence of this species will be evidenced by an increase in  $R_2$ , observation of the halide decay rate during the course of the titration will provide information on the stability of the dimer under experimental conditions.

## II. Theory

From simple equilibrium theory, it is possible to predict the dependence of  $R_2$  on the concentration of thiol and mercuric ion under varying conditions of pH and ionic strength. The following equilibria will be used to describe the species encountered here:



Dissociation constants for (56a) - (56d) are given by

$$K_1 = \frac{[\text{Hg}^{++}] [\text{Br}^-]^4}{[\text{HgBr}_4^{2-}]} \quad (57a)$$

$$K_2 = \frac{[\text{RS}^-] [\text{H}^+]}{[\text{RSH}]} \quad (57b)$$

$$K_3 = \frac{[\text{Hg}^{++}] [\text{RS}^-]^2}{[\text{RSHgSR}]} \quad (57c)$$

$$K_4 = \frac{[\text{RSHgBr}] [\text{RS}^-]}{[\text{RSHgSR}] [\text{Br}^-]} \quad (57d)$$

Available literature values for these constants except  $K_4$  are given in Table I. Of the compounds used in this study, all but mercaptoethanol bore either amino or carboxyl groups in addition to the sulphhydryl group. The effect of the charge of these species on the chemistry of the sulphhydryl group has been neglected in (56a) - (56d), an approximation which is valid at acid pH. Kolthoff (45) has shown that the charge of the carboxyl groups in cysteine and glutathione has no effect on the dissociation constants of the mercaptides. The values of  $K_3$  for these two compounds are those of the species with protonated amino groups; the concentration of other species may be ignored below the pH indicated in Table I, and  $K_3$  will be independent of pH within this range. In the case of mercaptoacetic acid, Kolthoff (47) has shown that the effect of the charge on the carboxyl groups must be taken into account. However, the dissociation constant for the mercaptide is constant below pH 4.7 and hence the above approximation will be valid within this range. Values for mercaptoacetic acid will be used in calculations for mercaptosuccinic acid. Combining equations (57a) - (57c) yields

$$[\text{HgBr}_4^{2-}] = \frac{K_3 [\text{RSHgSR}] [\text{H}^+]^2 [\text{Br}^-]^4}{K_2 K_1 [\text{RSH}]^2} \quad (58)$$

Table I. Equilibrium Constants for Thiols at 25°C.

	Glutathione (45)	Cysteine (45)	Mercaptoacetic Acid (47)
<sup>a</sup> K <sub>1</sub>	-----	2.46 x 10 <sup>-21</sup> (40)	-----
<sup>b</sup> K <sub>2</sub>	1.04 x 10 <sup>-9</sup>	2.19 x 10 <sup>-9</sup>	2.8 x 10 <sup>-11</sup>
<sup>c</sup> K <sub>2</sub>	1.1 x 10 <sup>-41*</sup>	5.6 x 10 <sup>-41**</sup>	4.8 x 10 <sup>-45†</sup>
	* at pH ≤ 7.5	** at pH ≤ 5.5	† at pH ≤ 4.7

a. Values determined from solvent distribution and polarographic studies.

b,c. Values determined by polarographic studies.

The amount of mercuric ion added and the amount of RSH originally present may be defined as

$$[\text{Hg}]_{\text{total}} = [\text{RSHgSR}] + [\text{HgBr}_4^{2-}] \quad (59)$$

$$[\text{RSH}]_{\text{total}} = [\text{RSH}] + 2[\text{RSHgSR}] \quad (60)$$

$\text{Hg}^{++}$  and  $\text{RS}^-$ , as is apparent from the equilibrium constants of Table I, will be present in negligible amounts. For the present, the species  $\text{RSHgBr}$  has been neglected, since the existence of this monomeric complex cannot be demonstrated polarographically (44, 45). The case where there is a detectable concentration of monomer will be discussed later.

Solving equations (59) and (60) for  $[\text{RSHgSR}]$  and  $[\text{RSH}]$ , substituting in equation (58), and rearranging results in a third order equation:

$$\boxed{X^3 + (V - 2W)X^2 + \left(\frac{V - 2W}{2}\right)^2 X + \mathfrak{R}(X - W) = 0} \quad (61)$$

where

$$X = [\text{HgBr}_4^{2-}] \quad (62a)$$

$$V = [\text{RSH}]_{\text{total}} \quad (62b)$$

$$\mathfrak{R} = \frac{K_3 [\text{H}^+]^2 [\text{Br}^-]^4}{4K_2^2 K_1} \quad (62c)$$

$$W = [\text{Hg}]_{\text{total}} \quad (62d)$$

From equation (47), it is apparent that knowledge of  $\alpha$  for the binding species  $[\text{HgBr}_4]^{2-}$  permits calculation of  $R_2$  for a given mercury concentration under prescribed conditions of pH and bromide concentration once equation (61) has been solved for X.

Equation (61) was solved for X as a function of W for a series of different values of  $\mathfrak{R}$  by the program shown in Fig. 15. The resulting family of curves is presented in Fig. 16. Two conclusions are at once apparent from Fig. 16:

1. In order to obtain an accurate and definitive end-point in this type of titration, conditions of pH and halide-ion concentration must be maintained so that  $\mathfrak{R}$  is less than  $10^{-10}$ .
2. In the region  $10^{-10} < \mathfrak{R} < 10^{-9}$ , extrapolation of the portion of the titration curve past the end-point to zero concentration of  $[\text{HgBr}_4]^{2-}$  would result in a value for the end-point which is up to 10% too low. In this range of  $\mathfrak{R}$ , an end-point correction or curve-fitting would be in order if an accurate end-point was desired.

Fig. 15. Program used to solve equation (61).



```
C CARDANO PROBLEM
  IMPLICIT REAL*8 (A-I,O-Z)
  W= 0.002
  H= 0.1
101 A1 = 0.1
100 A = A1*W
  B = (W - 2*A)
  C = ((W -2*A)/2)**2 + H
  D = -A*H
102 FORMAT(/' W =',D10.4,' H =',D10.4,' A =',D10.4,/)
  PRINT 102, W,H,A
  T = CROOT(B,C,D)
  A1=A1+0.1
  IF (A1.LE.1.001) GO TO 100
  H= H*0.1
  IF ( H.GT.1.D-11) GO TO 101
  STOP
  END

  REAL FUNCTION CROOT*8( B,C,D)
  IMPLICIT REAL*8 (A-I,O-Z)
21 FORMAT(/' LIMITING CASE'/)
44 FORMAT(///' B =',D16.8,' C =',D16.8,' D=',D16.8,/)
  Q = B*B*B/27 - B*C/6 + D/2
  P = ( 3*C - B*B)/9
  DELTA = Q*Q + P*P*P
  PI = 1.0471976
  PA = 6.2831856
  IF ( DELTA)1,2,3
1 ZEN = DABS(Q)
  R = Q*DSQRT(DABS(P))/ZEN
  FI =DARCOS(Q/R**3)
444 FORMAT(/' ARGUMENT FI = ',D16.8,/)
  X1 =-B/3 -2*R*DCOS(FI/3)
  X2 =-B/3 +2*R*DCOS( PI-FI/3)
  X3 = -B/3 +2*R*DCOS(PI + FI/3)
11 FORMAT(/' X1 =',D16.8,' X2 =',D16.8,' X3 =',D16.8 )
  PRINT 11,X1,X2,X3
  GO TO 35
2 PRINT 21
  GO TO 33
3 BAR =-Q +DSQRT(DELTA)
  ABA =DABS(BAB)
  BAL = -Q -DSQRT(DELTA)
  ABL =DABS(BAL)
  C1=1./3
  X11 = BAB * ABA**C1/ABA
  X12 = BAL * ABL**C1/ABL
  X1 = -B/3 +X11+X12
55 FORMAT(/' X1 =',D16.8)
  PRINT 55, X1
35 CRIT = (X1**3+B*X1**2 +C*X1 +D)/D
31 FORMAT(' CRITERION =',D16.8,/)
32 PRINT 31, CRIT
33 RETURN
  END
```

Fig. 16. Simulated titration curves for simple thiols at low pH produced by solution of equation (61).



Using the criterion that  $\alpha \leq 10^{-10}$  and the data of Table 1, (62c) may be used to predict the minimum pH at which thiol titrations may be performed without end-point error. The results of this calculation are presented in Fig. 17.

The present derivation can be generalized for a system where RSHgBr exists in a measurable quantity. In this case, equations (59) and (60) become

$$[\text{Hg}]_{\text{total}} = [\text{RSHgSR}] + [\text{HgBr}_4^{2-}] + [\text{RSHgBr}] \quad (63)$$

$$[\text{RSH}]_{\text{total}} = [\text{RSH}] + 2[\text{RSHgSR}] + [\text{RSHgBr}] \quad (64)$$

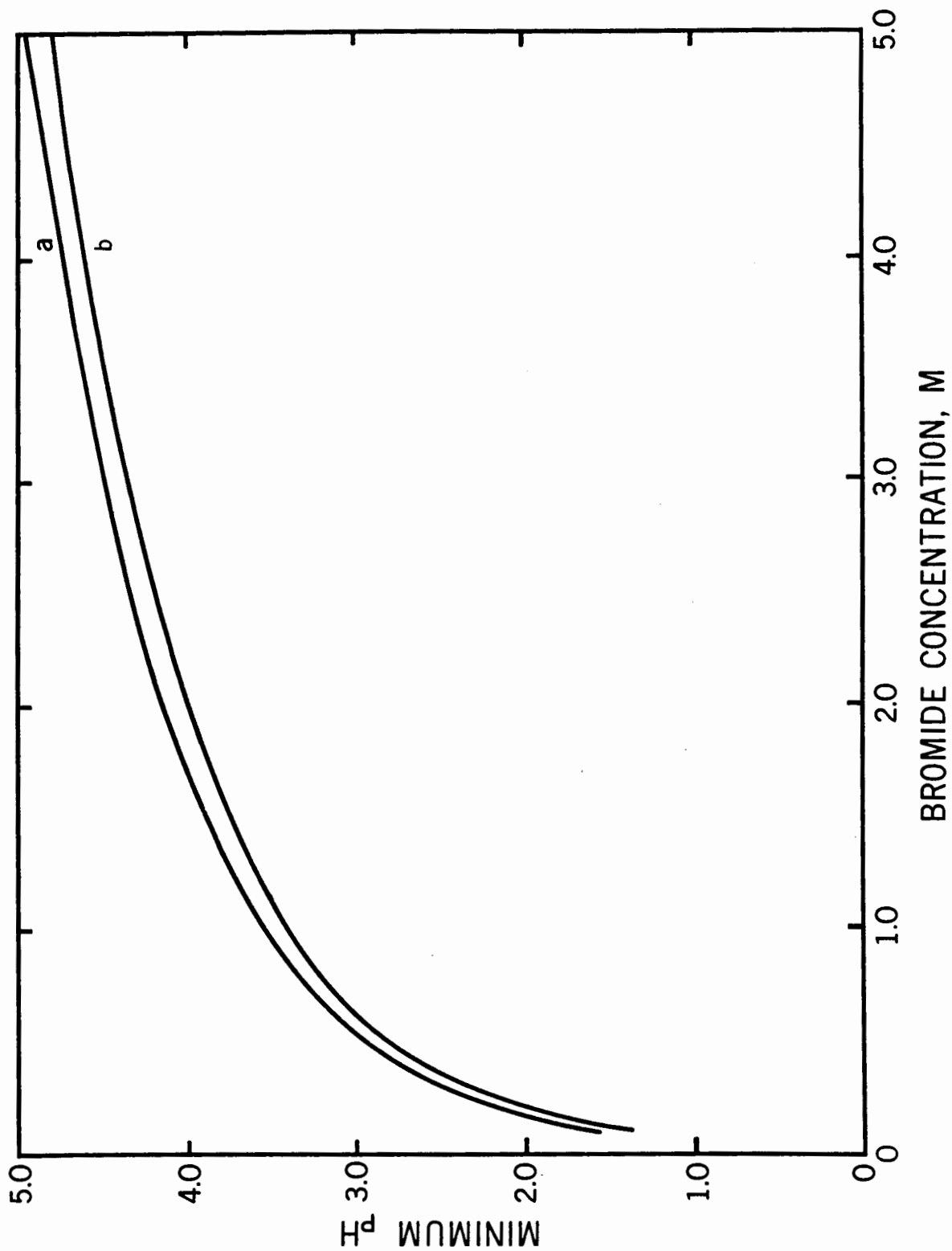
Solving for [RSHgSR] and [RSH] as before and substituting into equation (58) yields

$$\begin{aligned} X^3 + X^2(Y+V-2W) + \left(\frac{V-2W}{2}\right)^2 X + \alpha(X+Y-W) + XY\left(\frac{V-2W}{2}\right) \\ + \frac{Y^2 X}{2} = 0 \end{aligned} \quad (65)$$

where  $Y = [\text{RSHgBr}]$ . It is possible to eliminate the unknown  $Y$  by assuming that the value of  $\alpha$  is the same for RSHgBr and  $[\text{HgBr}_4^{2-}]$  (an assumption which would likely be valid for small peptides) and defining the parameter  $P = 4X + Y$ , where

$$\Delta R_2 = R_2 - R_{2F} = \frac{\alpha P}{[\text{Br}^-]} \quad (66)$$

Fig. 17. Minimum pH for which the condition  $\mathfrak{R} < 10^{-10}$  can be met as a function of bromide concentration. Curve a, cysteine and glutathione; curve b, mercaptosuccinic acid.



In the case where this assumption is clearly invalid, an estimation of the correlation time for the monomer may be made, and the expression for P modified accordingly. Replacing Y by P - 4X in (65) results in the expression

$$5X^3 - X^2(V-2W+3P) + X \left\{ \left( \frac{V-2W}{2} \right) \left( P + \frac{V-2W}{2} \right) - 3R + \frac{P^2}{2} \right\} + R(P-W) = 0 \quad (67)$$

Measurement of  $R_2$  during the titration of a thiol which produces some quantity of monomer will permit calculation of P for each point on the titration curve; once P is known, (67) can be solved for X and the concentration of RSHgBr determined. Solving (63) and (64) for [RSHgSR] and  $[RS^-]$  and substituting into (57d) then permits calculation of  $K_4$ :

$$K_4 = \left( \frac{K_2 Y}{[Br^-][H^+]} \right) \left( \frac{V - 2W + 2X + Y}{W - X - Y} \right) \quad (68)$$

In the present study, it has been possible to account for the observed titration curves by assuming that the tetrabromide ion is the only exchanging species. However, application of the present technique to the study of other peptides may result in the formation of appreciable amounts of monomer, ren-

dering a method of determining the monomer concentration quite valuable.



### III. Experimental

Crystalline glutathione (purity 98-100% claimed by manufacturer) was purchased from Sigma Chemical Company. Reagent grade mercaptosuccinic acid was supplied by Eastman Organic Chemicals. L-cysteine was a product of Matheson, Coleman, and Bell, and reagent grade mercaptoethanol was purchased from J.T. Baker Chemical Company. All were used without further purification. All other chemicals were reagent grade. Twice-distilled water was obtained from a Corning AG-10A Pyrex still and used to prepare all solutions.

Titration of thiol compounds were performed by preparing a 10 ml. sample of the thiol reagent in 0.5 - 2 molar NaBr solution. At pH 6, solutions were buffered with 0.05 molar phosphate, while very acidic or basic conditions were achieved by the addition of HCl or NaOH to unbuffered sodium bromide solution. After recording the initial bromide  $T_2$  decay, aliquots of 0.1 molar mercuric chloride solution were added, using Oxford micropipettes, and the decay was remeasured. Mercuric chloride was used as a titrant rather than mercuric bromide because of its greater solubility. Competition for mercury binding sites from the small amounts of chloride added was considered negligible. Solution temperature was assumed to be

that of the NMR probe,  $26 \pm 2^\circ\text{C}$ .

The pH of small volumes of solution was measured with a Fisher Accumet pH meter equipped with a Fisher 13-639-90 combination electrode; where greater accuracy was desired, a Corning model 12 expanded-scale pH meter with Corning 476022 glass electrode and Corning 470002 reference electrode was used. Sodium error was negligible under the conditions encountered in this series of experiments. Fisher standard buffers at pH 2, 4, 6 and 10 were used for calibration.

IV. Results and Discussion

Since  $\text{HgCl}_2$  was used as a titrant over a wide range of pH, it was deemed necessary to determine the effect of pH on the behaviour of the tetrabromide ion formed in the presence of NaBr. Data showing the dependence of  $R_2$  on the amount of mercuric ion added for pH 2.2 - 11.1 are presented in Fig. (18) - (20). Values for  $\alpha$  calculated from a linear least squares fit of these data are given in Table II.

Table II - Values of  $\alpha$  for  $[\text{HgBr}_4]^{2-}$  in 2 M. NaBr, 26°C.

pH	$\alpha, \text{ l m.}^{-1} \text{ s.}^{-1}$	Std. Deviation	Avg. $\alpha, \text{ l m.}^{-1} \text{ s.}^{-1}$
2.2	$2.71 \times 10^6$	$0.1 \times 10^6$	$2.75 \pm 0.1 \times 10^6$
6.1	$2.83 \times 10^6$	$0.06 \times 10^6$	
11.1	$2.72 \times 10^6$	$0.13 \times 10^6$	

Since  $\alpha$  is independent of pH over the range of experimental conditions encountered in this study, it will be permissible to use  $\alpha_{\text{AVG}}$  in calculations involving this constant of tetrabromide ion.

Titration curves for mercaptosuccinic acid, cysteine, glutathione, and mercaptoethanol are presented in Fig. (21) through (24). The reproducibility in the measured values of  $R_2$  was  $80 \text{ sec}^{-1}$  over the range of  $1200 < R_2 < 3000 \text{ sec}^{-1}$ . Error flags have been omitted for the sake of clarity.

Fig. 18. Dependence of  $R_2$  on the concentration of mercuric ion in 2.0 molar sodium bromide solution at pH 2.2.

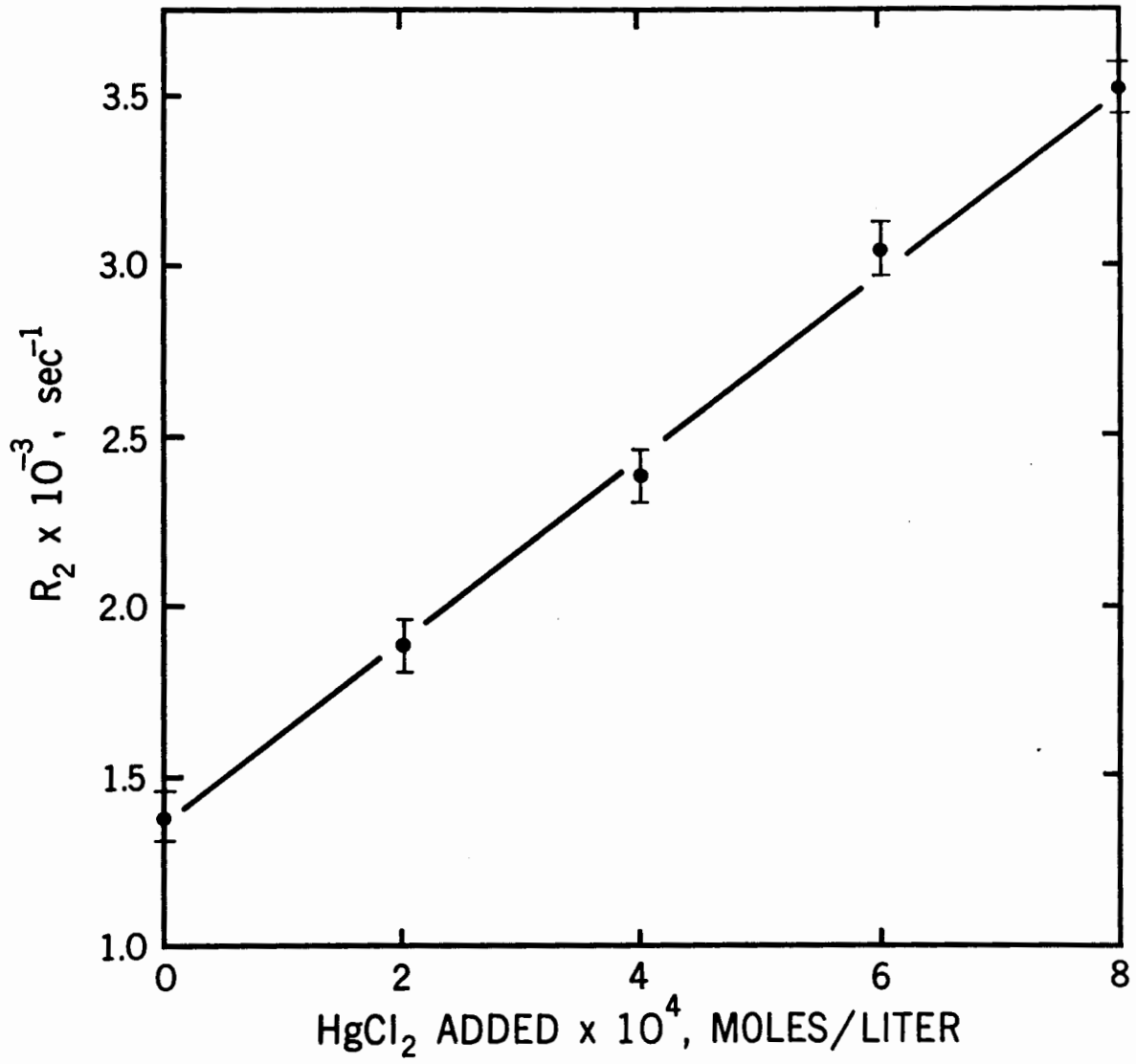


Fig. 19. Dependence of  $R_2$  on the concentration of mercuric ion in 2.0 molar sodium bromide solution at pH 6.1.

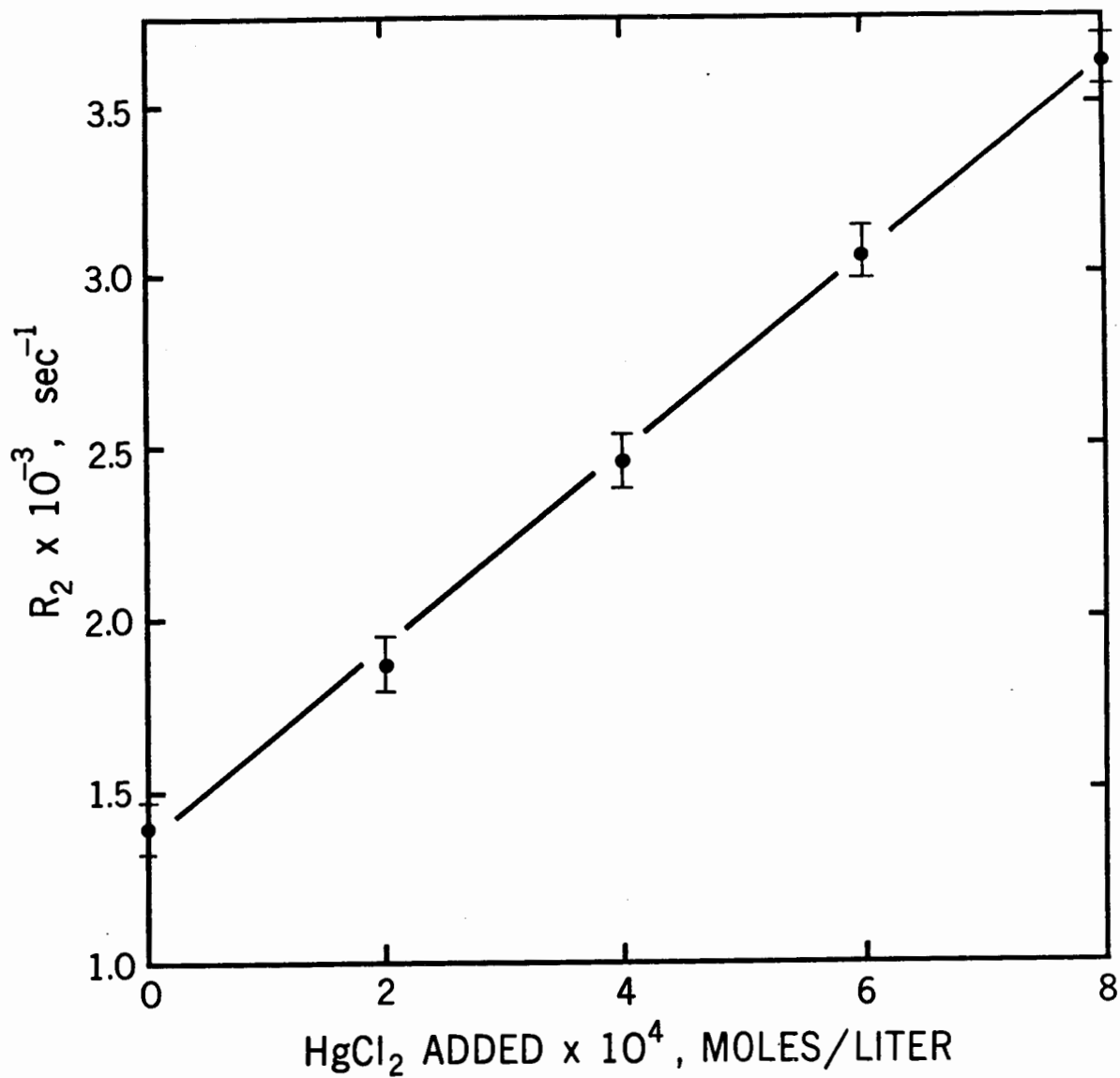


Fig. 20. Dependence of  $R_2$  on the concentration of mercuric ion in 2.0 molar sodium bromide solution at pH 11.1.



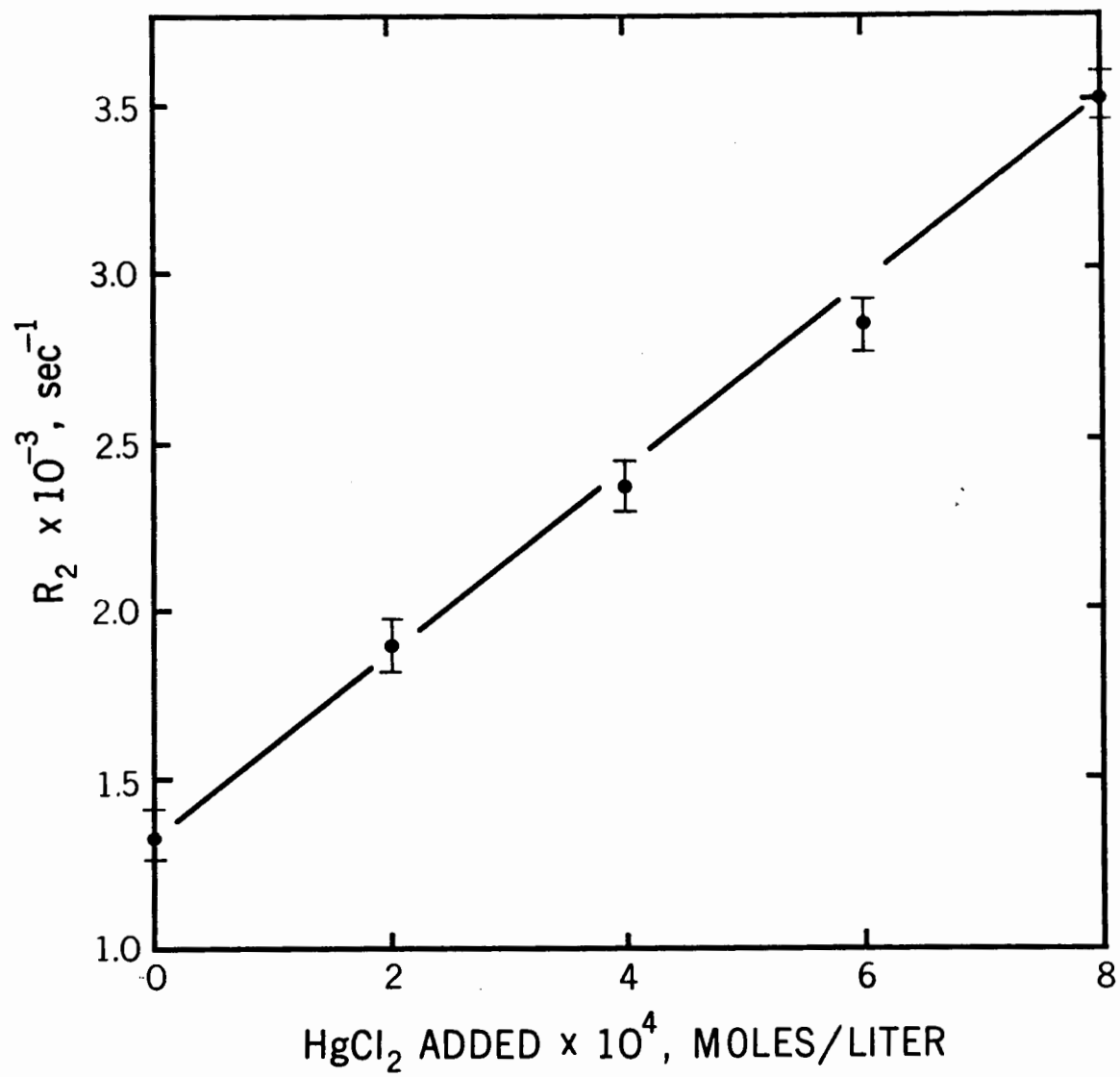


Fig. 21. Titration of  $1.2 \times 10^{-3}$  molar mercapto-  
succinic acid with  $\text{HgCl}_2$ . (●-●-●), pH  
2.5; (▲-▲-▲), pH 5.8; (■-■-■), pH 11.2;  
(-----), no thiol present.

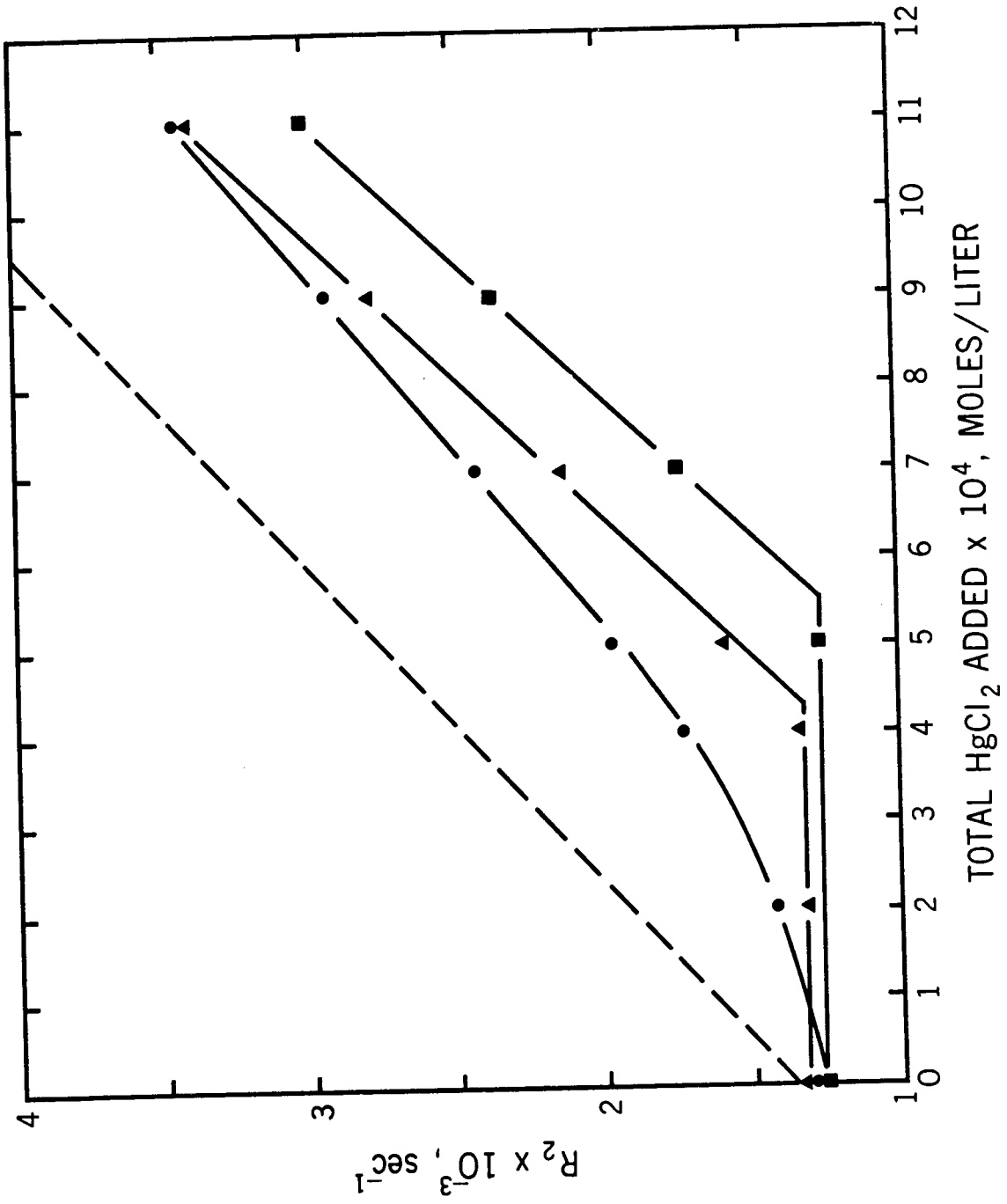


Fig. 22. Titration of  $1.2 \times 10^{-3}$  molar cysteine with  $\text{HgCl}_2$ . (●-●-●), pH 2.3; (▲-▲-▲), pH 6.0; (■-■-■), pH 11.2; (----), no thiol present.

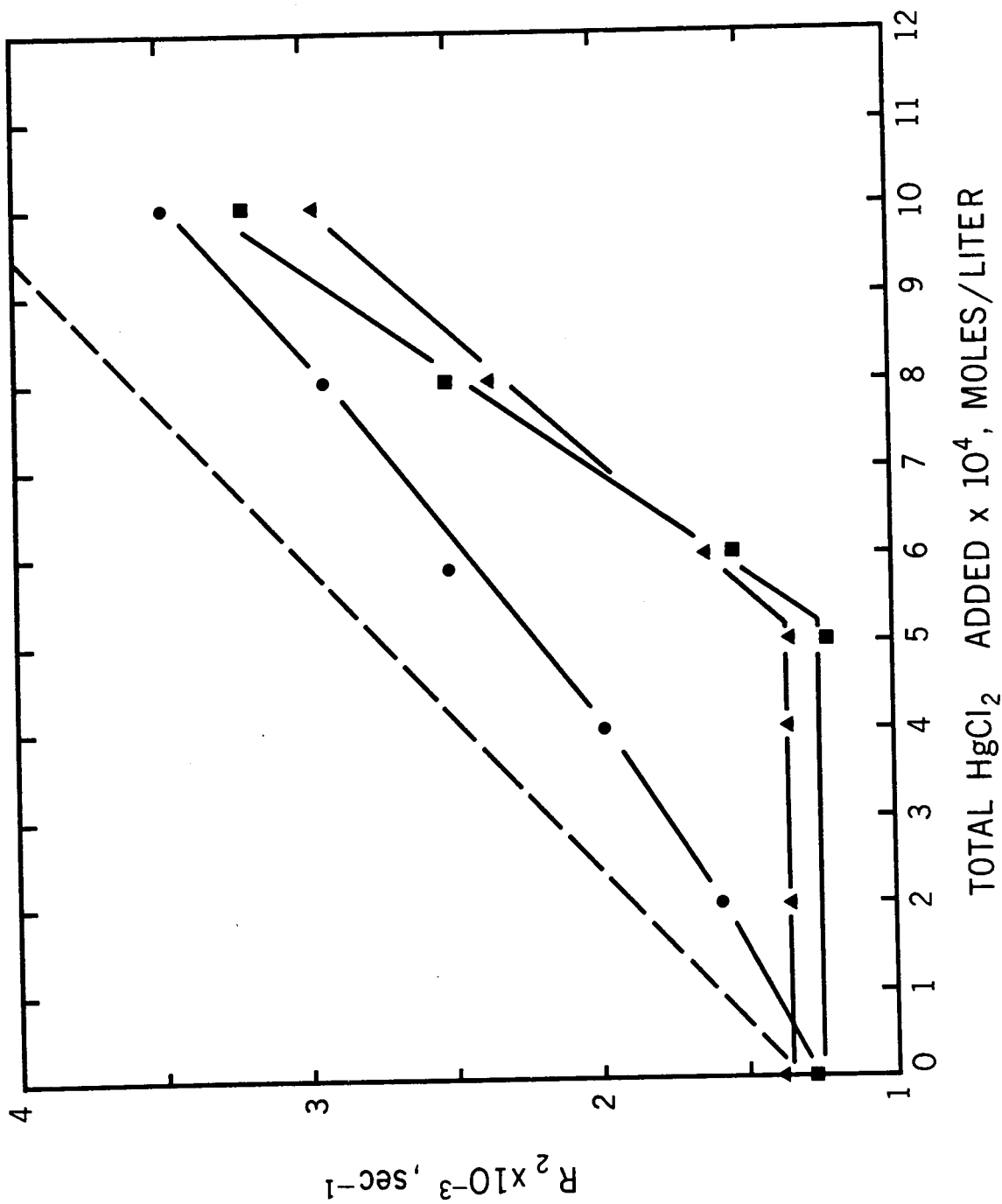


Fig. 23. Titration of  $1.0 \times 10^{-3}$  molar glutathione with  $\text{HgCl}_2$ . (●-●-●), pH 3.0; (▲-▲-▲), pH 6.1; (■-■-■), pH 11.2; (-----), no thiol present.

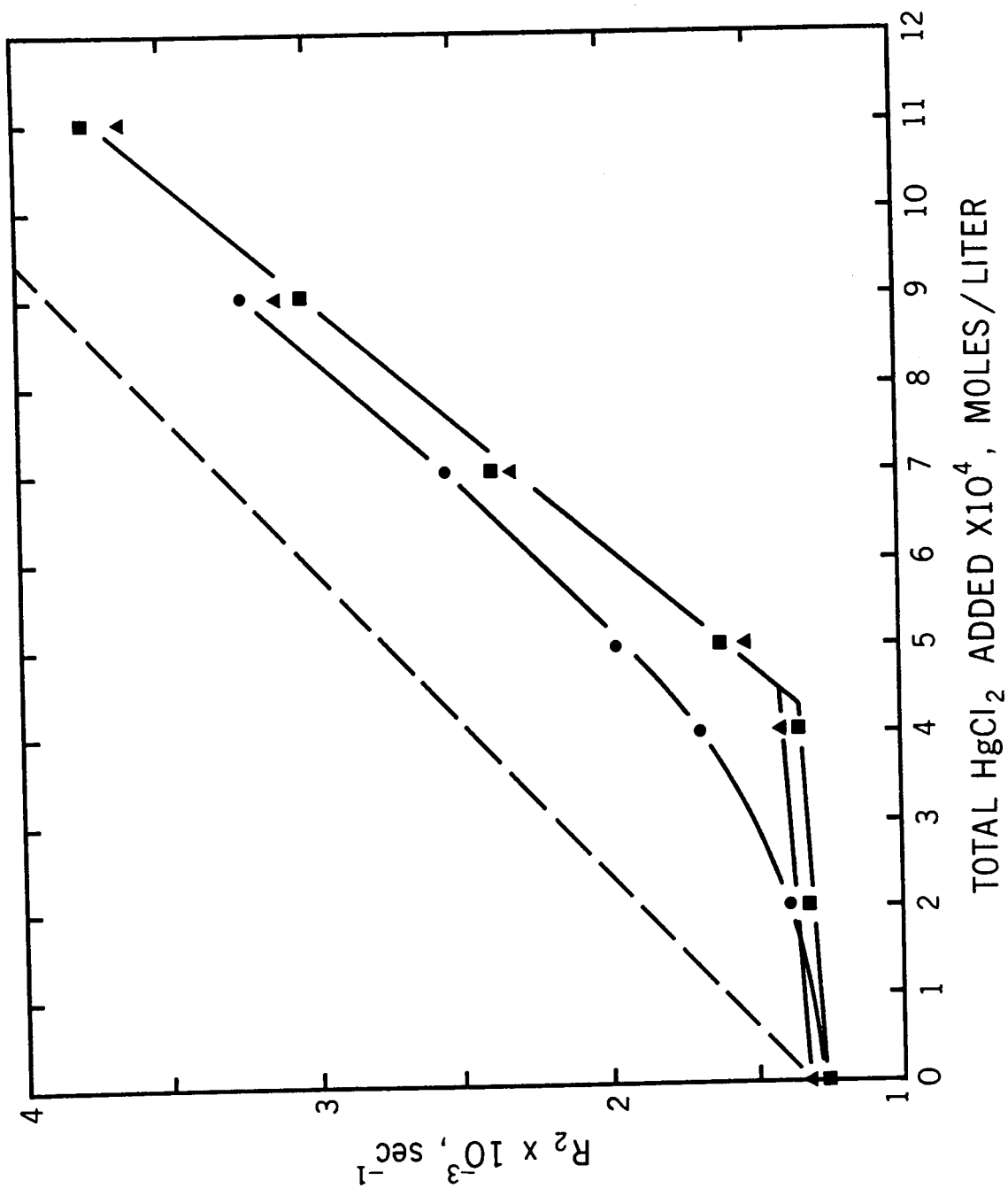
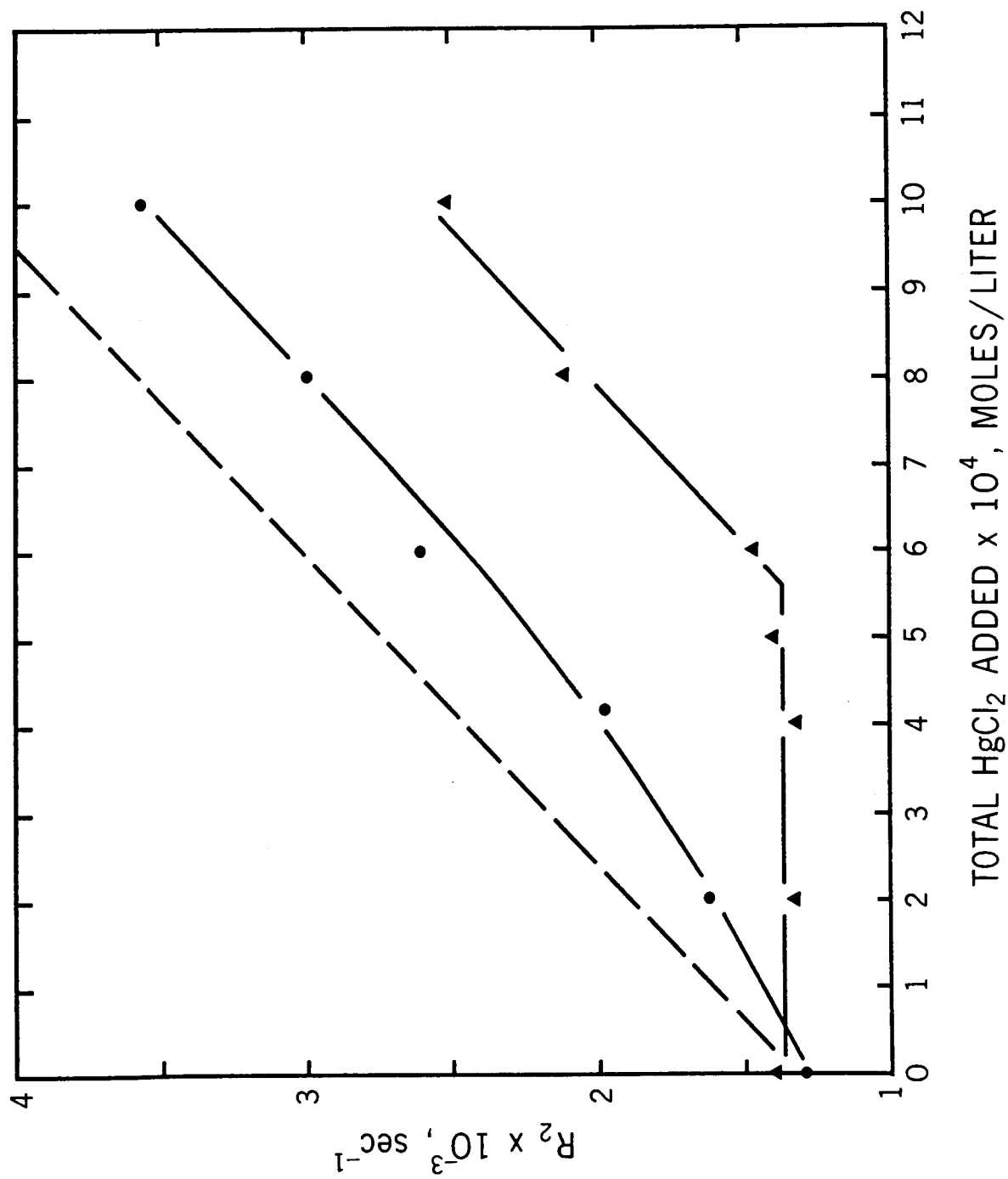


Fig. 24. Titration of  $1.25 \times 10^{-3}$  molar mercapto-  
ethanol with  $\text{HgCl}_2$ . (●-●-●), pH 2.4;  
(▲-▲-▲), pH 5.9; (-----), no thiol pre-  
sent.

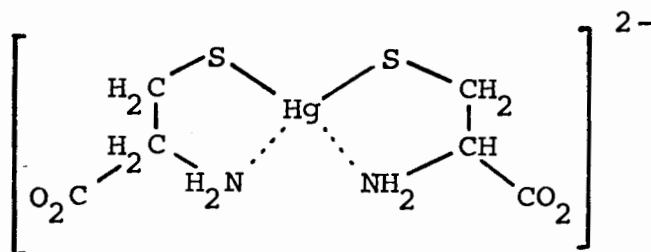




The results of this series of titrations support the conclusion by Kolthoff (44-47) that the final product of the reaction between a simply sulphydryl compound RSH and mercuric ion is the formation of the mercaptide RSHgSR. Consider those curves obtained near pH 6 and 11. Up to the end-point, occurring at

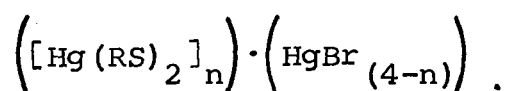
$$\frac{\text{RSH originally present}}{\text{Total HgCl}_2 \text{ added}} = 2$$

$R_2$  is constant for all the thiol compounds studied, indicating that the mercury in all cases exists in a form where it is inaccessible to halide exchange. The absence of exchange and the observed end-point suggest only one structure: the mercaptide  $\text{Hg}(\text{RS})_2$  where the four unfilled 5d orbitals on mercury are occupied in bonding to the 3p orbitals of sulphur and are not available for coordinate bonding to free halide ions. Further support for this conclusion may be drawn from the studies of Shindo and Brown (48) on the infrared spectroscopy of metal-thiol compounds. Shifts in the observed absorption maxima on complex formation demonstrated that dimers of the type



formed in the presence of excess RSH. Involvement of the amino and carboxyl groups in metal-thiol bonding was indicated, but the importance and exact nature of this type of binding is difficult to ascertain from the data presented in this study.

The amino and carboxyl groups also appear to have some role in interactions between the mercaptide dimer and free tetrabromide ion. In the case of mercaptosuccinic acid, cysteine, and glutathione, the slope of the portion of the titration curve past the end-point was greater than that found for the addition of  $\text{HgCl}_2$  to NaBr solution. A possible interpretation of this result is that the free carboxyl or amino groups displace one or more bromide ions from the tetrabromide complex to form a coordinately bound double complex,



The resulting increase in the overall rotation correlation time for the complex would appear as an increase in  $\alpha$ . The amino groups would be expected to participate more actively in coordinate binding in the unprotonated  $\text{NH}_2$  form and hence would bind more strongly at basic pH. The increase in  $\alpha$  for cysteine in going from pH 6.0 to 11.2 (Fig. 22) could be ascribed to this type of binding. Titration of solutions of

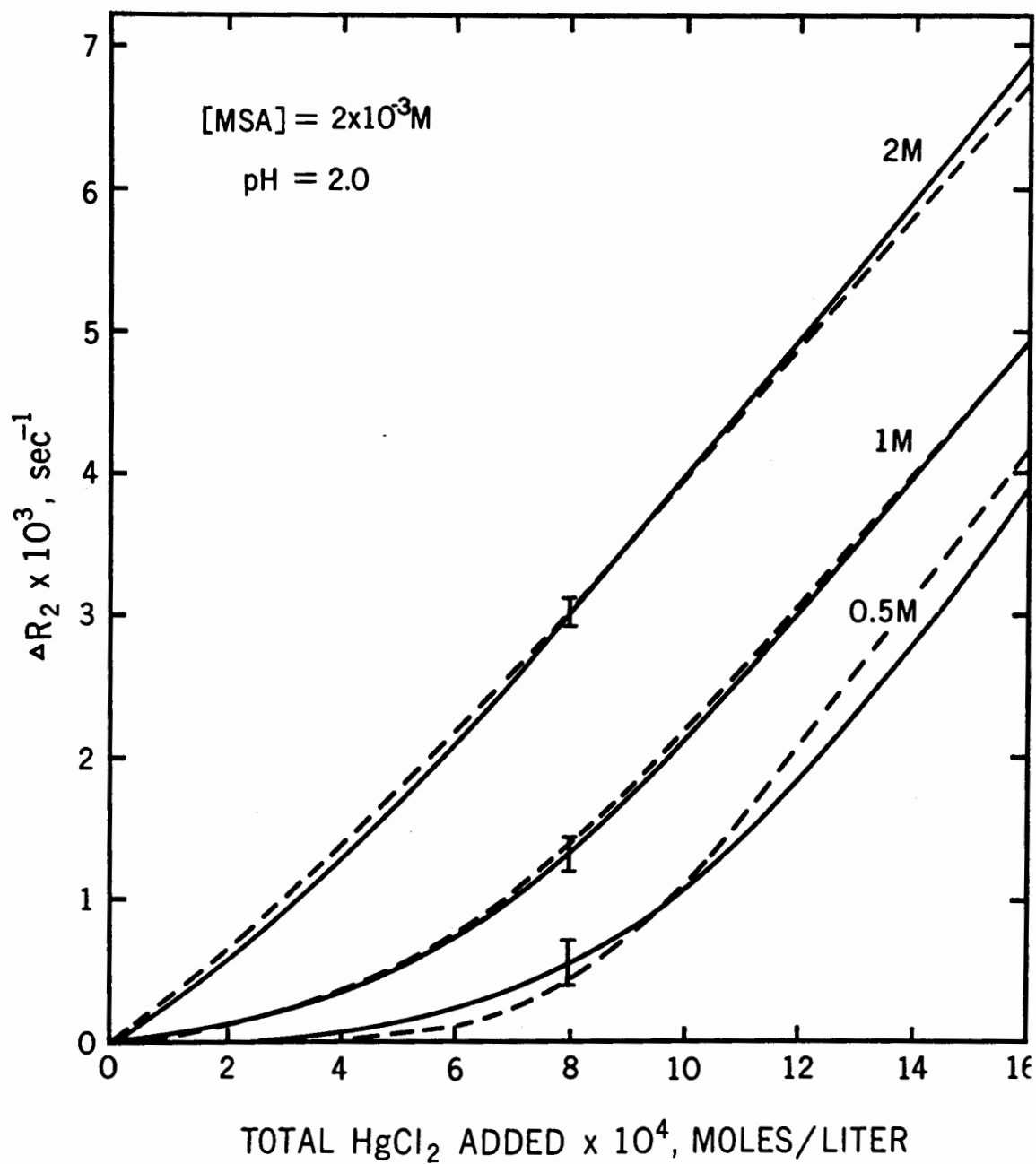
2 molar NaBr and 2 molar NaBr plus  $2 \times 10^{-3}$  molar succinic acid with  $\text{HgCl}_2$  produced identical values of  $\alpha$ , suggesting that the contribution of carboxyl groups to complex formation is of little importance. This view is supported by the fact that the slope of the second phase of the titration curve of mercaptosuccinic acid is much closer to the value found for 2 molar NaBr alone, than is the case for the two amino compounds. Complexes of this sort were postulated by Kolthoff (44, 45, 47), who observed formation of a compound  $\text{Hg}_2(\text{RS})_2$  in the presence of excess mercury with the second mercury atom appearing to be loosely bound. Shindo and Brown have also observed formation of such 1:1 complexes in several of the Ib and IIB metals. The situation is somewhat complicated by the fact that Kolthoff (45) was unable to observe the formation of the  $\text{Hg}_2(\text{RS})_2$  complex in the presence of 2 molar chloride. As expected, no increase in  $\alpha$  near pH 6 is observed with a non-complexing thiol such as mercaptoethanol (Fig. 24).

Some difficulty with decomposition of the thiol was encountered during the course of the titrations on cysteine and mercaptosuccinic acid, the latter compound being the least stable. Although titrations were performed as quickly as possible, shifts in the end-point were unavoidable with mercapto-

succinic acid and seemed particularly prevalent near pH 6, as may be seen from Fig. 21. In all cases, the end-point occurred at values of  $[RSH]/[HgCl_2]$  slightly less than two, which suggests that not all of the sulphhydryl groups in the thiol were active. The reason for this anomalous behaviour is not known.

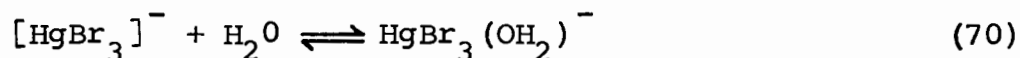
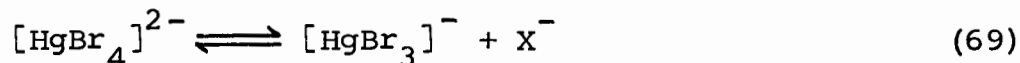
Near pH 2, the condition  $\mathfrak{R} < 10^{-10}$  was violated with all the compounds studied, with the result that no definitive end-point was obtained. Using the value for  $\alpha_{AVG}$  of  $2.75 \times 10^7$  liter mole<sup>-1</sup> sec<sup>-1</sup> derived from Table II, an attempt was made to fit the solutions of equation (61) to titration curves determined at low pH. Mercaptosuccinic acid was used as experimental material rather than cysteine or glutathione to eliminate any interference from the binding of mercury by amino groups. The results of a series of titrations performed on this compound at pH 2.0 for 0.5, 1.0 and 2.0 molar NaBr solutions are shown in Fig. 25; values for  $\Delta R_2 = R_2 - R_{2F}$  have been normalized to those expected for 1.0 molar NaBr to remove the  $[Br]^{-1}$  dependence of  $\alpha$  and to emphasize changes resulting from differences in  $\mathfrak{R}$ . It was found that in order to have a close fit, it was necessary to take into account thiol decomposition and set  $[MSA] = 1.83 \times 10^{-3}$  moles/liter in the calculation, this

Fig. 25. Dependence of the mercaptosuccinic acid titration curve at low pH on the bromide concentration. (—), experimental data; (----), theoretical relationship resulting from solution of equation (61). Error bars represent the error inherent in measurement of  $R_2$  at each bromide concentration. Values of  $\Delta R_2$  have been normalized to those expected for 1.0 molar NaBr.



value being based on the 8% decomposition apparent in Fig. 21. Under these conditions, an excellent fit was produced for 2.0 and 1.0 molar NaBr and a less exact fit for 0.5 molar NaBr.

Differences between the theoretical and experimental curves at 0.5 molar may be ascribable to the presence of other species such as  $\text{HgBr}_3(\text{OH}_2)^-$ . Since the equilibrium constant (40) for the reaction



is

$$K_o = \frac{[\text{HgBr}_4^{2-}]}{[\text{Br}^-][\text{HgBr}_3^-]} = 28.8 \text{ moles}^{-1} \quad (71)$$

it is apparent that in 0.5 NaBr, about 7% of the free mercuric ion exists as  $\text{HgBr}_3(\text{OH}_2)^-$  with one less site for exchange than the tetrabromide ion. This may explain why experimental values for  $\Delta R_2$  at higher mercury concentrations are approximately  $350 \text{ sec}^{-1}$  lower than expected. However, this is not the only possible explanation. The clarification of the exact phenomena occurring under these conditions would be an interesting problem but is outside the scope of this work.



A simple chemical model based only on the chemistry of the sulphhydryl group has been shown to be capable of describing much of the behaviour of the equilibria encountered in the study of these simple compounds. From nuclear lifetime measurements on these exchanging systems, it has been possible to draw conclusions concerning the structures of the complexes observed here. The major limitation of the simple mercuric bromide probe appears to be the instability of the mercury-sulphur bond at low pH, rendering difficult direct measurement on the sulphhydryl groups of proteins (for example, pepsin, rennin, or pepsinogen) requiring such conditions. On the basis of this information, the application of the probe to the study of protein structure may now be considered.

## STUDIES ON HEMOGLOBIN

### I. Introduction

To date, the majority of halide-probe studies on proteins have dealt with methods of estimating the number and availability of metal-ion binding sites from measurements of the  $^{35}\text{Cl}$  line-width  $\Delta\nu$ . Stengle and Baldeschwieler (5) have titrated the sulphhydryl groups of equine and human hemoglobin with mercuric chloride, finding two identical sites in the native protein. A similar study by Ellis et al. (12) revealed one and perhaps two sulphhydryl groups with different  $\alpha$  values in bovine hemoglobin and one group in horseradish peroxidase. Bryant (9) has reported detecting 0.5 sulphhydryl group in bovine mercaptalbumin and has evaluated the relative strengths of protein-metal bonding for the Group IIb metals. In all three cases,  $\Delta\nu$  was found to be dependent on pH and the presence of denaturants, presumably reflecting a structural change within the protein. However, changes in  $\alpha$  or  $\Delta\nu$  generally did not provide sufficient data to determine whether these effects were the result of differences in protein flexibility near the probe site, changes in the exchange rate, or increased binding at other sites on the molecule. Non-specific binding of halide ions to the protein has been observed in most studies; this phenomenon

has been studied in carboxypeptidase A by Bryant (10) and in several other proteins by Zeppezauer et al. (18). The binding of zinc as a coenzyme has been demonstrated by this method for carbonic anhydrase by Ward (17) and for pyruvate kinase by Cottam and Ward (11). The chloride probe method has also been used to titrate the sulphhydryl groups of the erythrocyte membrane (14).

Two authors have recently reported experiments wherein organic mercurials were used to study specific sites in macromolecules. Haugland et al. (6) have succeeded in titrating antidinitrophenyl antibody with a mercury-labelled hapten, while Marshall (7) has bound the inhibitor p-mercuribenzene-sulfonyl fluoride to the catalytic site of  $\alpha$ -chymotrypsin. In the latter study, rotational movement of the bound probe appeared to be hindered when a single methionine group was alkylated. These studies represent the most promising area for future halide-exchange studies and will be discussed in detail in the concluding section.

It is clear that the halide-probe technique is applicable to a number of biologically important systems and has considerable potential for the detection of structural changes within these systems. However, it is equally evident that a method of determining which effect is responsible for the observed phe-

nomena is needed before this technique can yield quantitative information about macromolecular conformational changes. The experiments described here will hopefully pave the way to a more quantitative description of these phenomena.

The method described in the section dealing with the theory of the exchange effect for measuring  $k_1$  and  $T_2$  for a bound halide-ion probe will be applied to the binding of bromide ions to the free sulphhydryl groups of equine methemoglobin. Experiments designed to detect conformational changes within the hemoglobin molecule by observing these parameters in the native and structurally modified protein will be described.

Hemoglobin was chosen as the subject of this study for a number of reasons. Present knowledge of the molecular structure of this protein is more exact than that of any other macromolecule, largely due to extensive X-ray crystallographic studies (49-52). The biochemistry of hemoglobin has been studied under a wide variety of conditions; the review by Rossi Fanelli *et al.* (53) provides a most comprehensive overview of this field. In its native state, the protein has four sulphhydryl groups that are not involved in disulphide bridging, one at cysteine residue G11 (#104) on each  $\alpha$  chain and one at cysteine residue F9 (#93) on each of the  $\beta$  chains (54). As may be seen from Fig. 26, only the latter two sites are accessible to the surrounding medium

Fig. 26. Structure of the tetrameric hemoglobin molecule (from Dickerson and Geis (55)). The free sulphhydryl group on the  $\alpha$  chain is buried within the molecule on the G-helix, while the sulphhydryl site responsible for binding mercuric ion to the  $\beta$  chain is situated on the F-helix and is in contact with the surrounding medium. Those residues which participate in the  $\alpha_1\beta_2$  contacts are labelled in bold type. Dissociation into dimers is believed to occur through breaking of the  $\alpha_1\beta_2$  and  $\alpha_2\beta_1$  contacts (71).

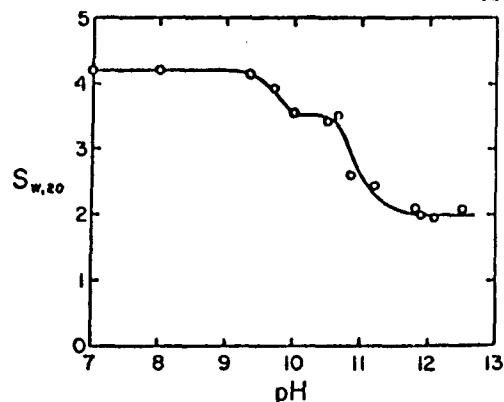


(53). Since free sulphhydryl sites are available on the protein, halide-exchange measurements may be performed using mercuric ion to bind bromide to the protein, thus avoiding the synthesis of more complex mercurials. Finally, this system has previously been studied by steady-state chloride NMR (5); hence a comparison of results with chloride and bromide probes is possible.

Of the many structural alterations exhibited by hemoglobin in response to changes in the molecular environment, the conformational changes induced by basic pH were chosen as a model system for evaluating the capabilities of the bromide-probe method. The results of the sedimentation studies of Kurihara and Shibata (56) provide insight into the behaviour of this system and will be summarized briefly here before discussion of the NMR data. The sedimentation constant  $S_{w,20}$  (extrapolated to zero protein concentration in water at 20°C) of equine hemoglobin solutions was measured between pH 7.0 and 12.5, and was found to decrease with increasing pH, as shown in Fig.

27. All of the observed sedimentation patterns showed only a

Fig. 27. Effect of high pH on the  $S_{w,20}$  of equine hemoglobin in 0.2 molar phosphate buffer.  $S_{w,20}$  expressed in Svedberg units. (from Kurihara and Shibata (56)).



single peak, suggesting that only a single hemoglobin type was present.

The denaturation process may be divided into two steps: the first step from the native molecule to the component of  $3.48 \pm 0.05$  S and the second step from the 3.5 S component to the component of  $2.01 \pm 0.06$  S which is completed above pH 11.9. Measurement of diffusion constants at pH 7.0, 10.5, and 12.1 yielded molecular weights of 67,800, 67,300 and 35,300 respectively. It was clear that the protein retained its tetrameric structure during the first step, but dissociated into halves in the second step. From these data, the frictional ratio  $f/f_0$ , where  $f$  is the observed frictional coefficient of the protein and  $f_0$  is the frictional coefficient for a hypothetical sphere, could be calculated (57). This quantity was found to be 1.31, 1.58, and 1.78 at pH 7.0, 10.5, and 12.1, respectively. Since the frictional ratio is related to the shape of the macromolecule (58), it is apparent that the conformation of the tetramer is altered by increasing pH. These changes were found to be reversible below pH 12.

Experiments were therefore performed to measure the exchange rate and correlation time for the bound bromide probe at pH 7.0 and 10.0 in an attempt to observe any conformational changes occurring within this range.  $\alpha$  was determined from the



slope of the curve for titration of the two free sulphhydryl groups with  $\text{HgCl}_2$ . Titrations were performed at different bromide concentrations and  $T_{2B}$  and  $k_1$  evaluated from a plot of  $\alpha^{-1}$  versus  $[\text{Br}^-]$  according to equation (48):

$$\alpha^{-1} = \frac{1}{k_1} + \frac{T_{2B}[\text{Br}^-]}{n}$$

where  $n$  represents the number of binding sites per molecule.

$\tau_c$  could then be calculated from the expression for  $T_{2B}$  (38).

## II. Characterization of the Hemoglobin Preparation:

Since the hemoglobin used in this study was a commercial preparation, experiments were performed to determine the purity of the samples received and the effect, if any, of preparation and storage on the protein. The results of these tests will be described briefly before discussion of the NMR experiments.

### A. Experimental

#### 1. Materials

Twice-recrystallized equine methemoglobin, lot #U3770, prepared by the method of Drabkin (59) was purchased from Mann Research Laboratories and used in the studies described here. A similar product purchased from Pentex Inc. was used initially but was abandoned because of variations in the sulphhydryl content. The protein was stored at 4°C in a dessicator over anhydrous manganese perchlorate. Before NMR studies were performed, all of the hemoglobin samples from Mann were thoroughly mixed to ensure homogeneity of the sample. All other chemicals were reagent grade.

#### 2. Cyanomethemoglobin Assay

The hemoglobin content of shipments from Mann and Pentex was determined by conversion to cyanomethemoglobin followed by measurement of the absorbance at 540 nm (60-63).

Stock solutions for the cyanomethemoglobin assay were prepared according to the method of Wootton and Blevin (60):

Stock Solution I: 200 mg  $K_4Fe(CN)_6$  per liter

50 mg KCN

140 mg  $KH_2PO_4$

Stock Solution II: 0.1 molar sodium tetraborate.

25 mg of hemoglobin were dissolved in 8 ml of solution I. After 15 minutes, 2.5 ml of solution II were added, followed by enough solution I to make the volume up to 25 ml. No turbidity could be detected in the resulting cyanomethemoglobin solutions. Absorbances at 540 nm were read at room temperature in a Cary 14 spectrophotometer using standard 10 mm path length cuvettes. An absorptivity of  $11.0 \times 10^3$  liter mole<sup>-1</sup> cm<sup>-1</sup> per heme (61-63) was used in calculating the hemoglobin content.

### 3. Spectra

The hemoglobin absorption spectrum was determined by dissolving samples in 0.2 molar sodium phosphate buffer at pH 7.0 and filtering the resulting solution under pressure through a 0.65  $\mu$ m Millipore filter before recording spectra. Solutions prepared in this way showed no signs of turbidity. Hemoglobin concentrations were such that the absorbances were between 0.45 and 1.10 for all the samples tested. Each absorptivity is the

average of measurements on two different samples, with the exception of the absorptivity for the Soret peak, which is the average of three samples. In all but one case the two measurements agreed to within 2%.

#### 4. Column Chromatography

Gel suspensions for gel filtration and ion-exchange chromatography were prepared according to instructions in the literature supplied by the manufacturer (64,65). These recommendations were followed in loading and eluting the columns. G-75 Sephadex of particle size 40-120  $\mu\text{m}$  and diethylaminoethyl (DEAE) Sephadex A-50 of the same particle size were a product of Pharmacia Fine Chemicals Ltd. Glass columns and accessories were a product of the same company. Columns were run in a cold room at 8°C. Samples were eluted from the G-75 column with 0.1 molar NaCl or NaBr in 0.05 molar phosphate buffer at pH 6.7. The gel column was loaded with 5.7 mg of hemoglobin dissolved in 0.5 ml of eluant. Dimensions of this column were 1.4 x 85 cm, and the flow rate was approximately  $3 \text{ ml cm}^{-2} \text{ hr}^{-1}$ . Hemoglobin was eluted from a 1.4 x 28 cm column of the DEAE anion exchanger by a linear NaCl gradient. Starting buffer was 0.1 molar tris(hydroxymethyl)aminomethane-HCl at pH 8.5. A volume of 2 ml of starting buffer containing 20 mg of hemoglobin was applied to the column. The flow rate

in this case was  $14 \text{ ml cm}^{-2} \text{ hr}^{-1}$ . Before the ion-exchange column was loaded, hemoglobin solutions were dialyzed overnight at  $8^{\circ}\text{C}$  against twenty-five volumes of 0.1 molar tris-HCl starting buffer at pH 8.5 to remove any salt present in the protein. Samples for gel filtration were not dialysed. Fractions were collected on an LKB fraction collector, and fraction volume was determined from the weight of a representative number of fractions. Spectra of column fractions were run in  $22 \times 2 \times 10$  mm microcuvettes.

pH measurements were performed as previously described. The pH of column eluants was measured on cold solutions in order to minimize any effects from the temperature dependence of the buffer pH.

## B. Results and Discussion

### 1. Cyanomethemoglobin Assay

The hemoglobin content of shipments from Mann and Pentex was determined by conversion to cyanomethemoglobin followed by measurement of the absorbance at 540 nm (60-63). Two portions of Pentex hemoglobin contained 79 and 80% hemoglobin by weight. Repetition of the assay on three portions of Mann hemoglobin yielded hemoglobin contents of 83, 85, and 86%, the average being 85%. All methemoglobin concentrations reported here

are corrected to this hemoglobin content.

## 2. Absorption Spectra

The absorption spectrum of the hemoglobin received from Mann is shown in Fig. 28, together with absorptivities calculated by Keilin and Hartree (66) and Scheler et al. (67). Exact values for these quantities are given in Table III. Peak position identified the hemoglobin as being in its ferric form. Some discrepancies between the calculated absorptivities and previously-published results (66,67) are apparent, particularly at the Soret band and in the range 460-590 nm. These differences could conceivably be due to the presence of 10-20% oxy-hemoglobin; however, addition of a 100-fold excess of ferri-cyanide to the methemoglobin solution caused only minor changes within this range (dotted line in Fig. 28), proving that 2% or less of the reduced form was present. Furthermore, Huisman et al (68) have published a spectrum of human methemoglobin similar in shape to that reported here. The clarification of these spectral inconsistencies must await future studies.

## 3. Column Chromatography

Methemoglobin samples were subjected to Sephadex gel filtration and ion-exchange chromatography on DEAE anion exchanger in order to evaluate the homogeneity and degree of dissociation of the protein and to determine whether the 15

Fig. 28. Absorption spectrum of equine methemoglobin. Absorptivities at wavelengths below 450 nm are to be read from the left-hand scale, while values for wavelengths above 450 nm are to be read from the right-hand scale. The solid line represents values for the equine methemoglobin from Mann. Absorptivities found for equine methemoglobin by Keilin and Hartree (66) and Scheler et al. (67) are shown by the dashed line and the crosses, respectively. The dotted line near 575 nm denotes the spectral change caused by addition of a 100-fold excess of ferricyanide.

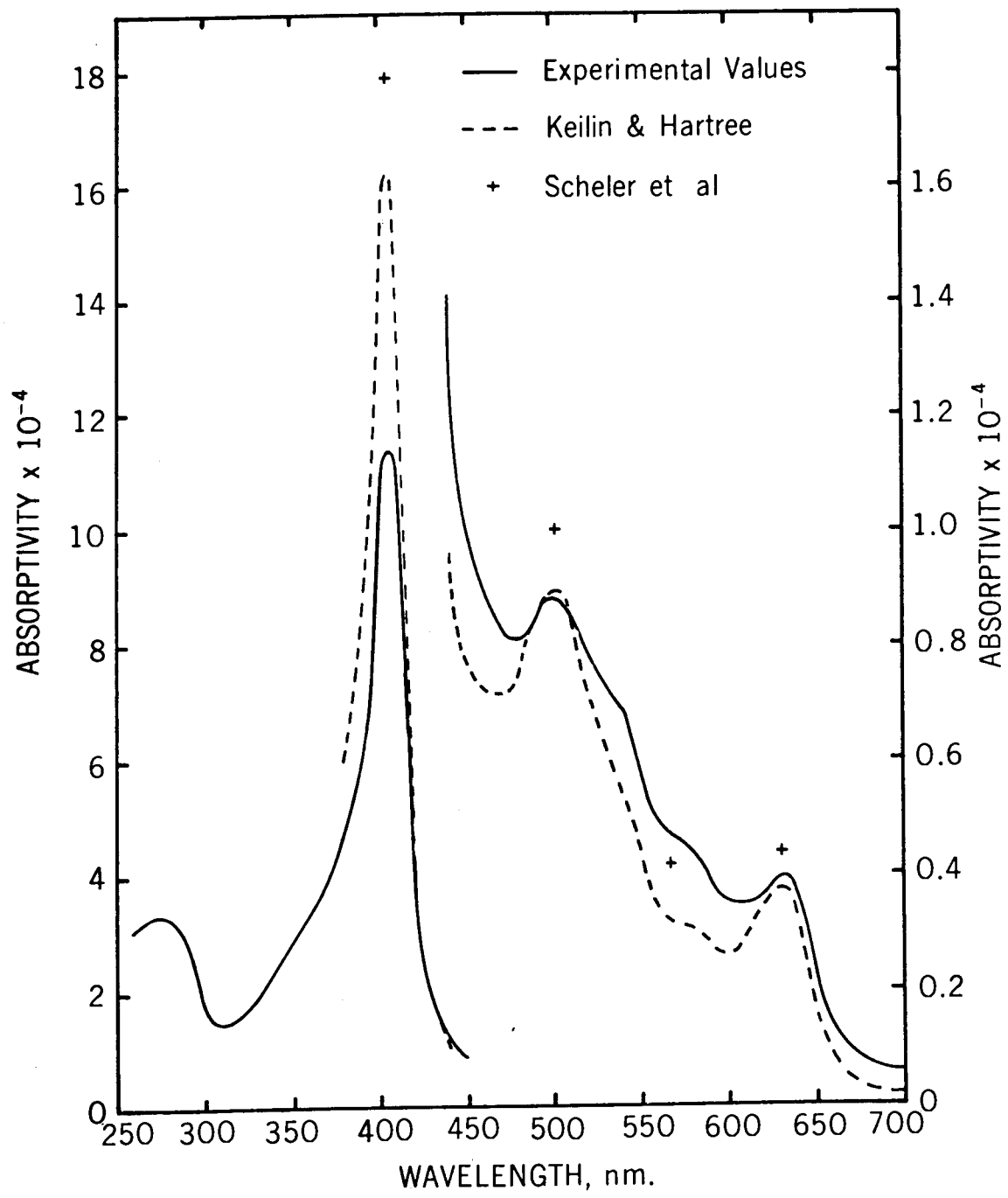




Table III. Absorptivities of equine methemoglobin in 0.2 molar phosphate buffer at pH 7.0.

$\lambda_{\text{max}}$ , nm	$\alpha/\text{heme} \times 10^{-4}$	$\alpha/\text{heme} \times 10^{-4}$ (a)	$\alpha/\text{heme} \times 10^{-4}$ (b)
275	3.30	-----	-----
405	11.4	17.9 (404.5 nm)	16.2 (404 nm)
500	0.89	1.0 (500 nm)	0.89 (505 nm)
534*	0.71*	-----	0.62 (531 nm) *
571*	0.47*	0.42 (575 nm)	0.31 (576 nm) *
630	0.40	0.44 (631 nm)	0.38 (632 nm)

(a) Scheler et al., pH 6.6 (67).

(b) Keilin and Hartree, pH 6.8 (66).

\* Peak height and position uncertain.

weight percent impurity was the result of bound water or was due to some proteinaceous contaminant. Gel filtration profiles for hemoglobin eluted from G-75 Sephadex by 0.1 molar NaBr and 0.1 molar NaCl are shown in Figs. 29 and 30 respectively. Theoretical molecular weights were calculated from the relationship (64,69)

$$K_{av} = \frac{V_e - V_o}{V_t - V_o} \quad (72)$$

where  $K_{av}$  is the partition coefficient of the protein between the liquid and gel phases.  $V_o$  is the elution volume for a substance completely excluded from the gel.  $V_t$  is the bed volume of the column, and  $V_e$  is the elution volume for the protein.  $V_o$  was determined as the elution volume of a 1% solution of Dextran blue. The relation between  $K_{av}$  and the molecular weight was taken from the literature supplied by the manufacturer (64). An error in the estimation of fraction volumes for Fig. 29 resulted in the values for  $V - V_o$  being 5-12% too low. Since the exact magnitude of this correction is uncertain, uncorrected values of  $V - V_o$  are given in Fig. 29. The elution profile for methemoglobin eluted from DEAE Sephadex at pH 8.5 by a linear NaCl gradient is shown in Fig. 31.

Heme (405 nm) and protein (275 nm) absorbance in Fig. 29 peak at the same elution volume, indicating that no signifi-

Fig. 29. Gel filtration of Mann equine methemoglobin on G-75 Sephadex. Flow rate:  $3.2 \text{ ml cm}^{-2} \text{ hr}^{-1}$ . Eluant: 0.1 molar NaBr in 0.05 molar phosphate buffer, pH 6.7. Sample: 5.7 mg in 0.5 ml eluant. Bed dimensions: 1.4 x 85 cm.

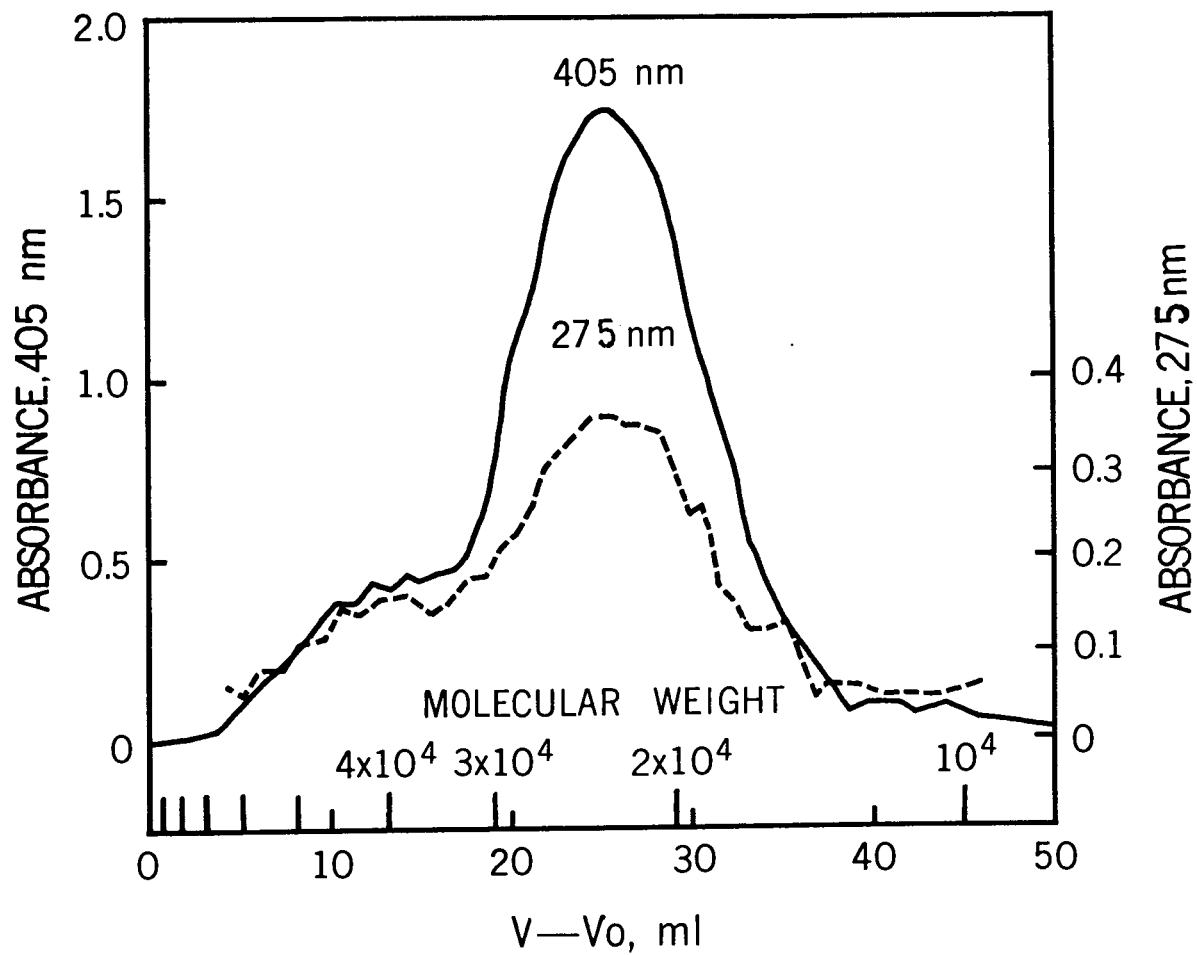


Fig. 30. Gel filtration of Mann equine methemoglobin on G-75 Sephadex. Flow rate:  $3.3 \text{ ml cm}^{-2} \text{ hr}^{-1}$ . Eluant: 0.1 molar NaCl in 0.05 molar phosphate buffer, pH 6.7. Sample: 5.7 mg in 0.5 ml eluant. Bed dimensions: 1.4 x 85 cm.

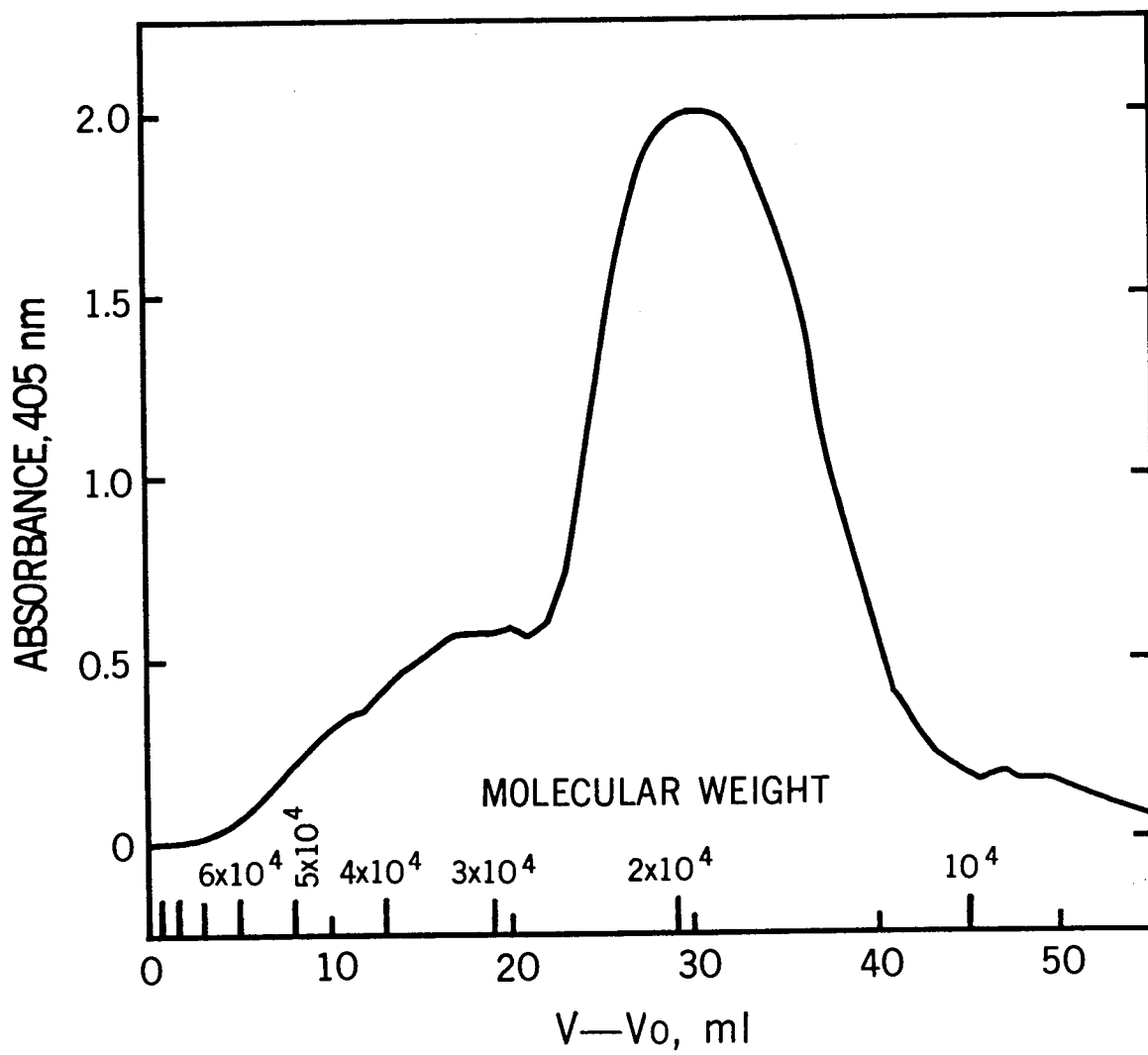
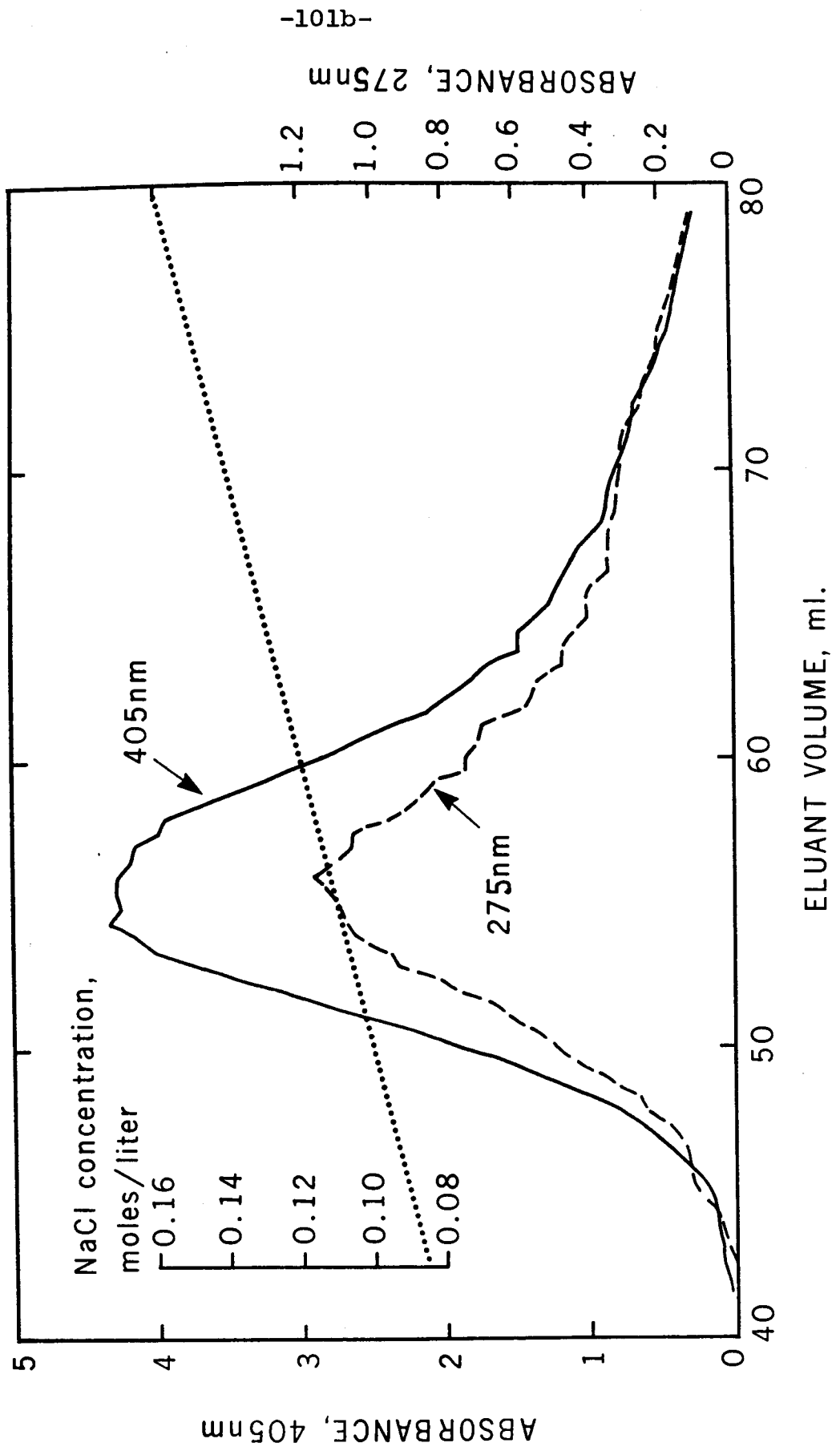


Fig. 31. Chromatography of Mann equine methemoglobin on DEAE Sephadex A-50 in 0.1 molar tris-HCl buffer at pH 8.5. Flow Rate:  $14 \text{ ml cm}^{-2}\text{hr}^{-1}$ . Sample: 20 mg hemoglobin in 2 ml starting buffer. Bed dimensions: 1.4 x 28 cm.



ABSORBANCE, 275nm

NaCl concentration,  
moles/liter

0.16  
0.14  
0.12  
0.10  
0.08

405nm

275nm

ABSORBANCE, 405nm

ELUANT VOLUME, ml.



cant amount of protein contaminant of molecular weight greater than 7,000 was present. The 15% non-heme portion of the sample must then be composed mostly of small organic molecules such as 2,3-diphosphoglycerate, salts, or bound water. Allowing for the volume error in Fig. 29, both gel profiles for the heme absorption consist of a peak at 19-20,000 molecular weight with a shoulder at 30-34,000 molecular weight. Chromatography of a sample of the equine hemoglobin from Pentex on this column resulted in a similar elution profile.

The reason for the existence of two peaks at relatively low molecular weight is not obvious at present. A large volume of literature supports the view that the hemoglobin tetramer exists in rapid equilibrium with the dimer and monomer (53), with dissociation occurring symmetrically (70,71):



Published studies (Table IV) suggest that at neutral pH and low ionic strength, the tetramer should predominate. The existence of this equilibrium causes the molecular weight estimated by the Sephadex method to increase towards the tetramer molecular weight as the concentration of the hemoglobin sample applied to the column is increased (73). The sample

Table IV. Molecular Weight of Hemoglobin Measured by Different Methods

Reference	Method	Conditions	Molecular Weight	Comments
56	Ultracentrifuge	0.2 molar phosphate buffer, pH 7.0	67,800	Horse hemoglobin
72	Light Scattering	0.05 molar phosphate buffer, pH 7.0 As above + 2 molar NaCl	67,500 40,300	Human oxyhemoglobin  As above
73	Gel Filtration, G-100 Sephadex	0.04 molar phosphate buffer +0.1 molar KCl, pH 6.8	~55,000	Bovine hemoglobin. Extrapolation of data to initial concentration employed here.
74	Gel Filtration, G-100 Sephadex	0.1 molar phosphate buffer +0.1 molar NaCl, pH 7.0 As above + 3 molar NaCl	47,000 38,000	Human methemoglobin. Protein concentration (4 mg/ml) less than half that employed here.  As above

concentration used here, 11.4 mg/ml, is higher than the concentrations used in published studies (73,74), suggesting that the molecular weights found here should be higher than the values in the literature. Based on the fact that Sephadex studies on hemoglobin generally show lower molecular weights than do other methods, it appears that the molecular sieve process encourages formation of monomer and dimer; however, molecular weight values as low as those found here have not been reported to date. It is also possible that some adhesion of the hemoglobin to the gel may occur, causing an increase in the elution volume. Horse hemoglobin may be more readily dissociated than the hemoglobin of other species, but the molecular weights calculated by Kurihara and Shibata (56) do not support this conclusion. Since the molecular weights of the peak and shoulder correspond closely to those expected for the monomer (17,000) and dimer (34,000) it is tempting to postulate the presence of stable monomer and dimer in this sample. However, unless the sample has undergone drastic chemical modifications, present knowledge of the hemoglobin dissociation process makes this situation highly unlikely. Further studies comparing weights calculated from gel filtration and from methods such as light scattering that do not involve partition of the different spe-

cies will be required to explain the low molecular weights calculated here. The fact that peaks occur at approximately the same molecular weights in Figs. 29 and 30 suggests that low concentrations of NaBr and NaCl have similar effects on the dissociation of equine hemoglobin. Investigation of the effect of high salt concentration on the elution profile was not carried out because of a tendency of the protein to aggregate at high ionic strength.

For a pure tetrameric protein in rapid equilibrium with dimer and monomer, the elution profile from gel filtration would be expected to be a single peak at the average molecular weight (75). The occurrence of a peak and a shoulder is therefore unexpected. However, studies on the elution of equine hemoglobin by a pH gradient from carboxymethylcellulose cation exchanger reveal the presence of two components in the proportion of 60 and 40% (68,76). Amino-acid analysis (77) reveals that equine hemoglobin exhibits four possible components arising from substitution of glutamine for lysine at 60 $\alpha$  and of tyrosine for phenylalanine at 24 $\alpha$ . Only two components can be separated electrophoretically. Perutz et al. (78) claim that the two species should be isomorphous. Although these substitutions occur at residues which are situated on the outside of

the molecule and are not involved in the  $\alpha_1\beta_2$  contact (49,51), it is conceivable that the two components may still have different dissociation constants  $K_1$  and  $K_2$ . A difference in the dissociation constants could cause each component to elute at a different average molecular weight. Bovine and normal human hemoglobin were found to consist of a single component (68) and would therefore not be expected to exhibit this type of behaviour. These data suggest a reason why this type of profile has not been reported in Sephadex studies on the latter two proteins (73,74), but they do not explain the presence of the single component observed for equine hemoglobin by Kurihara and Shibata (56). Alternatively, if adhesion of the protein to the gel were to occur, differences in the adhesion strength between the two components could easily cause the two hemoglobins to elute at different volumes. Further studies are obviously in order.

Only one peak appeared when the methemoglobin purchased from Mann was chromatographed on DEAE anion exchanger (Fig. 31). Apparently the anion exchange properties of the two components are not sufficiently different to permit their separation on this type of resin. Pharmacia claims separation of oxy- and carboxyhemoglobin on DEAE Sephadex under the conditions shown

in Fig. 31 (65). It is likely, therefore, that oxyhemoglobin, if present, would separate from methemoglobin under these conditions. The presence of a single peak in Fig. 31 supports the previous conclusion based on spectral data that the amount of oxyhemoglobin present is negligible.

### III. NMR Studies

#### A. Experimental

NMR titrations were performed on methemoglobin at pH 7.0 and 10.0 in 0.5-3.0 molar NaBr in 0.05 molar sodium phosphate and sodium bicarbonate buffers, respectively. At pH 7.0, hemoglobin solutions were not sufficiently stable for titrations to be carried out in the manner described for the simple thiols. At this pH, solutions became turbid after approximately 5 minutes in 3 molar NaBr and 20-30 minutes in 0.5 molar NaBr. Measurements were made on clear solutions whenever possible, although the presence of a slight turbidity did not produce any observable change in  $R_2$ . In performing the titrations at pH 7.0, separate methemoglobin portions were weighed out for each point on the titration curve, the portion was dissolved in the NaBr-buffer solution and mixed with the appropriate quantity of mercuric chloride solution, and  $R_2$  was measured as quickly as possible. For the addition of micro-liter quantities of  $HgCl_2$ , Oxford micropipettes were used as before. Sample volume was 10 ml in all cases.

At pH 10.0, methemoglobin solutions in 0.5 - 2.0 molar NaBr showed no sign of turbidity for over two hours. During this period, measurements of  $R_2$  performed on a sample of

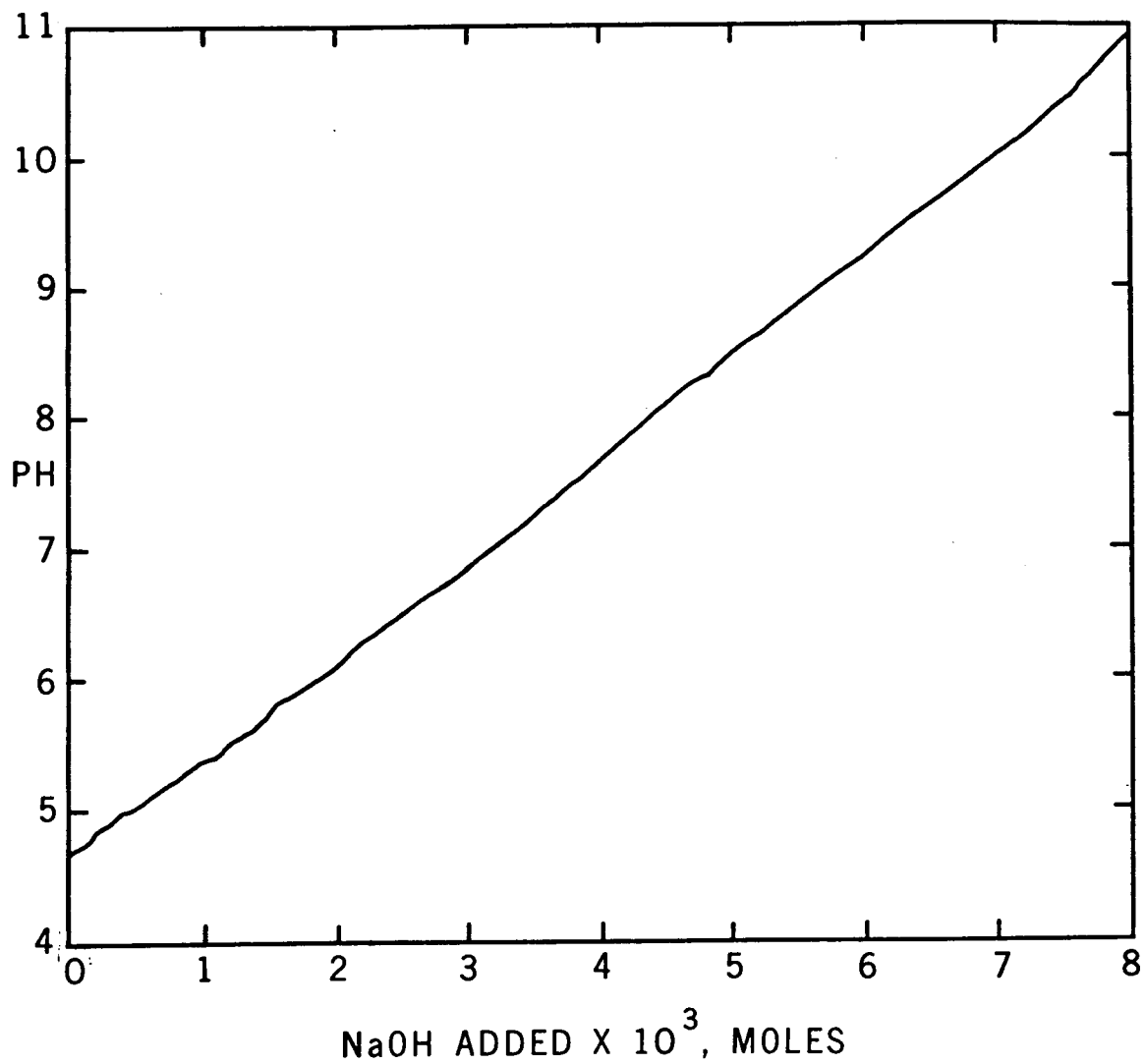
$4.1 \times 10^{-5}$  molar methemoglobin made  $5 \times 10^{-5}$  molar in  $\text{HgCl}_2$  did not detect any changes in  $R_2$  exceeding the error in the decay rate measurement. Because the protein showed no tendency at this pH to form aggregates which might cause  $R_2$  to change with time, titrations were performed by adding successive portions of  $\text{HgCl}_2$  to a hemoglobin solution. This procedure eliminated errors due to weighing and mixing a separate sample for each point on the titration curve. Protein instability precluded titrations in 3.0 molar NaBr at pH 10.0; under these conditions, methemoglobin solutions became turbid shortly after mixing, and precipitation of the majority of the protein occurred within minutes.

Two of the hemoglobin titrations reported here were performed using a mixed buffer composed of 0.05 molar succinic acid, 0.05 molar monobasic sodium phosphate, 0.05 molar Tris, and 0.05 molar glycine with sufficient NaOH to achieve the desired pH. This buffer had a practically uniform buffer capacity between pH 5 and 10.5 (Fig. 32) but was not used in the rate constant measurements because of its relatively high ionic strength.

Values of  $\alpha$  used in determination of  $T_{2B}$  and  $k_1$  were calculated by a linear least square fit of the titration data. Measurements of  $R_2$  were performed at  $[\text{HgCl}_2]/[\text{Protein}]$  ratios



Fig. 32. Titration curve of 0.2 molar mixed buffer composed of 0.05 molar succinic acid, 0.05 molar monobasic sodium phosphate, 0.05 molar Tris, and 0.05 molar glycine with sufficient NaOH to achieve the desired pH.



of approximately 0, 0.25, 0.50, 0.75, and 1.0. In order to maintain the decay rate within the range where accurate measurements could be performed, methemoglobin and  $\text{HgCl}_2$  concentrations were made proportional to the halide concentration. In 3.0 molar NaBr, a methemoglobin concentration of  $6.4 \times 10^{-5}$  molar was titrated with  $7.5 \times 10^{-3}$  molar  $\text{HgCl}_2$  solution. At pH 7.0, two titrations were performed for each halide concentration, with the value of  $R_2$  for each point being the average of decay-rate measurements on two separate hemoglobin samples. Titrations at pH 10.0 were repeated four times for each halide concentration.

Values of  $R_2$  were obtained by the two-point method. Usually 6-12 estimates of  $(t_1 - t_2)$  were made over different portions of the decay curve in order to average out the effect of any spurious signals superimposed on the decay. Each decay rate quoted here is the average of several separately tuned and averaged decays. The estimated error in decay rates measured by this procedure was  $40 \text{ sec}^{-1}$  in 2 molar NaBr and  $80 \text{ sec}^{-1}$  in 0.5 molar NaBr.

Measurement of pH was performed as previously described. Sample temperature was  $23 \pm 1^\circ \text{C}$ .

B. Results

The titration curve for  $3.8 \times 10^{-5}$  molar methemoglobin in 2.0 molar NaBr at pH 7.0 is shown in Fig. 33. One sample of methemoglobin was used per point. Results of similar titrations of  $2.5 \times 10^{-5}$  molar methemoglobin in mixed buffer at pH 7.0 and 8.5 are given in Fig. 34. Using a separate portion of methemoglobin for each point introduced an uncertainty in  $R_2$  resulting from errors inherent in dissolving the individual portions, with the uncertainty being greater as the amount of hemoglobin to be dissolved increased and as increasing halide concentration caused the protein to be less soluble. The magnitude of the total possible error was estimated from the deviation of individual  $R_2$  values from the titration curve and was found to be  $100 \text{ sec}^{-1}$  for  $3.8 \times 10^{-5}$  molar methemoglobin and  $60 \text{ sec}^{-1}$  for  $2.5 \times 10^{-5}$  molar methemoglobin in 2.0 molar NaBr. The titration curve for  $3.8 \times 10^{-5}$  molar methemoglobin in 2.0 molar NaBr at pH 10.0 is given in Fig. 35. As this experiment was performed by adding aliquots of  $\text{HgCl}_2$  to a methemoglobin solution, the uncertainty in  $R_2$  was simply the error in estimating the decay rate from the averaged signal, or  $40 \text{ sec}^{-1}$ . The titration curve of Fig. 33 was performed once, as were those in Fig. 34. Two titrations were performed at pH 10.0, with the resulting curves being identical. It is apparent that the value

Fig. 33. Titration of  $3.8 \times 10^{-5}$  molar equine methemoglobin in 2.0 molar NaBr in 0.05 molar sodium phosphate buffer, pH 7.0. Vertical dashed lines represent the  $\text{HgCl}_2$  concentration at which the first and second sulphhydryl groups would be titrated. Use of a different methemoglobin sample for each point caused  $R_2$  to be subject to errors resulting from weighing and dissolving the individual samples. Possible error in  $R_2$  using this method is  $100 \text{ sec}^{-1}$ .

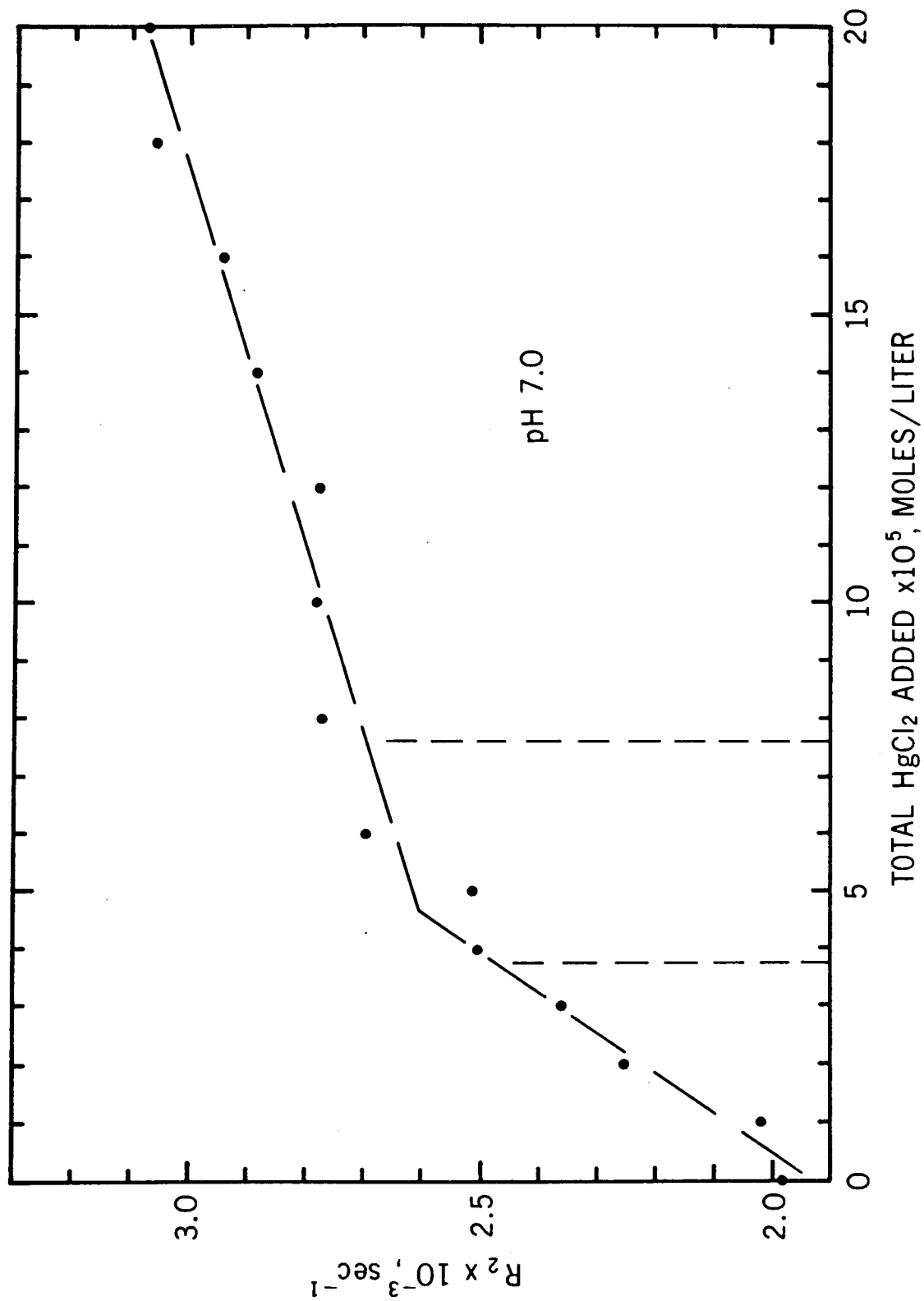


Fig. 34. Titration of  $2.5 \times 10^{-3}$  molar equine met-hemoglobin in 2.0 molar NaBr in 0.2 molar mixed buffer at pH 7.0 and 8.5. One met-hemoglobin sample used per point. Possible error in  $R_2$  is  $60 \text{ sec}^{-1}$ .

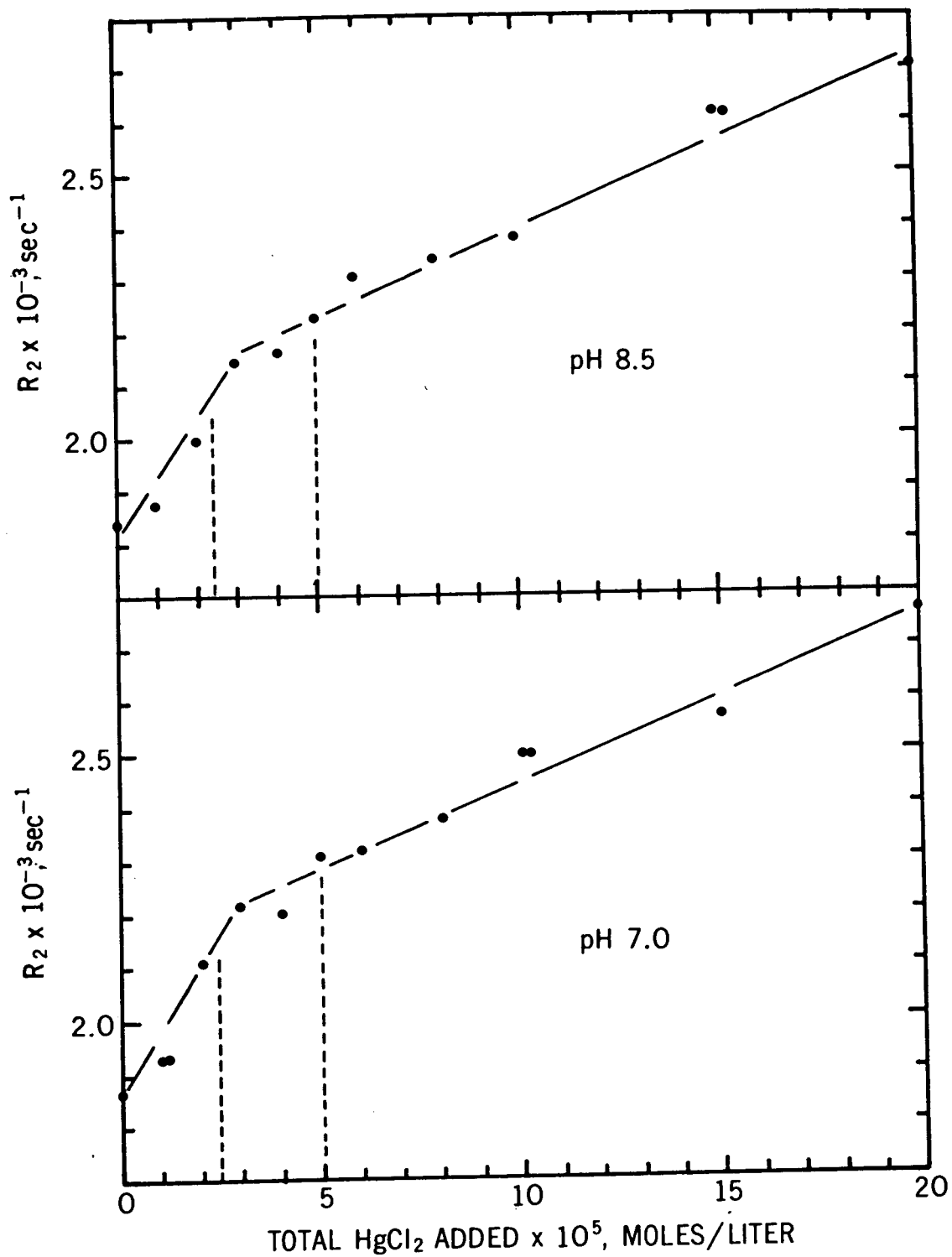
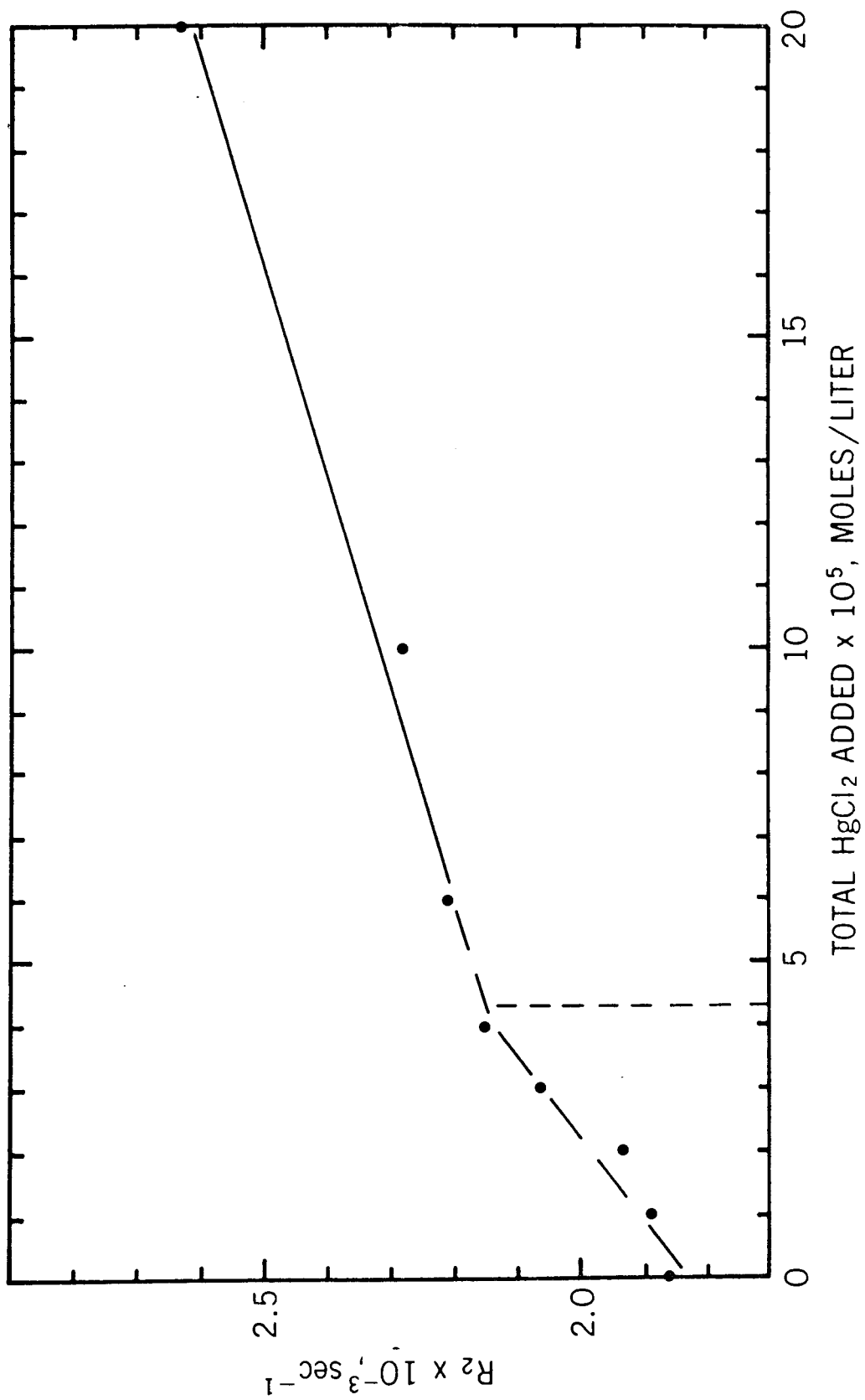




Fig. 35. Titration of  $3.8 \times 10^{-5}$  molar equine met-hemoglobin in 2.0 molar NaBr in 0.05 molar sodium bicarbonate buffer, pH 10.0. Estimated error in  $R_2$  is  $40 \text{ sec}^{-1}$ .

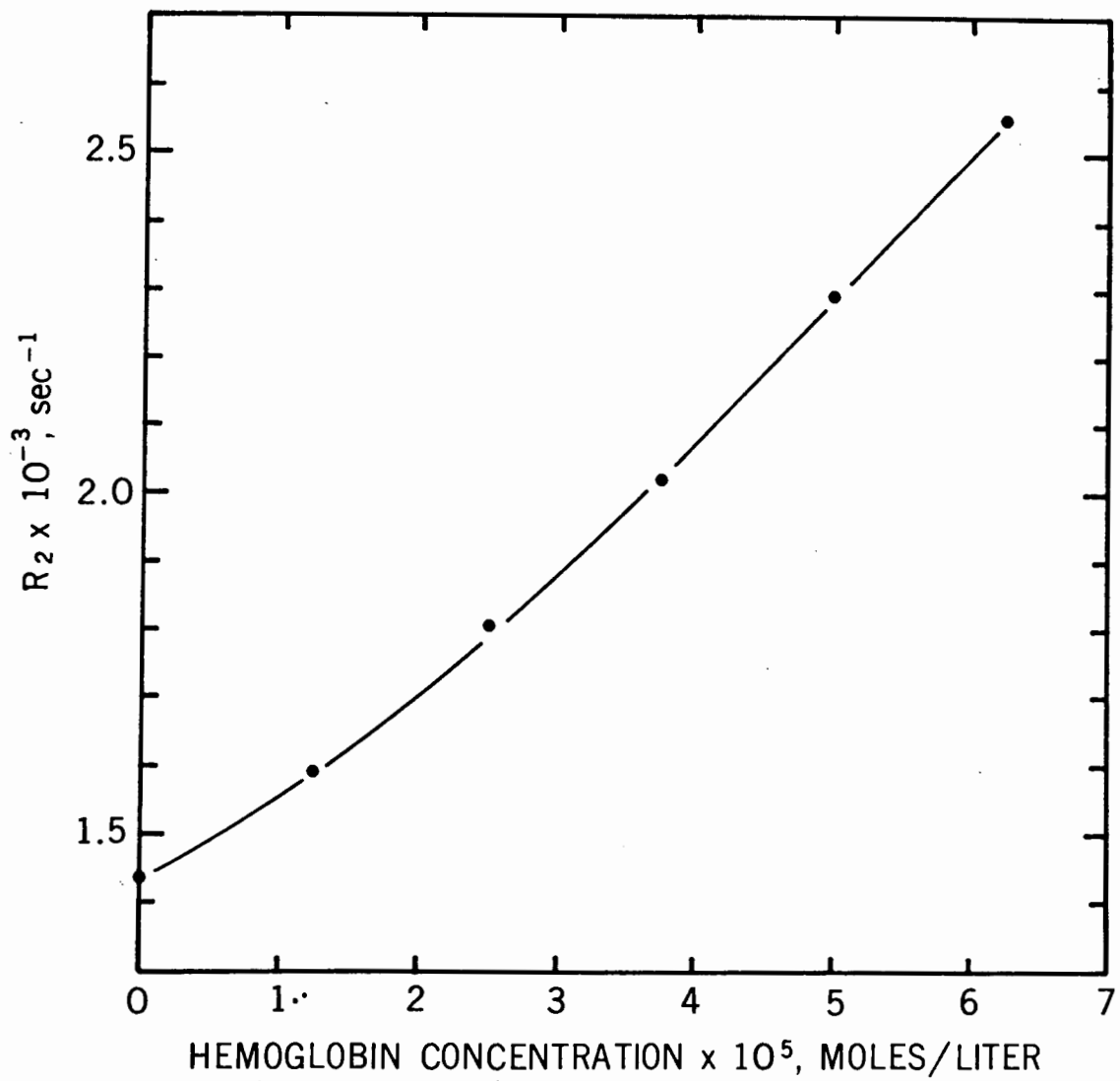


of  $\alpha$  is the same at pH 7.0 and 8.5, and approximately half that value at pH 10.0.

Assuming a molecular weight of 68,000 for the tetramer, the sulphhydryl titer for equine methemoglobin at pH 7.0 and 8.5 fell between 1.2 and 1.5 groups per molecule, while both titrations at pH 10.0 revealed the presence of 1.0 sulphhydryl group. Several titrations were carried out on the equine methemoglobin from Pentex Inc. One shipment of protein exhibited a sulphhydryl content of 2.5 - 2.7 groups per molecule, while a second shipment apparently contained only 1.3 - 1.5 groups. For this reason, this product was abandoned in favour of the methemoglobin from Mann Research Laboratories. Titrations that were performed on the second shipment of Pentex hemoglobin at pH 7.0 and 10.0 gave results similar to those shown for the product from Mann.

Besides halide exchange at the bound mercury atoms, hemoglobin was found to exhibit non-specific binding of bromide ions, as evidenced by the increase in the decay rate with increasing protein concentration shown in Fig. 36. This effect has been observed with a number of proteins by Zeppezauer et al. (18) and has been shown to be independent of the presence of bound metallic ions. Zeppezauer et al. concluded that this phenomenon is the result of quadrupolar relaxation resulting from interactions

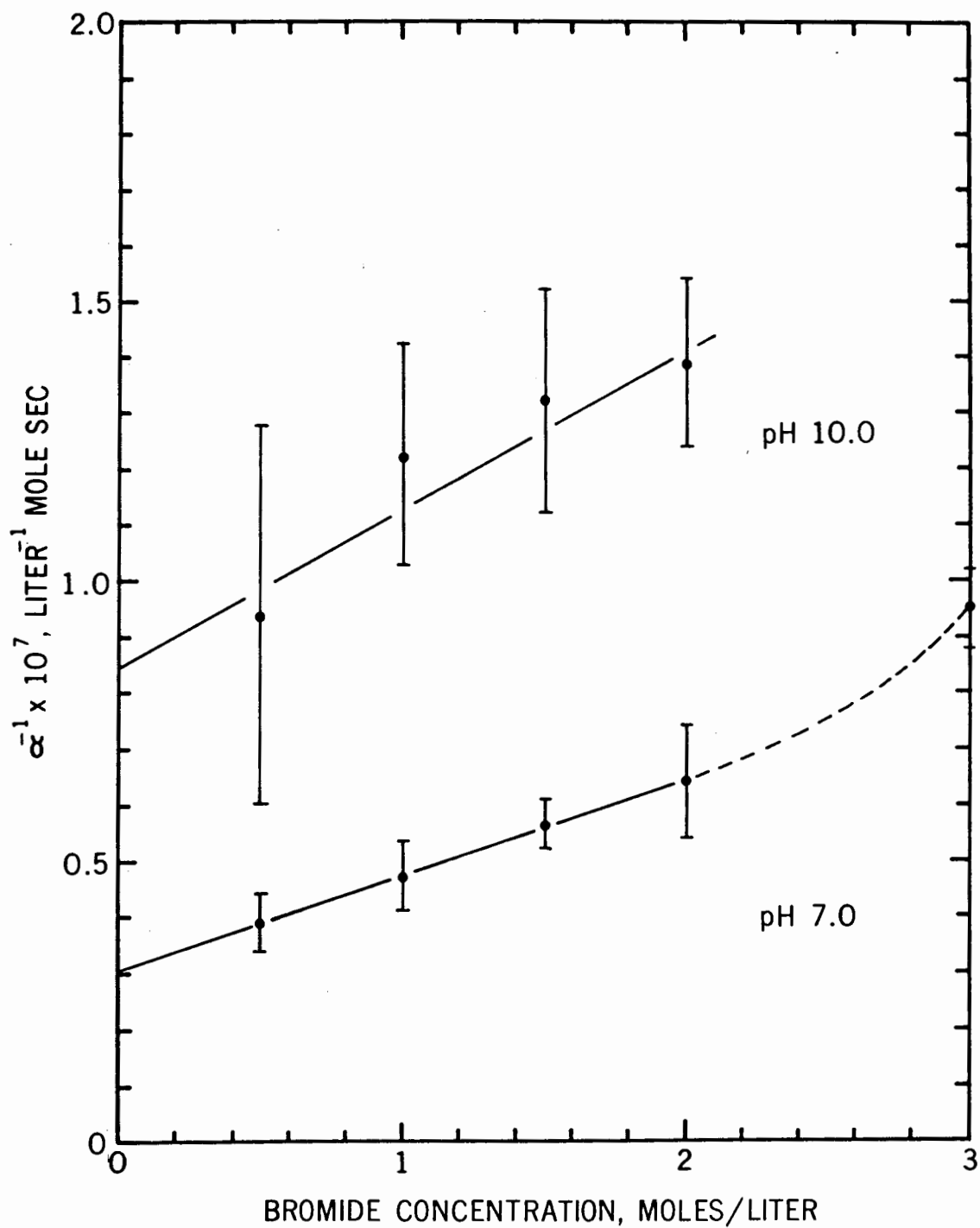
Fig. 36. Dependence of  $R_2$  on the methemoglobin concentration in the absence of mercury. Methemoglobin samples dissolved in 0.5 molar NaBr in 0.05 molar phosphate buffer, pH 7.0. Estimated error in  $R_2$  is  $80 \text{ sec}^{-1}$ .



between bromide ions and undetermined groups on the surface of the protein. Viscosity measurements performed in this laboratory on methemoglobin solutions showed that the increase in viscosity with increasing protein concentration contributes only slightly to this change in  $R_2$ . It is probable that the nonlinearity of the dependence of  $R_2$  on the methemoglobin concentration is due to dissociation of the tetramer at low protein concentration.

In order to separate the contributions of  $k_1$  and  $T_{2B}$  to the values of  $\alpha$  found for the sulphhydryl groups at pH 7.0 and 10.0, titrations were performed at different bromide concentrations and  $k_1$  and  $T_{2B}/n$  evaluated from the plots of  $\alpha^{-1}$  versus  $[\text{Br}^-]$  shown in Fig. 37 according to equation (48). For these experiments, the IBM 360 computer was programmed to calculate  $\alpha$  and its standard deviation by a least square fit of the titration data. Error bars in Fig. 37 represent the greater of either the average of the standard deviations of the individual  $\alpha$  values or the range of values of  $\alpha$ . A least square fit of the data in Fig. 37 produced values of  $k_1$  and  $T_{2B}/n$  given in Table V. Halide exchange was assumed to occur at two sulphhydryl sites per molecule of tetramer. Stated errors represent one standard deviation. Values for the cor-

Fig. 37. Determination of  $k_1$  and  $T_{2B}$  for equine methemoglobin at pH 7.0 and 10.0. Error bars represent the greater of either the average of the standard deviation of the individual  $\alpha$  values, or the range of values of  $\alpha$ .





relation time of the bound halide nucleus were calculated assuming an  $^{81}\text{Br}$  quadrupolar coupling constant of 320 MHz (40) and the expression of Abragam (38) for  $T_{2B}$ .

Several attempts were made to repeat the rate constant measurement at pH 7.0 with  $^{79}\text{Br}$  as an independent check on the calculated values of  $k_1$  and  $\tau_c$ . Because of field drifts in the magnet, reliable data could only be obtained in 2.0 molar NaBr, where the signal strength permitted short averaging periods. Two titrations at this bromide concentration yielded an average  $\alpha$  value of  $0.61 \pm 0.06 \times 10^{-7}$  liter mole $^{-1}$  sec $^{-1}$  for  $^{79}\text{Br}$ . Assuming that the correlation time for the bound probe at pH 7.0,  $0.74 \times 10^{-10}$  sec, is the same for both  $^{81}\text{Br}$  and  $^{79}\text{Br}$ , it is possible to estimate the magnitude of the exchange rate for  $^{79}\text{Br}$  from this value of  $\alpha$ . The exchange rate obtained using a value of 1.4 for the square of the ratios of the quadrupole moments of  $^{79}\text{Br}$  and  $^{81}\text{Br}$  is given in Table V. The estimated  $^{79}\text{Br}$  rate constant is in reasonable agreement with the rate constant measured for  $^{81}\text{Br}$ . Since equation (48) predicts that different isotopes should yield the same value for the rate constant, this result provides some verification of the data of Table V.

Table V. Experimental Values of  $k_1$  and  $T_{2B}/n$ .

Isotope	pH	$k_1 \times 10^7, \text{ l m}^{-1} \text{ s}^{-1}$	$T_{2B}/n \times 10^8, \text{ sec}$	$\tau_c \times 10^{10}, \text{ sec}$
$^{81}\text{Br}$	7.0	$3.27 \pm .06$	$1.68 \pm .04$	0.74
$^{81}\text{Br}$	10.0	$1.2 \pm 0.2$	$3 \pm 1$	0.4
$^{79}\text{Br}$	7.0	$3 \pm 1$	—	—

C. Discussion

It is not possible at present to put forward a satisfactory explanation of the low sulphhydryl contents found here. Published results generally confirm the existence of two free sulphhydryl sites per hemoglobin tetramer. X-ray structural studies (49,52) predict the existence of one exposed -SH group on each  $\beta$ -chain. Amperometric titration of equine hemoglobin (79) revealed 2.64 mercury-binding sites per molecule at 0°C. Stengle and Baldeschwieler (5) found approximately two sulphhydryls per molecule in 0.5-4.0 molar NaCl by  $^{35}\text{Cl}$  NMR, although no exact estimate of the sulphhydryl titer could be made from their data. Results of a similar titration performed on bovine hemoglobin (12) were interpreted in terms of two different mercury-binding sites; however, as there was considerable uncertainty in these data, the results could be construed as resulting from titration of only 1.5 sulphhydryl groups. This is the only published study which could be in agreement with the present values. The absence of evidence for  $\beta$ - $\beta$  chain contacts in the tetramer (59-52) and the fact that hemoglobin would be dissociated into  $\alpha\beta$  dimers by the concentrated salt solutions (Table IV) and sulphhydryl reagents (71) used in the halide-probe method, rule out the possibility that titration of one 93 $\beta$  cysteine resi-

due prevents titration of the corresponding site on the second  $\beta$ -chain via a conformational change.

It seems unlikely that the sulphhydryl content has decreased on storage; Cole et al. (80) have kept lyophilized human hemoglobin for two years without loss of sulphhydryl content. These authors do, however, mention recording lower sulphhydryl titers with lyophilized samples that were reluctant to dissolve.

The results of Kurihara and Shibata (Fig. 27) and the NMR data in Figs. 33-35 are in excellent agreement. Kurihara and Shibata found the protein structure unchanged between pH 7.0 and 9.0, but by pH 10.0 observed a conformational change occurring without dissociation.  $\alpha$  was the same at pH 7.0 and 8.5 but had decreased by half at pH 10.0, suggesting that the environment of the 93 $\beta$  sulphhydryl groups had undergone some structural alteration. Since hemoglobin is dissociated into dimers by the conditions encountered here, and yet exhibits the same pH effects found for the tetramer, conformational changes induced by basic pH are apparently not sensitive to the degree of dissociation of the tetramer.

The correlation time of  $0.74 \times 10^{-10}$  sec calculated at pH 7.0 is in excellent agreement with the value of  $10^{-10}$  sec estimated by Ellis (12) for the sulphhydryl groups of

bovine hemoglobin at pH 6.3. Correlation times obtained by the NMR halide-probe method are shorter by two orders of magnitude than those found by other methods; Haugland and Stryer (81) for example, used depolarization of fluorescence to calculate a rotational correlation time of  $5 \times 10^{-8}$  sec for anthraniloyl chymotrypsin. It is apparent that the probe is indicating motion at the binding site rather than rotation of the macromolecule as a whole.

Reference to Fig. 5 reveals that the values of  $k_1$  and  $\tau_c$  in Table V place bromide exchange in methemoglobin well into the intermediate region between the fast and slow exchange limits, where both  $k_1$  and  $\tau_c$  may be measured. Since other proteins may be expected to exhibit similar values for these quantities, it is likely that both parameters will in general be measurable with bromide probes.

The fact that the bromide exchange rates calculated here for protein-bound mercury are close to those found for the tetrabromide ion ( $3.7 \pm 4 \times 10^7$  liter mole<sup>-1</sup>sec<sup>-1</sup>) is a result of some consequence, since these rates are close to the theoretical diffusion limit (40). In this limit, the exchange rate will be sensitive only to steric effects limiting the rate of diffusion to and from the binding site and will not

depend on the chemistry of the mercury-bromide or mercury-sulphur bond. This result implies that the rate of bromide exchange with protein-bound mercuric ion should in general be dependent on the configuration of the protein chains surrounding the binding site. This prediction is verified by the pH-dependent change of  $k_1$  from  $3.27 \times 10^7$  liter mole<sup>-1</sup> sec<sup>-1</sup> (pH 7.0) to  $1.2 \times 10^7$  liter mole<sup>-1</sup> sec<sup>-1</sup> (pH 10.0). Exchange-rate measurements may therefore be expected to yield considerable information concerning the nature of conformational changes at specific sites in macromolecules.

The data of Table V demonstrates that the changes observed in  $\alpha$  between pH 7.0 and 10.0 result from alterations in both  $k_1$  and  $\tau_c$ . It is apparent that basic pH causes an increase in the flexibility of the environment of the 93 $\beta$  site (characterized by  $\tau_c$ ) and a decrease in its accessibility (characterized by  $k_1$ ).

Since the exact nature of the conformational changes occurring between pH 7.0 and 10.0 is unknown, interpretation of these data in terms of the structure of hemoglobin is difficult. Hemoglobin in acid medium has been found to adopt a highly disordered structure accompanied by the loss of  $\alpha$ -helical regions, but is believed to be much more stable toward alkaline

pH (82). Optical rotary dispersion spectra for equine met-hemoglobin show small changes in the ultraviolet between pH 6.0 and 9.5, but are difficult to interpret owing to interference from the Soret band Cotton effect (83). The decrease of  $\tau_c$  from  $0.74 \times 10^{-10}$  sec at pH 7.0 to  $0.4 \times 10^{-10}$  sec at pH 10 must result from enhanced flexibility of the polypeptide chain at or near the 93 $\beta$  site at this pH. Presumably this enhanced flexibility reflects some disordering of the  $\alpha$ -helix or the removal of a steric hindrance imposed by the proximity of another part of the protein chain.

Some general inferences may also be drawn on the basis of the atomic model of the tetramer at neutral pH. Under these conditions, the 93 $\beta$  sulphhydryl group is believed to be exposed to the surrounding medium. The present NMR data yield a value for the exchange rate at this site which is close to that calculated for free mercuric bromide ion ( $3.7 \pm 0.4 \times 10^7$  liter mole<sup>-1</sup>sec<sup>-1</sup> (40)), suggesting that solvated bromide ions have free access to this group. These data are therefore in accordance with the predictions of the X-ray model. The decrease in the exchange rate at high pH implies that diffusion of the bromide ion to and from this site is in some manner hindered. The helix H $\beta$  is closest to cysteine 93 $\beta$  (Fig. 27)

and could conceivably cause the observed effect by closely approaching the F $\beta$  helix and shielding the bound mercury from the solution. Alternatively, this steric hindrance may be the result of deformation of the F $\beta$  helix near the cysteine site. Elucidation of the exact cause of these phenomena must await further structural studies.

The results presented here represent a preliminary study of the 93 $\beta$  site of hemoglobin. According to the atomic model, this residue occupies a strategic position within the tetramer. Perutz (52) concludes that the salt bridge between histidine 146 $\beta$  and aspartate 94 $\beta$  is broken on oxygenation, with resulting alterations in the  $\beta$ -chain conformation near the probe site. The chain segment histidine 97--aspartate 102 bearing five of the nine  $\beta$  residues participating in  $\alpha_1\beta_2$  contacts (Table 1 of reference (51)) is nearby and may affect the 93 $\beta$  site when contacts between the monomers are modified by ligation of the heme. Recently, the sensitivity of the 93 $\beta$  sulphhydryl site to oxygenation-dependent conformational changes has been demonstrated with horse and human hemoglobin by the ESR probe technique. Changes in the paramagnetic resonance spectrum of iodoacetamide spin labels attached to this group were observed on oxygenation of either the  $\alpha$  or  $\beta$  chains (84). Providing that a satisfactory solution can be found to the problem of protein aggregation, halide-exchange studies on this site



may also yield information regarding ligand binding. It is apparent that the possibilities for probe studies on this system have only begun to be explored.

STUDIES ON OTHER PROTEINS

I. Papain

Papain (EC 3.4.4.10) is a proteolytic enzyme of molecular weight 20,700 (85) bearing one free sulphhydryl group at the active site (86,87). Since a monomeric protein with a single mercury-binding group would be an ideal system for halide-exchange studies, NMR titrations were performed on this enzyme at the beginning of this study to determine its feasibility for halide-probe experiments.

Twice-recrystallized papain was purchased as a suspension in acetate buffer, pH 4.5, from Sigma Chemical Co. Protein concentration was determined from the absorbance at 278 nm using an absorptivity of 51,800 liter mole<sup>-1</sup>cm<sup>-1</sup> (88).

The initial titration, performed on a suspension of  $6.4 \times 10^{-5}$  molar papain in 2.0 molar NaBr in 0.05 molar acetate buffer, pH 4.5, did not show any break in the curve indicative of a reactive sulphhydryl group and appeared very similar to the bottom titration curve of Fig. 38. Repetition of the titration at pH 6.0 yielded the upper titration curve of Fig. 38. The break in this curve suggests the presence of a reactive sulphhydryl group, but the change is small enough to conceivably be the result of improper tuning of the resonance condition.

$R_2$  was determined graphically in this case, and with this method mistuning is often not as obvious as with the two-point method. These experiments were performed within a few days of the sample being opened.

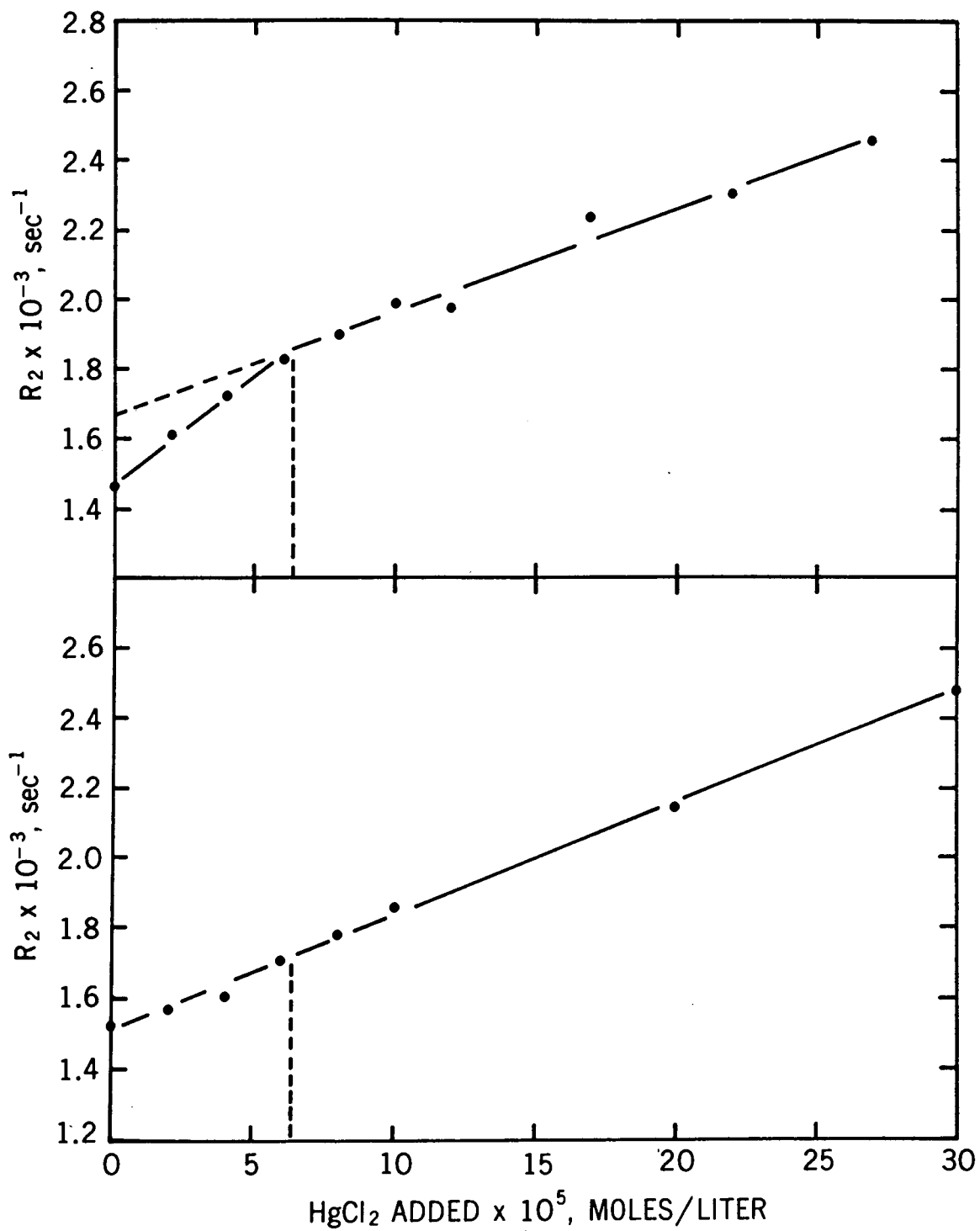
Titration were repeated on this sample two months later under the following conditions:

- (a)  $3.2 \times 10^{-5}$  molar papain dissolved in 0.5 molar NaBr, pH 6.6.
- (b)  $6.4 \times 10^{-5}$  molar papain suspended in 2.0 molar NaBr, pH 6.0.
- (c)  $6.4 \times 10^{-5}$  molar papain suspended in 2.0 molar NaBr, pH 8.3.

The titration curve from (b) is shown in the lower part of Fig. 38. No evidence for any sulphhydryl group was seen in these experiments. These results were particularly puzzling in view of the fact that Mensch (89) reports titrating 0.5 sulphhydryl group in papain using  $^{35}\text{Cl}$  NMR. Correlation time for the bound probe was calculated to be  $3 \pm 1 \times 10^{-10}$  sec.

Recent studies on the activation of papain shed some light on this dilemma. Crystalline papain prepared by the method of Kimmel and Smith (90) commonly exhibits low enzymatic activity and a sulphhydryl titer of 0.5 or less. The inactive

Fig. 38. Titration curves of papain. Top, titration of  $6.4 \times 10^{-5}$  molar papain suspended in 2.0 molar NaBr in 0.05 molar phosphate buffer, pH 6.0.  $R_2$  was measured by the graphical method, causing the possible error in  $R_2$  to be  $100 \text{ sec}^{-1}$ . The titration was performed a few days after the sample was opened. Bottom, titration performed under the same conditions two months later.  $R_2$  was measured by the two-point method (see text) and the possible error in  $R_2$  is  $80 \text{ sec}^{-1}$ .



form of the protein has been shown (91,92) to exist as a disulphide formed between papain and free cysteine present in the last steps of the purification procedure. Activation frees the bound protein sulphhydryl group. In the presence of cysteine, activated papain has been found to undergo rapid oxidation by air to the inactive form (91). The experiments reported by Mensch were apparently carried out on a partially active preparation of the enzyme; hence the low sulphhydryl content. If the results shown in Fig. 38 (top) are indicative of the presence of one free sulphhydryl group, then the disappearance of this group may be ascribed to air oxidation of the enzyme in the vial after breaking the seal. If the apparent break in this curve is attributed to experimental error, then the enzyme was obviously in the inactive form when received. Since further NMR studies would require activation of all samples of the enzyme followed by careful removal of the activator, and since the presence of traces of free cysteine could result in variations in the sulphhydryl content of the protein, halide-probe studies on this system were abandoned.

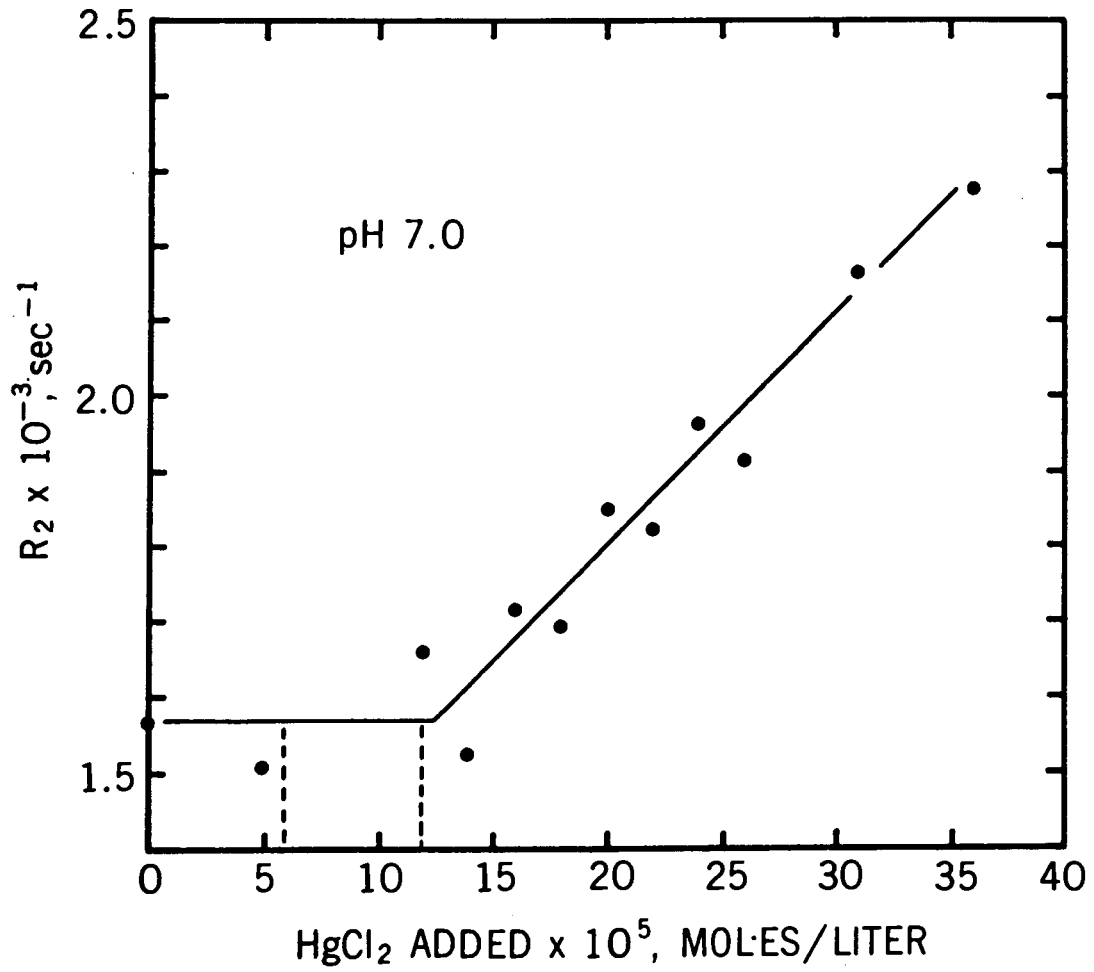
## II. Ovalbumin

Ovalbumin is a globular protein of molecular weight 45,000 bearing three free sulphhydryl groups (93). One ti-

tration performed on a solution of  $5.9 \times 10^{-5}$  molar ovalbumin in 2.0 molar NaBr at pH 7.0 revealed that this protein binds approximately two equivalents of mercury at sites where exchange with bromide ions in the solution does not occur. Protein concentration was calculated from the sample weight and no effort was made to determine the purity of the sample. Twice-recrystallized, lyophilized, and salt-free ovalbumin was a product of Sigma Chemical Company.

Fig. 39. Titration of  $5.9 \times 10^{-5}$  molar ovalbumin in 2.0 molar NaBr in 0.05 molar phosphate buffer, pH 7.0.  $R_2$  was determined graphically<sub>1</sub> and has an estimated error of 100 sec<sup>-1</sup>.





## GENERAL CONCLUSIONS

The halide-exchange technique described here has proven to be a method capable of detailed probing into the structural and dynamic properties of proteins and peptides. On the basis of experience with this method, it is possible to draw some conclusions regarding the use of  $\text{Br}^-$  as an NMR probe and to suggest promising avenues for extension of the present studies.

### I. Comparison of Chloride, Bromide, and Iodide as NMR Probes

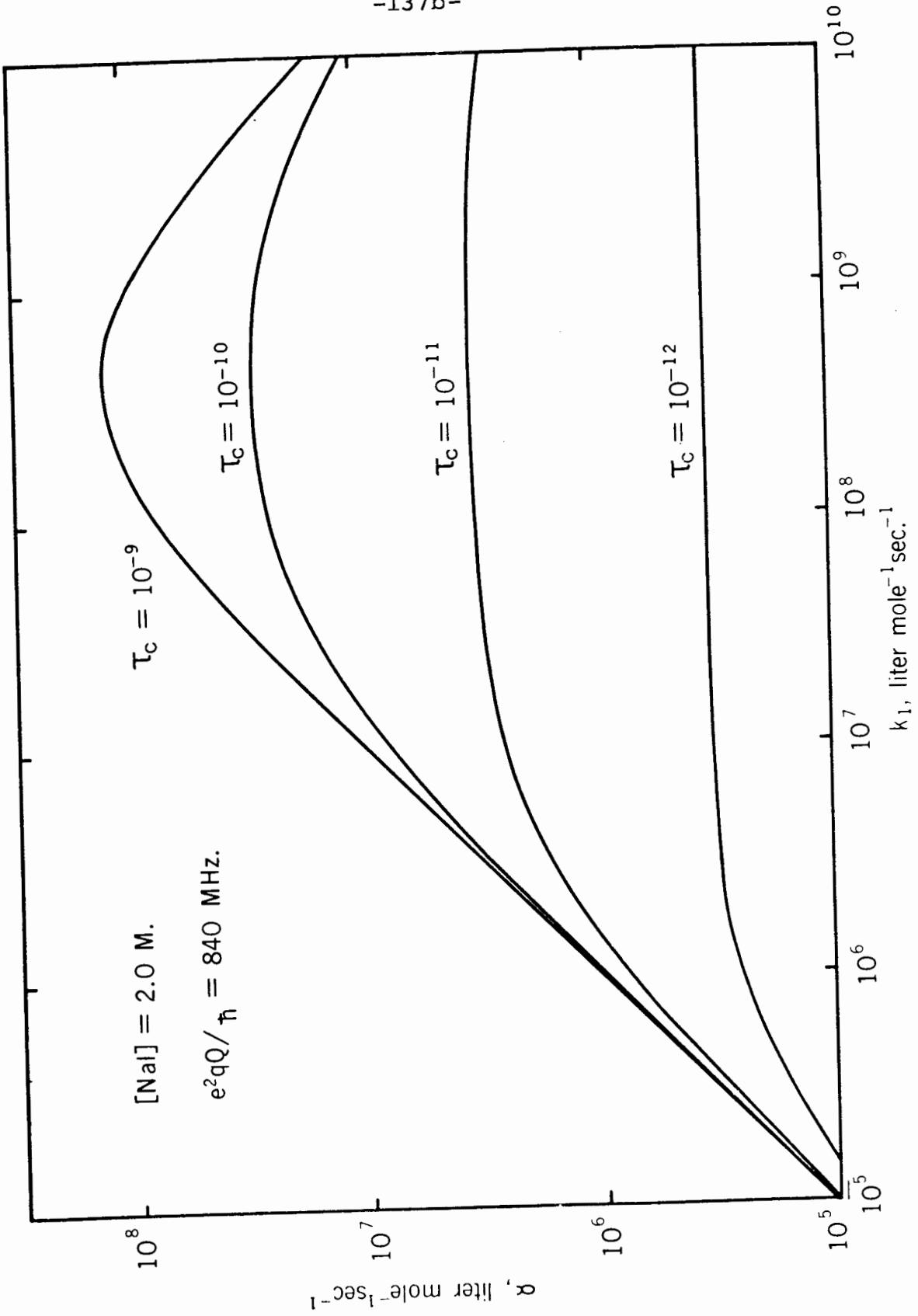
As the magnitude of  $\Delta R$  increases with the square of the quadrupolar moment  $Q$ , it would seem that  $\text{I}^-$  would be a superior probe to  $\text{Br}^-$ , and  $\text{Br}^-$  to  $\text{Cl}^-$ . However, comparison of the decay rates for aqueous  $\text{NaCl}$  and  $\text{NaBr}$  reveals that  $R_{2F}$  is  $50 \text{ sec}^{-1}$  for the chloride nucleus but  $1200 \text{ sec}^{-1}$  for bromide nuclei. Solvation asymmetry obviously has more drastic effects on the nucleus with the greater quadrupole moment. For this reason, observed changes in  $R_2$  relative to  $R_{2F}$  for  $\text{Br}^-$  are actually smaller than is the case for chloride. In this sense, iodide would probably be the least sensitive of the three probes, with chloride being the best. Also, the shorter the decay time, the more difficulty is encountered in accurately determining  $R_2$ .

Since the correlation times estimated by Mensch (89) for papain and Ellis (12) for bovine hemoglobin are of the same order as those measured here,  $10^{-10}$  sec, it seems likely that this is a typical value for sulphhydryl-bound halide probes. If the halide-exchange rate is  $9 \times 10^7$ ,  $4 \times 10^7$ , and approximately  $10^7$  liter mole<sup>-1</sup>sec<sup>-1</sup> (40) for I<sup>-</sup>, Br<sup>-</sup>, and Cl<sup>-</sup> respectively, this correlation time would situate bromide and iodide exchange well into the intermediate region between the slow and fast exchange limits (Figs. 5 and 40) while placing chloride exchange nearly at the fast exchange limit (Fig. 9).  $\alpha$  would therefore depend mostly on  $\tau_c$  with chloride probes. It is probable that only with bromide and iodide probes can both  $k_1$  and  $\tau_c$  be measured for sulphhydryl groups by this method. Other halide probes than mercuric ion (see next section) may exhibit quite different correlation times and it may be necessary to use a different halide to measure both  $k_1$  and  $\tau_c$  in each case.

## II. Improvements to the Spectrometer and Data Acquisition System

Several modifications to the present equipment would result in considerable saving of time and some improvement in

Fig. 40. Calculated dependence of  $\alpha$  on the rate of halide exchange for 2.0 molar iodide.

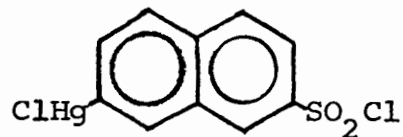


the accuracy of this method. Use of a signal averager with a minimum dwell time of 1  $\mu$ sec would permit measurements of  $R_2$  to be made on the off-resonance beat signal, thus eliminating the necessity for critical resonance tuning and the consequent danger of off-resonance modulation effects.  $R_2$  could be accurately determined from one measurement under these conditions. Better field stabilization is definitely in order if long averaging periods are to be used. The practicality of the bromide-probe method would be greatly enhanced by such technical improvements.

### III. Other Possible Probes

Extension of this technique to the study of more complex and informative probes suggests attractive possibilities for future research. Since mercury is a popular heavy-metal label for X-ray crystallographic studies, a number of organo-mercury compounds suitable for halide-probe studies are now available. The review by Blake (94) presents an excellent summary of recent progress in this field. Marshall (19) has recently bound a series of these bromomercurinaphthalenesulfonyl chloride inhibitors (I) to the essential serine in the active site of  $\alpha$ -chymotrypsin. Complexes of the enzyme with inhibi-

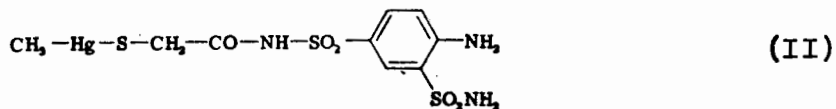
tors bearing mercury at different sites exhibited different  $^{35}\text{Cl}$  and  $^{81}\text{Br}$  linewidths, the results being



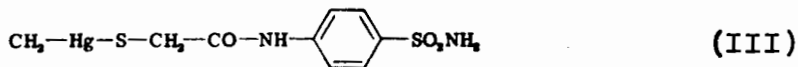
(I)

interpreted as variations in the correlation time of the bound label. In theory, titrations performed with these probes could yield values of  $k_1$  and  $\tau_c$  for each site on the inhibitor. These results might then yield detailed information regarding the fit of the inhibitor into the active site.

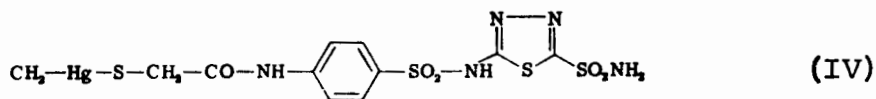
Several sulfonamide inhibitors (II-IV) used in X-ray studies on carbonic anhydrase require only complexing of the mercury to a halide atom for halide-exchange studies:



(II)



(III)



(IV)

Analogues of these inhibitors prepared with the substituents meta and para to each other would be expected to fit differently into binding sites and be sensitive to different conformational changes. Probes with varying lengths of carbon chain between the mercuric halide and the protein-specific group could act as biochemical rulers. Measurement of the length of probe required to increase the halide exchange rate to the value for free tetrabromide ion (that is, the chain length required to leave the mercury atom outside the protein) might permit estimation of the depth of buried active sites. More sophisticated experiments utilizing the findings of Huntress (25,34) might permit some estimate of the anisotropy of the movement of these probes. It should be possible to synthesize NMR probes to fit any given site. The flexibility of this method appears limited only by the imagination with which it is applied.



BIBLIOGRAPHY

1. Edelman, G.M. and McClure, W.O. 1968. Fluorescence Probes and the Conformation of Proteins. *Acc. Chem. Res.* 1:65.
2. Hamilton, C.L. and McConnell, H.M. 1968. in: A. Rich and N. Davidson (eds). Structural Chemistry and Molecular Biology. W.H. Freeman Co., San Francisco.
3. McConnell, H.M. and McFarland, B.G. 1970. Physics and Chemistry of Spin Labels. *Quart. Revs. Biophys.* 1:91.
4. Stengle, T.R. and Baldeschwieler, J.D. 1966. Halide Ions as Chemical Probes for NMR Studies of Proteins. *Proc. N.A.S.* 55:1020.
5. Stengle, T.R. and Baldeschwieler, J.D. 1967. Halide Ions as Probes for NMR Studies of Proteins. The Sulphydryl Groups of Hemoglobin. *J. Am. Chem. Soc.* 89:3045.
6. Haugland, R.P., Stryer, L., Stengle, T.R. and Baldeschwieler, J.D. 1967. Nuclear Magnetic Resonance Studies of Antibody-Hapten Interactions Using a Chloride-Ion Probe. *Biochem.* 6:498.
7. Marshall, A.G. 1968. Study of a Sulfonyl Derivative of  $\alpha$ -Chymotrypsin by Chlorine Nuclear Magnetic Resonance. *Biochem.* 7:2450.
8. Bryant, R.G. 1969. Nuclear Magnetic Resonance Study of Calcium-43. *J. Am. Chem. Soc.* 91:1870.
9. Bryant, R.G. 1969. Halogen Ion Probe Study of Bovine Mercaptalbumin. *J. Am. Chem. Soc.* 91:976.
10. Bryant, R.G., Yeh, H.J.C. and Stengle, T.R. 1969. The Disulfide Bond in Carboxypeptidase A. A Chloride Ion Nuclear Magnetic Resonance Study. *Biochem. Biophys. Res. Comm.* 87:603.
11. Cottam, G.L. and Ward, R.L. 1969. <sup>35</sup>Cl-NMR Studies on Zinc-Pyruvate Kinase Complexes. *Arch. Biochem. Biophys.* 132:308.

12. Ellis, W.D., Dunford, H.B. and Martin, J.S. 1969. Studies on Heme Proteins Using the NMR Halide-Probe Technique. *Can. J. Biochem.* 47:157.
13. Happe, J.A. and Ward, R.L. 1969. Chlorine-35 Nuclear Magnetic Resonance Study of Zinc Nucleotide Diphosphate Complexes. *J. Am. Chem. Soc.* 91:4906.
14. Sandberg, H.E., Bryant, R.G. and Piette, L.H. 1969. Studies on the Location of Sulphydryl Groups in Erythrocyte Membranes with Magnetic Resonance Spin Probes. *Arch. Biochem. Biophys.* 133:144.
15. Sykes, B.D. 1969. An Application of Transient Nuclear Magnetic Resonance Methods to the Measurement of Biological Exchange Rates. The Interaction of Tri-fluoroacetyl-D-phenylalanine with the Chymotrypsins. *J. Am. Chem. Soc.* 91:949.
16. Sykes, B.D. and Parravano, C. 1969. A Nuclear Magnetic Resonance Study of the Inhibition of Lysozyme by N-acetyl-D-glucosamine and Di-N-acetyl-D-glucosamine. *J. Biol. Chem.* 244:3900.
17. Ward, R.L. 1969. <sup>35</sup>Cl Nuclear Magnetic Resonance Studies of a Zinc Metalloenzyme Carbonic Anhydrase. *Biochem.* 8:1879.
18. Zeppezauer, M., Lindman, B., Forsen, S. and Lindqvist, I. 1969. A <sup>81</sup>Br Nuclear Magnetic Resonance Study of Bromide Ion Binding to Proteins in Aqueous Solution. *Biochem. Biophys. Res. Comm.* 37:137.
19. Marshall, A.G. Private Communication.
20. Navon, G., Shulman, R.G., Wylunda, B.J. and Yamane, T. 1970. Nuclear Magnetic Resonance Study of the Binding of Fluoride Ions to Carboxypeptidase A. *J. Mol. Biol.* 51:15.
21. Sykes, B.D., Schmidt, P.G. and Stark, G.R. 1970. Aspartate Transcarbamylase: A Study by Transient Nuclear Magnetic Resonance of the Binding of Succinate to the Native Enzyme and its Catalytic Subunit. *J. Biol. Chem.* 245:1180.

22. Pople, J.A. Schneider, W.G. and Bernstein, H.J. 1959. High-Resolution Nuclear Magnetic Resonance. McGraw-Hill, Toronto. p. 25.
23. Ref. 22, p. 46.
24. Abragam, A. 1961. The Principles of Nuclear Magnetism. Oxford University Press, London. p. 313.
25. Huntress, W.T. 1970. The Study of Anisotropic Rotation of Molecules in Liquids by NMR Quadrupolar Relaxation. *Adv. Mag. Res.* 4:1.
26. Wallach, D. 1967. Effect of Internal Rotation on Angular Correlation Functions. *J. Chem. Phys.* 47:5258.
27. Slichter, C.P. 1963. Principles of Magnetic Resonance. Harper and Row, New York. p. 137.
28. Dirac, P.A.M. 1958. The Principles of Quantum Mechanics. Clarendon Press, Oxford. p. 130.
29. Ref. 27, p. 129.
30. Ref. 24, p. 277.
31. Ref. 24, p. 162.
32. Rose, M.E. 1957. Elementary Theory of Angular Momentum. John Wiley and Sons, Inc., New York. Ch. IV.
33. Ref. 24, p. 166.
34. Huntress, W.T. 1968. Effects of Anisotropic Molecular Rotational Diffusion on Nuclear Magnetic Relaxation in Liquids. *J. Chem. Phys.* 48:3524.
35. Ref. 24, p. 271.
36. Ref. 24, p. 299.
37. Pitzer, K.S. 1953. Quantum Chemistry. Prentice-Hall Inc., New York. p. 49.
38. Ref. 24, p. 314.

39. Margenau, H. and Murphy, G.M. 1965. The Mathematics of Physics and Chemistry. D. Van Nostrand Co. Inc., Princeton, New Jersey. p. 309.
40. O Reilley, D.E., Schacher, G.E. and Schug, K. 1963. Rate of Exchange of Halide Nuclei with Mercury (II) in Aqueous Solution. J. Chem. Phys. 39:1756.
41. Ref. 22, p. 361.
42. Marshall, A.G. 1970. Calculation of NMR Relaxation Times for Quadrupolar Nuclei in the Presence of Chemical Exchange. J. Chem. Phys. 52:2527.
43. Kolthoff, I.M. and Barnum, C. 1940. The Anodic Reaction and Waves of Cysteine at the Dropping Mercury Electrode and the Platinum Micro Wire Electrode. J. Am. Chem. Soc. 62:3061.
44. Stricks, W. and Kolthoff, I.M. 1952. Polarography of Glutathione. J. Am. Chem. Soc. 74:4646.
45. Stricks, W. and Kolthoff, I.M. 1953. Reactions Between Mercuric Mercury and Cysteine and Glutathione. Apparent Dissociation Constants, Heats and Entropies of Formation of Various Forms of Mercuric Mercapto-Cysteine and -Glutathione. J. Am. Chem. Soc. 75:5673.
46. Kolthoff, I.M., Stricks, W. and Morren, L. 1954. Amperometric Mercurimetric Titration of Sulphydryl Groups in Biologically Important Substances. Anal. Chem. 26:366.
47. Stricks, W., Kolthoff, I.M., and Heyndrickx, A. 1954. Formation and Properties of Various Mercuric Mercapto Thioglycolates Formed in Reactions between Mercuric Mercury and Thioglycolic Acid. J. Am. Chem. Soc. 76:1515.
48. Shindo, H. and Brown, T.L. 1965. Infrared Spectra of Complexes of L-Cysteine and Related Compounds with Zinc (II), Cadmium (II), Mercury (II), and Lead (II). J. Am. Chem. Soc. 87:1904.

49. Perutz, M.F., Muirhead, H., Cox, J.M. and Goaman, L.C.G. 1968. Three-dimensional Fourier Synthesis of Horse Oxyhemoglobin at 2.8 Å<sup>o</sup> Resolution: The Atomic Model. *Nature* 219:131.
50. Perutz, M.F. 1969. The Hemoglobin Molecule. *Proc. Roy. Soc. B.* 173:113.
51. Bolton, W. and Perutz, M.F. 1970. Three Dimensional Fourier Synthesis of Horse Deoxyhemoglobin at 2.8 Å<sup>o</sup> Resolution. *Nature* 228:551.
52. Perutz, M.F. 1970. Stereochemistry of Cooperative Effects in Hemoglobin. *Nature* 228:726.
53. Rossi Fanelli, A., Antonini, E. and Caputo, A. 1964. Hemoglobin and Myoglobin. *Adv. Prot. Chem.* 19:73.
54. Dayhoff, M.O. and Eck, R.V. 1968. Atlas of Protein Sequence and Structure. National Biomedical Research Foundation, Silver Spring, Md. p. 130, 144.
55. Dickerson, R.E. and Geis, I. 1969. The Structure and Action of Proteins. Harper and Row, New York. p. 56.
56. Kurihara, K. and Shibata, K. 1960. Dissociation of Horse Hemoglobin at High pH. *Arch. Biochem. Biophys.* 88:298.
57. Tanford, C. 1961. Physical Chemistry of Macromolecules. John Wiley and Sons, Inc., New York. p. 357, 365.
58. Ref. 57, p. 324-328.
59. Drabkin, P.B.C. 1945. Crystallographic and Optical Properties of Human Hemoglobin. *Am. J. Med. Sci.* 209:268.
60. Wootton, I.D.P., and Blevin, W.R. 1964. The Extinction Coefficient of Cyanmethaemoglobin. *Lancet* No. 7357, p. 434.

61. Zijlstra, W.G. and Van Kampen, E.J. 1960. Standardization of Hemoglobinometry I. The Extinction Coefficient of Hemoglobinocyanide at 540 m $\mu$ . Clin. Chim. Acta 5:719.
62. Morningstar, D.A., Williams, G.Z. and Suutarinen, P. 1966. The Millimolar Extinction Coefficient of Cyanmethemoglobin from Direct Measurement of Hemoglobin Iron by X-ray Emission Spectroscopy. Am. J. Clin. Pathology 46:603.
63. Stigbrand, T. 1967. Molar Absorbancy of Cyanmethemoglobin. Scand. J. Clin. Lab. Invest. 20:252.
64. Sephadex Gel Filtration in Theory and Practice. Pharmacia Fine Chemicals, Uppsala, Sweden.
65. Sephadex Ion Exchangers. Pharmacia Fine Chemicals, Uppsala, Sweden.
66. Keilin, D. and Hartree, E.F. 1951. Purification of Horse-Radish Peroxidase and Comparison of its Properties with Those of Catalase and Methemoglobin. Biochem. J. 49:88.
67. Scheler, W., Schoffa, G. and Jung, F. 1957. Lichtabsorption und Paramagnetische Suszeptibilitat bei Derivaten des Pferde-und Chironomous-Methamoglobins sowie des Pferde Metmyoglobins. Biochem. Zeit. 329:232.
68. Huisman, T.H.J., Martis, E.A. and Dozy, A. 1958. Chromatography of Hemoglobin Types on Carboxymethylcellulose. J. Lab. and Clin. Med. 52:312.
69. Determann, H. 1968. Gel Chromatography. Springer-Verlag, New York. p. 67.
70. Guidotti, G., Konigsberg, W. and Craig, L.C. 1963. On the Dissociation of Normal Adult Human Hemoglobin. Proc. N.A.S. 50:774.
71. Rosemeyer, M.A. and Huehns, E.R. 1967. On the Mechanism of the Dissociation of Hemoglobin. J. Mol. Biol. 25:253.

72. Rossi-Fanelli, A., Antonini, E. and Caputo, A. 1961. Studies on the Relations Between Molecular and Functional Properties of Hemoglobin. I. The Effect of Salts on the Molecular Weights of Human Hemoglobin. *J. Biol. Chem.* 236:391.
73. Andrews, P. 1964. Estimation of the Molecular Weights of Proteins by Sephadex Gel-Filtration. *Biochem. J.* 91:222.
74. Merrett, T. 1966. Observations on the Dissociation of Oxy-, Deoxy-, and Ferrihemoglobin in Relation to pH and Ionic Strength by the Sephadex Method. *Biochim. Biophys. Acta.* 124:389.
75. Ref. 69, pp. 89 and 118.
76. Gutter, F.J., Peterson, E.A. and Sober, H.A. 1959. Chromatography of Proteins. III. Human, Horse, and Dog Hemoglobins on Cation-Exchange Cellulose. *Arch. Biochem. Biophys.* 80:353.
77. Kilmartin, J.V. and Clegg, J.B. 1967. Amino-acid Replacements in Horse Hemoglobin. *Nature* 213:269.
78. Perutz, M.F., Steinrauf, L.K., Stockell, A. and Bingham, A.D. 1959. Chemical and Crystallographic Study of the Two Fractions of Adult Horse Hemoglobin. *J. Mol. Biol.* 1:402.
79. Murayama, M. 1958. Titratable Sulfhydryl Groups of Horse, Sheep, Dog, and Cow Hemoglobins at 0° and 38°. *J. Biol. Chem.* 233:594.
80. Cole, R.D., Stein, W.H. and Moore, S. 1958. On the Cysteine Content of Human Hemoglobin. *J. Biol. Chem.* 233:1359.
81. Haugland, R.P. and Stryer, L. 1967. A Fluorescent Probe at the Active Site of  $\alpha$ -Chymotrypsin in: International Symposium on the Conformation of Biopolymers. Vol. I. Academic Press, New York, p. 321.
82. Tanford, C. 1968. Protein Denaturation. *Adv. Protein Chem.* 23:121.

83. Beychok, S. 1964. Effects of Ligands on the Optical Rotary Dispersion of Hemoglobin. I. Ferrihemoglobin Cyanide, Ferrihemoglobin Azide, Ferrihemoglobin Hydroxide, and Carbonmonoxyhemoglobin. *Biopolymers* 2:575.
84. Deal, W.J., Mohlman, S.G. and Sprang, M.L. 1971. Conformational Equilibria in Spin-Labelled Hemoglobin. *Science* 171:1147.
85. Smith, E.L. and Kimmel, J.R. 1960. Papain. In: Boyer, P.D., Lardy, H. and Myrback K. (eds.) The Enzymes. Academic Press, New York.
86. Light, A., Frater, R., Kimmel, J.R. and Smith, E.L. 1964. Current Status of the Structure of Papain. *Proc. N.A.S.* 52:176.
87. Drenth, J., Jansonius, J.N., Koekoek, R., Swen, H.M. and Wolthen, B.G. 1968. Structure of Papain. *Nature* 218:929.
88. Wetlaufer, D.B. 1962. Ultraviolet Spectra of Proteins and Amino Acids. *Adv. Protein Chem.* 17:303.
89. Mensch, J.C. 1969. Private Communication.
90. Kimmel, J.R. and Smith, E.L. 1954. Crystalline Papain. I. Preparation, Specificity, and Activation. *J. Biol. Chem.* 207:515.
91. Sluyterman, A.E. 1967. The Activation Reaction of Papain. *Biochim. Biophys. Acta.* 139:430.
92. Klein, I.B. and Kirsch, J.F. 1969. The Mechanism of the Activation of Papain. *Biochem. Biophys. Res. Comm.* 34:575.
93. Cunningham, L.W., Neuenke, B.J. and Strayhorn, W.D. 1957. Sulphydryl Content and Tryptic Susceptibility of Thermally Denatured Ovalbumin. *J. Biol. Chem.* 228: 835.
94. Blake, C.C.F. 1968. The Preparation of Isomorphous Derivatives. *Adv. Protein Chem.* 23:59.



CURRICULUM VITAE

T. Rand Collins

Personal History:

Place of birth: Vancouver, B.C., Canada  
Date of birth: October 15, 1946.  
Marital status: Married to Janie L. Trute on  
December 12, 1969.

Educational Background:

1961-1965 West Vancouver Secondary School, West Van-  
couver, B.C. (High School and Senior  
Matriculation).  
1965-1968 Simon Fraser University, Burnaby 2, B.C.  
(Undergraduate Studies).  
1969-1971 Simon Fraser University, Burnaby 2, B.C.  
(Graduate Studies).  
Summer, 1969 Marine Biological Laboratory, Woods Hole,  
Massachussetts, U.S.A. (Physiology  
Course).

Degrees:

B. Sc. (First Class Honours) Chemical Physics.  
Simon Fraser University, Burnaby 2, B.C. 1969.

Awards:

First Class B.C. Government Scholarships--Simon Fraser University, Burnaby 2, B.C. 1965-1968.

Vancouver Postal Club Scholarship--Simon Fraser University, Burnaby 2, B.C. Fall, 1965.

National Research Council Postgraduate Scholarship--Simon Fraser University, Burnaby 2, B.C. 1969-1971.

President's Research Grant Award--Simon Fraser University, Burnaby 2, B.C. Spring, 1970.

Medical Research Council Studentship--University of California, Berkeley. 1971-1972.

Experience:

Research Assistant--Simon Fraser University, Burnaby 2, B.C. Summer, 1966. Photobiology.

Research Assistant--Pacific Oceanographic Group, Fisheries Research Board of Canada, Nanaimo, B.C. Summer, 1967. Physical Oceanography.

Research Assistant--Simon Fraser University, Burnaby 2, B.C. Fall, 1968. Biophysics of Photoreceptors.

Teaching Assistant--Simon Fraser University, Burnaby 2, B.C. Summer, 1971. Bisc. 101. Introduction to Biology.